SMIP97

SMIP97 SEMINAR ON UTILIZATION OF STRONG-MOTION DATA

Los Angeles, California
May 8, 1997

PROCEEDINGS

Sponsored by

California Strong Motion Instrumentation Program
Division of Mines and Geology
California Department of Conservation

Supported in Part by

California Seismic Safety Commission
Federal Emergency Management Agency

DEPARTMENT OF CONSERVATION
DIVISION OF MINES AND GEOLOGY

SMIP97

SMIP97 SEMINAR ON UTILIZATION OF STRONG-MOTION DATA

Los Angeles, California
May 8, 1997

PROCEEDINGS

Edited by

M.J. Huang

Sponsored by

California Strong Motion Instrumentation Program
Division of Mines and Geology
California Department of Conservation
801 K Street, MS 13-35
Sacramento, California 95814-3531

Supported in Part by

California Seismic Safety Commission
Federal Emergency Management Agency

The California Strong Motion Instrumentation Program (CSMIP) is a program within the Division of Mines and Geology of the California Department of Conservation and is advised by the Strong Motion Instrumentation Advisory Committee (SMIAC), a committee of the California Seismic Safety Commission. Current program funding is provided by an assessment on construction costs for building permits issued by cities and counties in California, with additional funding from the California Department of Transportation, the Office of Statewide Health Planning and Development, and the California Department of Water Resources.

In January 1997, a joint project, TriNet, between CDMG, Caltech and USGS was funded by the Federal Emergency Management Agency (FEMA) through the California Office of Emergency Services (OES). The goals of the project are to record and rapidly communicate ground shaking information in southern California, and to analyze the data for the improvement of seismic codes and standards.

DISCLAIMER

PREFACE

The California Strong Motion Instrumentation Program (CSMIP) in the Division of Mines and Geology of the California Department of Conservation promotes and facilitates the improvement of seismic codes through the Data Interpretation Project. The objective of this project is to increase the understanding of earthquake strong ground shaking and its effects on structures through interpretation and analysis studies of CSMIP and other applicable strong-motion data. The ultimate goal is to accelerate the process by which lessons learned from earthquake data are incorporated into seismic code provisions and seismic design practices.

Since the establishment of CSMIP in the early 1970s, over 600 stations, including 400 ground-response stations, 145 buildings, 20 dams and 45 bridges, have been installed. Significant strong-motion records have been obtained from many of these stations. One of the most important sets of strong-motion records is from the 1994 Northridge earthquake. During this earthquake strong-motion records were obtained from 116 ground-response stations and 77 extensively-instrumented structures. In addition to these records, CSMIP in cooperation with the City of Los Angeles and other agencies, collected and archived accelerograms recorded at over 300 high-rise buildings during the Northridge earthquake. These buildings were instrumented by the building owners as required by the City's Building Code. The strong-motion records from the Northridge earthquake have been and will be the subject of CSMIP data interpretation projects.

The SMIP97 Seminar is the ninth in a series of annual events designed to transfer recent interpretation findings on strong-motion data to practicing seismic design professionals and earth scientists. The purpose of the Seminar is to increase the utilization of strong-motion data in improving seismic design and practices. In the presentations, six invited experts who have utilized strong-motion data in specific studies will present the applications of strong-motion data to a variety of areas including earthquake resistant design, near fault ground motion, UBC ground shaking criteria, seismic rehabilitation guidelines, computer modeling of buildings, and utilization for bridges and dams. In addition, CSMIP staff will present two papers; one on the recent development on near-real-time strong motion and data dissemination through Internet, and the other on the EERI/FEMA Profession Fellowship project on site response. Director Richard Andrews of the Governor's Office of Emergency Services will present a luncheon address on the funding of TriNet project to improve earthquake planning, response and early warning.

Anthony F. Shakal
CSMIP Program Manager

Moh J. Huang
Data Interpretation Project Manager

TABLE OF CONTENTS

SMIP97 SEMINAR ON UTILIZATION OF STRONG-MOTION DATA

Sheraton Universal Hotel, Universal City, California
May 8, 1997

PROGRAM

8:30 - 9:30	**Registration**
9:30 - 9:40	**Welcoming Remarks** *Jeffrey Johnson*, Seismic Safety Commission, and Chair, Strong Motion Instrumentation Advisory Committee (SMIAC) *James Davis*, State Geologist, Division of Mines and Geology
9:40 - 9:50	**Introductory Remarks** *Anthony Shakal* and *Moh Huang*, Strong Motion Instrumentation Program
SESSION I	**Moderator:** *Bruce Bolt*, UC Berkeley Chair, SMIAC Ground-Response Subcommittee
9:50 - 10:20	**Use of Strong-Motion Data in Earthquake Resistant Design** *Paul Jennings*, California Institute of Technology, Pasadena
10:20 - 10:50	**Engineering Characteristics of Near Fault Ground Motion** *Paul Somerville*, Woodward-Clyde, Pasadena
10:50 - 11:00	**Questions and Answers for Session I**
11:00 - 11:20	Break
SESSION II	**Moderator:** *Chris Poland*, Degenkolb Engineers Chair, SMIAC Buildings Subcommittee
11:20 - 11:50	**1997 Uniform Building Code Ground Shaking Criteria** Charles Kircher and *Robert Bachman*, Fluor Daniel, Irvine
11:50 - 12:20	**Near-Real-Time Strong-Motion, TriNet Data and Data Dissemination through Internet** *Anthony Shakal*, V. Graizer, C. Petersen and R. Darragh, CDMG/SMIP, Sacramento
12:20 - 12:30	**Questions and Answers for Session II**

12:30 - 1:50	**Luncheon** Introduction *James Davis*, State Geologist, Division of Mines and Geology Speaker *Richard Andrews*, Director, Office of Emergency Services
SESSION III	**Moderator:** *Jeffrey Johnson*, Seismic Safety Commission Chair, SMIAC
1:50 - 2:20	**FEMA-273 Seismic Rehabilitation Guidelines: The Next Step - Verification** *Ronald Hamburger*, EQE International, San Francisco
2:20 - 2:50	**Shear-Wave Velocities and Design Response Spectra - An Examination Using Strong-Motion Data from the Gilroy Array** *Robert Darragh* and I.M. Idriss, CDMG/SMIP and UC Davis
2:50 - 3:00	**Questions and Answers for Session III**
3:00 - 3:20	Break
SESSION IV	**Moderator:** *Vern Persson*, Division of Safety of Dams, DWR Chair, SMIAC Lifelines Subcommittee
3:20 - 3:50	**Importance of Measured Full-Scale Building Response in the Computer Modeling of Buildings** *Gary Hart*, University of California, Los Angeles
3:50 - 4:20	**Utilization of Strong-Motion Data from Bridges and Dams** *Gregory Fenves*, University of California, Berkeley
4:20 - 4:30	**Questions and Answers for Session IV**
4:30	**Closing Remarks**

USE OF STRONG-MOTION DATA IN EARTHQUAKE RESISTANT DESIGN

Paul C. Jennings

Division of Engineering and Applied Science
California Institute of Technology
Pasadena, California

ABSTRACT

The study first reviews some simple methods of calculating maximum displacement, base shear and interstory drift from acceleration response records. A record from a 17-story building in Los Angeles obtained during the Northridge earthquake is used for illustration. More detailed analyses of similar records are suggested as attractive subjects for Master's theses and senior projects. Simple analyses of records from Northridge and other earthquakes convincingly indicate base shears and drifts that are substantially in excess of those used in design. The author urges that earthquake resistant design be based increasingly on measurements of earthquake response and measured properties of materials, and less on empiricism and qualitative assessments of earthquake performance.

INTRODUCTION

The records obtained from the earthquake response of structures are the basic data against which methods of earthquake resistant design and techniques for the analysis of earthquake response must be judged. The records are also useful for quickly informing the technical communities involved in earthquake damage assessment and recovery of the scope of the problems they may face. For the design engineer of a building that has been heavily shaken, the records can be helpful in assessing the likelihood of structural and non-structural damage that is not readily visible. The records also provide a means for educating the media and the public about the nature and extent of earthquake response. This paper reviews some of the simple methods whereby important results can be determined quickly from the measurements of earthquake response and notes the importance of recorded motions in improving the process of earthquake resistant design.

REVIEW OF ELEMENTARY METHODS

Figure 1 shows an example of the measurements which can be obtained from the response of a structure to strong ground motion. In this case the records are the accelerations measured at various points in a 17-story building during the Northridge earthquake of January 17, 1994 (CSMIP, 1995).

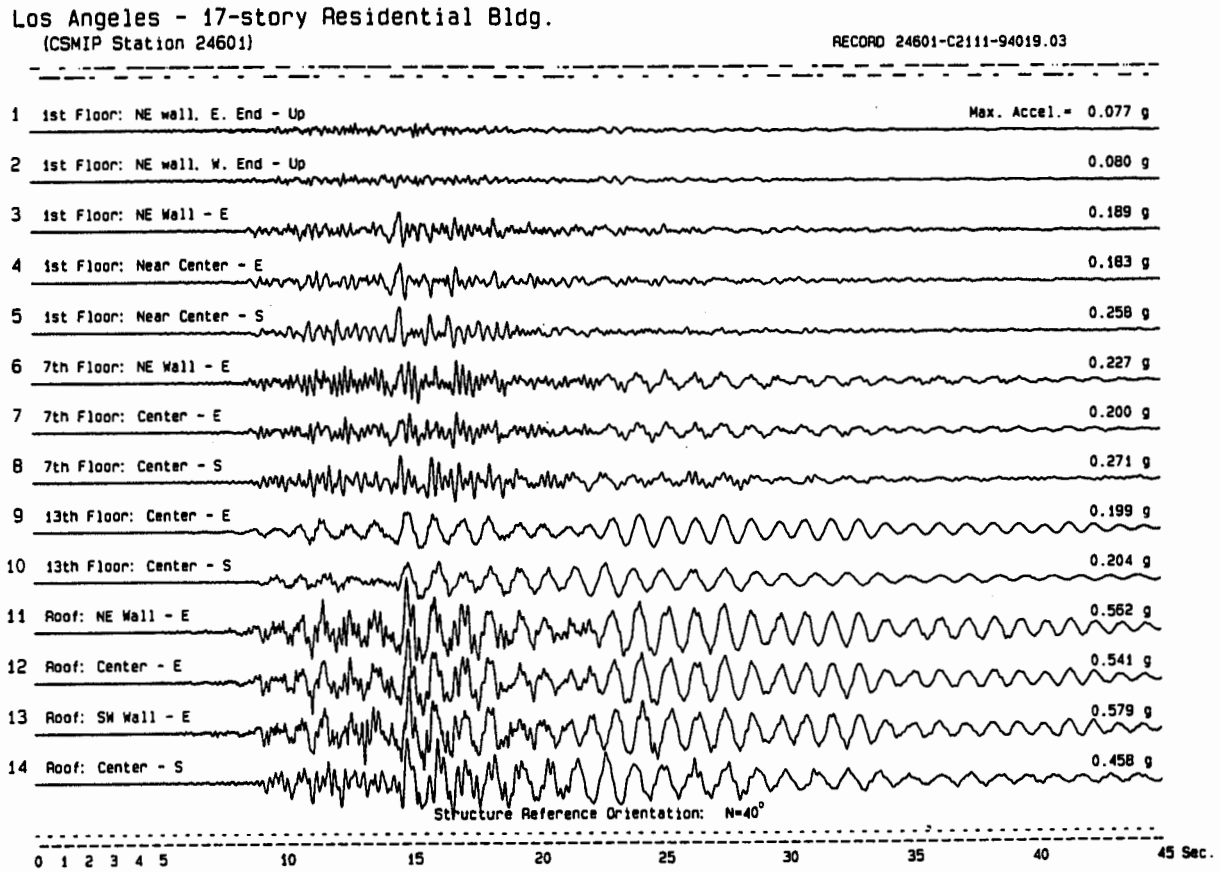

Figure 1. The acceleration measured in a 17-story residential building in Los Angeles during the Northridge earthquake of January 17, 1994 (Station 24601, CSMIP, 1995).

In accordance with common practice, a will denote acceleration, v, velocity, and d, displacement. The symbol for interstory drift will be γ. Attention is focused first on the acceleration recorded at the top of the structure; in some cases this and the corresponding acceleration at the base may be the only records available. One can draw a base line through the trace and use the indicated maximum acceleration to find a calibration factor if a scale factor is not given in the report. In the case of the Center-E component of the roof response (trace 12) in Figure 1, for example, a factor of $0.077g/mm$ was found before reproduction for the PROCEEDINGS (It is a coicindence that the maximum value of trace 1 is $0.077g$). Although the maximum acceleration occurred at about fifteen seconds, the oscillatory response of what appears to be the fundamental mode of the building produces almost equally large accelerations in the 22 to 35 second range. This is the portion of the response that will be examined as the largest displacement, base shear and interstory drift are expected during this time.

Applying the scaling factor to the large peaks in the Roof Center-E (trace 12) record around 25 seconds gives a value of $0.27g$ for the maximum acceleration of the roof in the fundamental mode. This total response can also be taken as the response of

the structure with respect to its base, as the ground motion at this time (trace 4) appears small and unrelated to the response. A calculation similar to that for the acceleration shows the building to have a fundamental period of vibration of 1.1 sec in this time frame.

Acceleration at the Roof

The record of acceleration obtained on the roof is of direct interest, particularly to mechanical engineers because of the large amount and variety of equipment that is often installed there. The measured acceleration can be compared to the design motions for such equipment and the response spectra distributed with the processed records can be used to compare the earthquake response of equipment to values used in the design.

A comparison of the roof acceleration to the acceleration at the base of the building also provides a measure of how much the structure amplified and altered the ground motion. This comparison can help engineers answer the obvious question of how much stronger the shaking may have been for occupants of the upper floors in comparison to those near the ground. In the present example the structure amplified the motions by roughly a factor of three, increasing the pulse of ground motion at about 15 seconds from a value of $0.183g$ at the first floor (trace 4) to a value of $0.541g$ on the roof (trace 12).

Maximum Displacement

The acceleration in the time range of 22 to 35 seconds is essentially sinusoidal, which allows the maximum displacement at the center of the roof in this direction to be evaluated from

$$d_{max} = \left(\frac{T}{2\pi}\right)^2 a_{max}. \qquad (1)$$

Using the values for acceleration, $0.27g$, and period, 1.1 sec, determined above, the maximum displacement of the 17-story building in its fundamental mode is found to be 8.2 cm. If processed records are available, scale factors are included with the plots of individual traces and this approximate calculation of displacement need not be done, as velocity and displacement calculations are part of the package of processed data. The value of the maximum displacement reported in the processed records in this case is 10.5 cm, but a value of 8.2 cm is quite representative of the maximum oscillatory displacement in the selected time period.

Base Shear

The base shear can also be approximated from the acceleration records with little detailed knowledge of the building. The records in Figure 1 can be used to estimate the acceleration profile of the structure during the time of maximum response (note that floors 13 and 7 (traces 9 and 7) are responding in phase with the roof in the selected time frame). However, to illustrate the most general approach, only the roof acceleration will be used; in this case one must assume an acceleration profile. In the present example it

appears justified to assume that the structure is vibrating only in its fundamental mode in the 22 to 35 second range.

In general, the base shear, V, can be written from Newton's law as

$$V = m_n a_n + m_{n-1} a_{n-1} + \cdots + m_2 a_2 + m_1 a_1, \tag{2}$$

in which the subscripts refer to one of the n floor levels. Defining m as the average floor mass, Eqn. 2 can be written

$$V = m a_n \left(\frac{m_n}{m} + \frac{a_{n-1} m_{n-1}}{a_n m} + \cdots + \frac{a_2 m_2}{a_n m} + \frac{a_1 m_1}{a_n m} \right). \tag{3}$$

Using the fact that the total mass, M, is n times the average mass, m, and assuming for the moment that the floor masses are all equal, the base shear as a fraction of the weight of the building becomes

$$\frac{V}{Mg} = \frac{a_n}{g} \frac{1}{n} \left(1 + \frac{a_{n-1}}{a_n} + \cdots + \frac{a_2}{a_n} + \frac{a_1}{a_n} \right). \tag{4}$$

If the structure is vibrating in the fundamental mode, the term in parentheses is just the sum of the mode shape ordinates, with the mode shape normalized so the ordinate at the roof is equal to unity. This quantity times $1/n$ is therefore simply the average value of the fundamental mode, a quantity that does not vary much. The fundamental mode of most buildings lies somewhere between the half sine wave of a uniform shear beam, typical of short frame buildings, and a straight line, shown by tall structures. If the fundamental mode is a straight line normalized to unity at the top of the structure, the average modal ordinate is 0.5; if the mode shape is the half sine wave of a uniform shear beam, the value increases to $2/\pi = 0.64$. Applying this to Eqn. 4, and using the middle of the range,

$$\frac{V}{Mg} = 0.6 \frac{a_n}{g} \pm 15\%. \tag{5}$$

In Eqn. 5, the factor 0.6 should be increased if the fundamental mode is believed to be close to that of a uniform shear beam, and decreased if the mode is thought to be closer to a straight line.

For a structure with unequal floor masses, the effect of such differences is seen from Eqns. 3 and 4 to be the same as having a different mode shape. For most structures, only a few floors will have masses much different from the average, and the final result, the average value of the modal ordinates, will not be changed very much.

In the 17-story building being used as an example, $a_n/g = 0.27$ and the mode shape is thought to be closer to a straight line than indicated by the factor of 0.6 in Eqn. 5 because shear walls provide most of the resistance for this direction of response. The floors of the structure have the same area, so the assumption of regular masses seems justified. Putting this together, the base shear experienced in the earthquake in the 22 to 35 sec time frame was about 15 percent of its weight. The base shear might have been as high as 17 percent of its weight, or as low as 13 percent, but it very unlikely to be outside this range, because the values come so directly from the measured response and from a reasonable range of relative accelerations (or displacements) of the structure at the time of maximum response.

Interstory Drift

A similar approach can be used to estimate the maximum interstory drift indicated by the recorded motion. The additional information needed is the height of the building, h, and the interstory height, l_j. The average interstory height, $l = h/n$, is also introduced. Using Eqn. 1, and assuming that the floors are vibrating in phase in the fundamental mode, the maximum drift at the j^{th} level can be expressed as

$$\gamma_j = \frac{d_{j+1} - d_j}{l_j} = \frac{T^2 a_n}{4\pi^2 l_j}\left(\phi_{j+1} - \phi_j\right), \tag{6}$$

in which ϕ_j is the value of the fundamental mode at the j^{th} level. In estimating the drift it is useful to look again at the cases of a straight line mode and a half sine wave mode. For a straight line mode normalized to unity at the top of the structure, the difference between modal ordinates for any two adjacent floors is l_j/h, and Eqn. 6 reduces to

$$\gamma = \frac{T^2 a_n}{4\pi^2 h} = \frac{d_{max}}{h}, \tag{7}$$

taking the same value for all stories. In the case of a half sine wave mode, $(\phi_{j+1} - \phi_j)/l_j$ is well-approximated by the slope of the mode shape at the height, x_j, of interest. Applying this to Eqn. 6 gives, in comparison to Eqn. 7

$$\gamma_j = \frac{T^2 a_n}{4\pi^2 h}\frac{\pi}{2}\cos\frac{\pi x_j}{2h}. \tag{8}$$

If the fundamental mode resembles a half sine wave, the maximum drift is at the first floor level and even for a building of four or five stories, the cosine function in Eqn. 8 is near unity. Using unity for the cosine and $\pi/2 = 1.57$, Eqns. 7 and 8 can be combined to estimate the range of the maximum first story drift,

$$1.3\frac{d_{max}}{h} \pm 25\%. \tag{9}$$

For the example structure, d_{max} was been found to be 8.2 cm and the height of the building is given (CSMIP, 1995) as 149 ft. 8 in. Using these values in Eqn. 9 gives a maximum drift between 0.2 and 0.3 percent.

Although the value of maximum acceleration experienced by the structure was quite high, $0.541g$, the values of base shear, displacement and drift associated with the maximum response of the fundamental mode are sufficiently moderate that significant damage is deemed unlikely in this case.

ADDITIONAL METHODS OF ANALYSIS

The previous section shows that much can be learned very quickly from a single acceleration record and rudimentary knowledge of the structure. Naturally, if more is known about the structure, or if additional records are available in or near the structure, more detailed analyses can be done. Two case studies of reading and interpreting strong-motion records are presented, for example, in Housner and Jennings (1982). Although more involved than what was presented above, these studies are still sufficiently simple that they can be easily done and readily explained.

Advances in the capabilities of computers and developments in software make it possible to perform easily even more involved calculations, calculations that not so long ago were feasible only as research studies. With this in mind, the author notes that studies of the measured earthquake response of selected buildings would make excellent topics for Master's theses and senior projects and suggests to his academic colleagues that they take advantage of these opportunities. Not only would such studies provide valuable experiences for the students, but they would also help structural engineers assimilate the important information in the strong-motion data base.

IMPLICATIONS FOR EARTHQUAKE ENGINEERING PRACTICE

It is critical to realize that the earthquake records are telling us some very important things in a very direct way about what is actually happening to structures, independent of how the structures are designed, where the strength comes from, and whether the response is linear or nonlinear. The maximum base shear, for example, is dependent only on the acceleration profile in the structure at the time of maximum response. Similarly, the maximum displacement of the structure is determined by the acceleration record, even when the response is not sinusoidal. Even more information will be available in the future, when dense instrumental arrays in structures that are now in the planning stages produce records. Data from these arrays will greatly increase the

precision of calculations of structural response including interstory shears, interstory drifts and, in some cases, strains in structural members.

The 17-story building used as an example exhibited quite significant response, even though it was rather distant from the area of strongest shaking during the Northridge earthquake. Using the technique described above, the drifts and base shears in two buildings in the San Fernando Valley, one in Sherman Oaks and one in Tarzana, were calculated. These buildings were closer to the region of strongest shaking and showed periods of 3.1 and 2.5 seconds, drifts of 0.8 percent and 1.6 percent, and base shears of 8 percent and 17 percent, respectively. The drifts and base shears substantially exceed the design limits recommended, for example, by the latest SEAOC Blue Book (SEAOC, 1996). Nor were these structures in the area of strongest shaking, which is generally understood to be further to the north, where the motions may have been roughly twice as strong as they were in the southern part of the San Fernando Valley. Furthermore, earthquakes significantly larger than the Northridge earthquake have obviously occurred in California and are entirely possible in most of the urbanized regions of the state.

Such considerations and other recent studies (Hall et. al., 1996, Jennings, 1997) lead the author to conclude that structures that respond successfully to nearby major earthquakes (M=7 and above), will exhibit interstory drifts on the order of 3 percent, or more, and/or base shears of 30 to 40 percent of their weight, or more. Although one may disagree with the specifics of this assessment, it does seem that the records of earthquake response are showing us convincingly that the values of excitation and response formally considered in the building codes are distinctly less than what actually happens during major earthquakes. For comparison to the numbers discussed above, SEAOC (1966) gives a design base shear for a two second period building (zone 4, I=1, S=1.2) of between 3 and 9 percent, depending on the reduction factor, R_w, and an allowable drift of 0.4 percent (or $0.03/R_w$).

A difference between code design values and measured earthquake response of this magnitude--approaching a factor of ten--is not a tenable situation. As more records become available and understood, it seems inevitable that the process of earthquake resistant design will be increasingly, and quite appropriately, based more and more upon records and measured properties of materials, and less and less upon empiricism and qualitative assessments of earthquake performance. This process is well along now in the design of special structures.

We should work hard to speed this process of change and improvement of the building codes; not only is the appropriate level of public safety a concern, but pushing for betterment of governing codes is part of our professional responsibility. In addition, if we are proven slow in responding to the challenges of incorporating new information into earthquake resistant design practices, it will become increasingly difficult for structural engineering to attract its share of the brightest young people, given the opportunities in competing fields of technology.

REFERENCES

California Strong Motion Instrumentation Program (CSMIP) (1995). "Processed Data for Los Angeles - 17-Story Residential Building", Report OSMS 95-01D, California Department of Conservation, Division of Mines and Geology, Sacramento, California.

Jennings, P. C., "Earthquake Response of Tall Regular Buildings" (1997). Earthquake Engineering Research Laboratory Report 97-01, California Institute of Technology, Pasadena, California.

Hall, J. F., T. H. Heaton, M. W. Halling and D. J. Wald (1996). Near-Source Ground Motion and its Effects on Flexible Buildings, *Earthquake Spectra*, Vol. 11, No. 4, pp. 569-605.

Housner, G. W. and P. C. Jennings (1982). "*Earthquake Design Criteria*", Earthquake Engineering Research Institute, Berkeley, California.

Structural Engineers Association of California (SEAOC) Seismology Committee (1996). "Recommended Lateral Force Requirements and Commentary, Sixth Edition, Structural Engineers Association of California, Sacramento, California.

ENGINEERING CHARACTERISTICS OF NEAR FAULT GROUND MOTION

Paul Somerville
Woodward-Clyde, Pasadena, CA

ABSTRACT

This paper explains the effects of rupture directivity on near-fault ground motions, describes an empirical model of these effects, provides guidelines for the specification of response spectra and time histories to represent near-fault ground motions, and provides guidelines for the selection of time histories.

INTRODUCTION

An earthquake is a shear dislocation that begins at a point on a fault and spreads at a velocity that is almost as large as the shear wave velocity. The propagation of fault rupture toward a site at very high velocity causes most of the seismic energy from the rupture to arrive in a single large long period pulse of motion which occurs at the beginning of the record (Somerville and Graves, 1993). This pulse of motion, sometimes referred to as "fling," represents the cumulative effect of almost all of the seismic radiation from the fault. The radiation pattern of the shear dislocation on the fault causes this large pulse of motion to be oriented in the direction perpendicular to the fault, causing the strike-normal peak velocity to be larger than the strike-parallel peak velocity. The effect of forward rupture directivity on the response spectrum is to increase the level of the response spectrum of the horizontal component normal to the fault strike at periods longer than 0.5 seconds. This causes the peak response spectral acceleration of the strike-normal component to shift to longer periods, for example from 0.25 seconds to as much as 0.75 seconds. Near fault effects cannot be adequately described by uniform scaling of a fixed response spectral shape; the shape of the spectrum must become richer in long periods as the level of the spectrum increases. Figure 1 shows these effects of rupture directivity in the time history and response spectrum of the Rinaldi recording of the 1994 Northridge earthquake.

Forward rupture directivity effects occur when two conditions are met: the rupture front propagates toward the site, and the direction of slip on the fault is aligned with the site. The conditions for generating forward rupture directivity effects are readily met in strike-slip faulting, where the fault slip direction is oriented horizontally in the direction along the strike of the fault, and rupture propagates horizontally along strike either unilaterally or bilaterally. However, not all near-fault locations experience forward rupture directivity effects in a given event. Backward directivity effects, which occur when the rupture propagates away from the site, give rise to the opposite effect: long duration motions having low amplitudes at long periods. This is illustrated in Figure 2, which shows the directivity effect in strike-slip faulting using the strike-normal components of ground velocity from two near-fault recordings of the magnitude 7.3 Landers earthquake of 1992 (Wald and Heaton, 1994). The Lucerne record, which is located 1.1 km from the surface rupture and 45 km from the epicenter of the Landers earthquake, consists of a large, brief pulse of motion (due to forward directivity effects), while the Joshua Tree record, located near the epicenter, consists of a long duration, low amplitude record (due to backward directivity effects).

The conditions required for forward directivity are also met in dip slip faulting, including both reverse and normal faults. The alignment of both the rupture direction and the slip direction up the fault plane produces rupture directivity effects at sites located around the surface exposure of the fault (or its updip projection if it does not break the surface). Consequently, it is generally the case that all sites located near the surface exposure of a dip-slip-fault experience forward rupture directivity when an earthquake occurs on that fault. Unlike the case for strike-slip faulting, where we expect forward rupture directivity effects to be most concentrated away from the hypocenter, dip slip faulting produces directivity effects on the ground surface that are most concentrated updip from the hypocenter. Recordings of the 1994 Northridge earthquake from the northern margin of the San Fernando Valley, such as the one at Rinaldi shown in Figure 1, contain forward rupture directivity effects.

EMPIRICAL MODEL OF NEAR-FAULT GROUND MOTIONS

Somerville et al. (1997) used a large set of near fault strong motion recordings to develop a quantitative model of rupture directivity effects. This model can be used to modify existing ground motion attenuation relations to incorporate directivity effects in ground motions used for seismic design. The ground motion parameters that are modified for directivity effects include the average horizontal response spectral acceleration; the average duration of the two horizontal acceleration time histories; and the ratio of strike normal to strike parallel spectral acceleration. *Strike-normal* refers to the horizontal component of motion *normal* to the strike of the fault. *Strike-parallel* refers to the horizontal component of motion *parallel* to the strike of the fault. Following the method of Husid (1969), duration is defined as the time between 5% and 75% of the cumulative squared acceleration, following the convention of Abrahamson and Silva (1997b).

In this model, amplitude variations due to rupture directivity depend on two geometrical parameters. First, the smaller the angle between the direction of rupture propagation and the direction of waves travelling from the fault to the site, the larger the amplitude. Second, the larger the fraction of the fault rupture surface that lies between the hypocenter and the site, the larger the amplitude. The duration of strong motion is modeled using the same two parameters, with an inverse relationship between duration and amplitude. The azimuth and zenith angles and length and width ratios are illustrated for strike-slip and dip-slip faulting in Figure 3. For strike-slip faults, the angle θ and length ratio X are measured from the epicenter to the site in the horizontal plane. For dip-slip faults, the angle ϕ and width ratio Y are measured from the hypocenter to the site in the vertical plane oriented normal to the fault.

The effects of rupture directivity on ground motion amplitudes and duration are modeled using the function X cos θ for strike-slip faults and Y cos ϕ for dip-slip faults. For strike-slip faults, the variation of ground motion parameters with θ is independent of the distance from the rupture, r_{rup}. However, between the ends of a dip-slip fault, the variation of ground motion parameters with ϕ is indistinguishable from its variation with rupture distance r_{rup}. Since rupture distance is a primary ground motion parameter already included in attenuation relations, we find more spatial variability of strike-slip motions with cos θ than of dip-slip motions with cos ϕ. The strike normal to strike parallel ratio was modeled using a cos 2ξ dependence of the strike normal to strike parallel ratio, where ξ is θ for strike-slip and ϕ for dip-slip in the range of 0 to 45 degrees.

The dependence of the spectral amplification factor on X cos θ for strike-slip faulting and Y cos ϕ for dip-slip faulting is shown in Figure 4a. These effects begin at 0.6 seconds period

and increase with period. For strike-slip faulting, maximum directivity conditions (X cos θ = 1) cause an amplitude about 1.8 times larger than average at 2 seconds period, while minimum directivity effects cause an amplitude about 0.6 times average. In the model for dip-slip faulting, which excludes sites off the ends of the fault as shown in Figure 3, the effects lie in the range of about 1.2 to 0.8.

The dependence of the duration factor on X cos θ for strike-slip faulting and on Y cos ϕ for dip-slip faulting is shown in Figure 4b. As expected, there is an inverse correlation between duration residuals and amplitude residuals. For maximum directivity conditions (X cos θ or Y cos ϕ = 1), the duration is about 0.55 times the average duration for both strike-slip and dip-slip faulting. For minimum directivity conditions, the ground motion durations are 2.1 and 1.6 times longer than average for dip-slip and strike-slip faulting respectively.

The model of the strike-normal to average horizontal ratio, which is independent of faulting mechanism, is displayed in Figure 5. The top part of the figure shows the period dependence of the ratio for various magnitudes and distances, and the bottom part of the figure shows the distance dependence of the ratio for various magnitudes and periods, averaged over all values of the angles θ and ϕ. The strike-normal motion is obtained by multiplying the attenuation relation value by the strike-normal to average horizontal ratio, and the strike-parallel motion is obtained by dividing the attenuation relation value by this ratio. The bottom right part of the figure shows the dependence of the ratio on θ or ϕ for M = 7 and r_{rup} = 5 as a function of period. The period dependence of the ratio indicates a transition, at a period of about 0.6 seconds, from coherent source radiation and wave propagation conditions at long periods to incoherent source radiation and wave propagation conditions at short periods.

SPECIFICATION OF RESPONSE SPECTRA FOR NEAR-FAULT GROUND MOTIONS

Scenario Earthquake Approach

The ground motions used in the design or evaluation of a structure are usually specified in the form of a response spectrum or set of response spectra. In some instances, the response spectrum may represent a specified earthquake magnitude and distance. In California, seismic design criteria for dams and bridges are specified in whole or in part in this way. Until recently, the state of practice was to assume that near-fault effects are adequately represented in empirical ground motion models that are used to estimate the response spectrum for the specified magnitude and distance. The ground motions predicted by these empirical models represent the average of all rupture directivity conditions: forward, backward and neutral. However, ground motions influenced by forward rupture directivity are much larger than those for average rupture directivity for periods longer than 0.5 seconds. Since forward directivity has a high likelihood of occurring at any near-fault site, it may be appropriate to include forward rupture directivity as a criterion for the development of ground motions for the maximum credible event. The common practice of using the 84th percentile ground motion instead of the mean may in part accomplish this objective.

During the past 5 years, response spectra for the design of retrofits of Caltrans toll bridges have contained modifications of these empirical models to incorporate near-fault effects. These modifications consist of increasing the response spectrum level of the average horizontal component of ground motion at periods longer than 1 second, and specifying separate response spectra for the strike-normal and strike-parallel components of motion, using models such as that

described by Somerville et al. (1995). These modifications provide a response spectrum that is more nearly representative of forward rupture directivity effects. To date, Caltrans is the only organization that has adopted the use of different response spectra in the strike-normal and strike-parallel directions.

Modifications to the response spectral level have been included in the SEAOC Strength Code Change (SEAOC, 1996) in the form of the near source factor N. This factor modifies the basic response spectrum using factors N_a and N_v that depend on the distance to the fault, the slip rate of the fault, and the maximum magnitude that the fault can generate. At distances close to major active faults in California, the design values ("maximum considered") ground motion map in the 1997 NEHRP provisions (Building Seismic Safety Council, 1996) was also developed using near-fault factors applied to a standard seismic zone 4 response spectrum.

In Figure 6 we compare response spectra for the same earthquake (magnitude 7 strike-slip, distance 5 km, stiff soil conditions) but two different rupture directivity conditions. The spectra at the top are for average rupture directivity conditions (sites located randomly around the fault), while the spectra at the bottom are for forward rupture directivity conditions (where rupture propagates towards the site). In each case, we show the strike-normal, strike-parallel, and average horizontal response spectra based on the model of Somerville (1996). For comparison, we show proposed 1997 SEAOC code spectra including the near-fault factor for the appropriate source category (B) and site category (S_D). We use the "design basis" spectrum for comparison with average rupture directivity conditions, and the "maximum capable" spectrum from the base isolation part of the code (a factor of 1.25 higher) for comparison with forward rupture directivity conditions. The modifications for rupture directivity effects in Somerville (1996) are based not on the general model described above, but on a model derived from ten recordings at close distances to the 1989 Loma Prieta, 1994 Northridge, and 1995 Kobe earthquakes. This model has larger modifications than the general model for periods between 0.5 and 2.0 seconds.

The model for average directivity conditions shown at the top of Figure 6 does not change the average horizontal spectrum given by the empirical model (Abrahamson and Silva, 1997), but gives a strike-normal component that is larger and a strike-parallel component that is smaller. The model for forward directivity conditions, shown at the bottom of Figure 6, not only has a larger difference between these two components, but also increases the average horizontal component above that given by the empirical attenuation relation. The combination of these two modifications for forward directivity conditions results in the strike normal motion being about 2 times higher than the average given by the empirical attenuation relation for periods longer than about 0.5 second, and the strike parallel motion being about the same as the average given by the empirical attenuation relation.

Comparing the response spectral models at the top and bottom of Figure 6, we see that the most important effect of forward rupture directivity on the response spectrum is to increase the level of the response spectrum at periods longer than 0.5 seconds. This is manifested in a shift in the peak of response spectral acceleration from 0.3 seconds (which is also the peak for the strike parallel component) to 0.5 seconds for the average of the horizontal components and to 0.75 for the strike normal component. This indicates that near fault effects cannot be adequately described by uniform scaling of a fixed response spectral shape; the shape of the spectrum must become richer in long periods as the level of the spectrum increases. This has been implemented in the proposed 1997 SEAOC code change by using separate near-fault factors N_a and N_v for the acceleration and velocity parts of the code response spectrum.

The "design basis" spectrum at the top of Figure 6 envelopes both the strike-normal and strike-parallel components of motion for average directivity. However, the "maximum capable" spectrum at the bottom of Figure 6 lies below the strike-normal component for forward rupture directivity. Should engineers be concerned about the possibility of the strike-normal component exceeding the design criterion? There are two reasons for thinking that the answer is yes. First, recent destructive earthquakes have shown evidence of near-fault damage occurring in preferred directions that correspond to the strike-normal direction (north-south in the 1994 Northridge earthquake; northwest-southeast in the 1995 Kobe earthquake). Second, the difference between strike-normal and average motions is statistically significant close to large earthquakes. For example, in the case shown in the lower part of Figure 6, (forward rupture directivity at a distance of 5 km from a magnitude 7 earthquake), the strike-normal component is a factor of 1.4 times larger than the average horizontal component at long periods, with a standard error of a factor of 1.28.

In Figure 7, we compare the near-fault spectra for average (top) and forward (bottom) directivity conditions with the ground motion model of Abrahamson and Silva (1997) from which they were modified. For periods longer than about 0.75 second, the strike normal component for forward rupture directivity is about 25% larger than the 84th percentile ground motion for the average of the two horizontal components for average rupture directivity conditions, as given by the Abrahamson and Silva (1995) model. This indicates that use of the 84th percentile may partly if not completely accommodate the ground motion level in the strike normal direction for forward rupture directivity conditions.

Since fault strike is usually well known close to major faults, it is straighforward to take the difference between the strike normal and strike parallel components of motion into account in the evaluation of near-fault ground motions, especially for base isolated buildings, bridges, dams, and other structures that are particularly sensitive to long-period ground motions. Consideration of these differences may be especially important for the retrofit of existing structures near active faults (e.g. Salah-Mars et al., 1994). For new structures, the stronger ground motion in the strike normal direction could be accommodated by orienting the structure with its long axis normal to the fault, as shown in Figure 8. The implications of the orientation of dams with respect to fault-controlled valleys and range fronts for the specification of design ground motions have been described by Somerville and Graves (1996). Even if the specific location and orientation of faults is not known, there may be a high enough level of certainty in the strike of faults in a region (for example, of blind thrust faults in the Los Angeles basin) to warrant consideration of larger strike-normal ground motions.

Probabilistic Approach

In many instances, the response spectrum is defined probabilistically as that having a specified annual probability of exceedance. A probabilistic response spectrum contains contributions from the entire range of magnitude-distance pairs that affect the site. This is the approach that is used to generate response spectra using the site-specific method prescribed by the UBC. It is also the approach used by the USGS to generate the National Seismic Hazard Maps. The "maximum capable" ground motion used in the base isolation code is associated with a specified probability of occurrence (10% in 100 years), and ground motion criteria for bridges and dams are also informally associated with annual probabilities of occurrence.

The current state of practice in the development of probabilistic response spectra is to assume that near-fault effects are adequately represented in the empirical ground motion models that are used to estimate the response spectrum for the specified magnitude and distance. However, the means now exist to incorporate near-fault effects in a more specific way by using the empirical model of Somerville et al. (1997) which is summarized in Figures 4 and 5. This model can be implemented by randomizing the location of the hypocenter on the fault planes of earthquakes having magnitudes larger than 6. The model has not yet been implemented in a probabilistic seismic hazard analysis. However, the main anticipated effect is a larger strike-normal response spectrum and a smaller strike-parallel response spectrum than the average horizontal spectrum estimated by current methods. At low probabilities, there may also be some increase in the average response spectrum due to the larger variability in ground motions predicted by the model.

SPECIFICATION OF TIME HISTORIES FOR NEAR-FAULT GROUND MOTIONS

Design and analysis of large structures is often done using time histories that are representative of the design response spectrum. The time histories, which may be from recorded earthquakes or from strong motion simulations of the kind described below, are sometimes spectrally matched to a design response spectrum. The modifications that we have developed to incorporate rupture directivity effects in the response spectrum are not sufficient to ensure the appropriate incorporation of rupture directivity effects in time histories that are matched to these spectra. This is because the forward rupture directivity effect is manifested in the time domain by a large pulse of long period ground motion, and the spectral matching process cannot build a rupture directivity pulse into a record where none is present to begin with. Forward rupture directivity effects are present in some but not all near-fault strong motion recordings. Since the response spectrum developed for design or evaluation of a near-fault site will be influenced by forward rupture directivity effects at most sites, it is important to select an appropriate proportion of time histories that include forward rupture directivity effects if time histories are being used to represent the response spectrum.

Orientation of Time Histories

If it is desired to fully represent near-fault conditions in the time histories, then it is necessary to initially specify the strike-normal and strike-parallel components of the time histories. If the axis of the structure is aligned at some angle θ to the strike of the fault, then the longitudinal and transverse time histories should then be derived from the strike-normal (SN) and strike-parallel (SP) time histories using the following equation:

$$\text{long} = SP \cos\theta + SN \sin\theta$$
$$\text{trans} = SP \sin\theta - SN \cos\theta$$

In Figure 8a, we schematically illustrate the recording of strong motion near fault A on the north and east components, the rotation of the north and east to strike-normal and strike-parallel, the transposition of the strike-normal and strike-parallel components to the structure site near fault B, and the rotation of the strike-normal and strike-parallel components into longitudinal and transverse components at the structure site. To avoid the first rotation step, we should archive near-fault strong motion recordings and simulations in their strike-normal and strike-parallel components.

Although near-fault ground displacements contain permanent displacements due to the static displacement field of the earthquake, analog systems traditionally used to record strong motion do not retain these displacements, and in any case they are removed by highpass filtering in traditional processing methods. However, in some cases the permanent ground displacements may be significant for design, and in these cases it is important to specify the correct orientation of the static and dynamic ground displacements. In Figure 8b, we show the sense of motion of the permanent ground displacement near left-lateral and right-lateral unilateral strike-slip faults for rupture propagation in either direction (that is, for epicenters at either end of the fault). The sense of strike normal displacement is continuous across the fault, whereas the sense of strike parallel displacement is discontinuous across the fault (reflecting the displacement on the fault). For a given sense of slip (e.g. strike-slip), the polarity of the strike parallel displacement is the same for rupture in either direction, but the polarity of the strike normal displacement is opposite for rupture in opposite directions. Current building codes assume that the two horizontal components are uncorrelated, and prescribe interchanging the two horizontal components in structural analyses. This is clearly inappropriate for near-fault ground motions, in which there are systematic differences between the strike-normal and strike-parallel components. Interchanging the components can represent physically unrealizable scenarios given the known orientation of the fault.

Scenario Earthquake Approach

If the response spectrum is derived from a scenario earthquake, then the magnitude and distance of the earthquake are specified, and time histories representative of that magnitude and distance need to be selected. If the response spectrum is based on the median level ground motion, then it represents average directivity conditions, and it is appropriate to select time histories that span a range of directivity conditions. However, if the response spectrum is based on the mean plus one standard deviation ground motion level, then it represents forward directivity conditions, and most if not all of the time histories should be for forward rupture directivity conditions. As described in Figure 7, the strike normal ground motion level for forward rupture directivity conditions is about as large as or larger than the 84th percentile response spectrum for average directivity conditions.

With the exception of Caltrans toll bridges noted above, design or analysis response spectra apply to the average of the two horizontal components of ground motion. When scaling a time history to match this spectrum, a scaling factor should be found that matches the average of the two horizontal components of the time history to the design spectrum. This factor should then be applied to each of the two horizontal components in order to leave unchanged the ratio between the two horizontal components. In the case when the response spectra of the strike-normal and strike-parallel components of motion are separately specified (e.g. for Caltrans toll bridges), then the time histories can be scaled separately to these response spectra.

Probabilistic Approach

A probabilistic seismic hazard analysis (PSHA) takes into account the ground motions from the full range of earthquake magnitudes that can occur on each fault or source zone that can affect the site. The time histories that are selected must represent the dominant combinations of magnitude, distance and ϵ that contribute to the response spectrum. The parameter ϵ is defined as the number of standard deviations above or below the median ground motion level for that magnitude and distance that is required to match the probabilistic spectrum. The magnitude,

distance and ϵ combinations are identified through deaggregation of the seismic hazard (McGuire, 1995; Silva and Toro, 1996).

If the probabilistic seismic hazard analysis were to include the near-fault modifications for rupture directivity effects described above, then the deaggregation could include values of the directivity function X cos θ for strike-slip faults and Y cos ϕ for dip-slip faults, and the directivity content of time histories could be selected based on the predominant value of the directivity function. Otherwise, some estimate of the appropriate directivity content of the time histories can be obtained from the parameter ϵ defined above. If the predominant value of ϵ is near zero, then the response spectrum approximately represents average directivity conditions, and it is appropriate to select time histories that span a range of directivity conditions. However, if the predominant value of ϵ is one, then the response spectrum is at the mean plus one standard deviation ground motion level for that event, representing forward directivity conditions, and most if not all of the time histories should be for forward rupture directivity conditions. In the deaggregation of seismic hazard at 10% probability of exceedance in 50 years in Los Angeles and San Francisco, Silva and Toro (1996) found that the ϵ value was approximately one on average for the predominant contribution to the hazard. This indicates the need to select time histories having predominantly forward rupture directivity conditions in order to represent the 10% in 50 year ground motions in Los Angeles and San Francisco.

SELECTION OF TIME HISTORIES FOR NEAR-FAULT GROUND MOTIONS

If time histories are used in conjunction with the response spectrum, it is important to select time histories which appropriately include rupture directivity effects because the spectral matching process cannot build a rupture directivity pulse into a record where none is present to begin with. As a guide to the selection of time histories for use in design and evaluation of structures that are sensitive to long-period ground motions, we have listed a set of near-fault strong motion recordings and indicated the nature of the rupture directivity effects that they contain. The catalog of records given in Table 1 includes those whose closest distance to the fault rupture is 10 km or less in the data set that was used by Somerville et al. (1995, 1997) to develop an empirical model of directivity effects on strong ground motions. The influence of rupture directivity effects on each record is indicated, based on the geometrical relationships between the recording site, the fault rupture, the epicenter, and the direction of slip on the fault. The table lists the peak horizontal accelerations and velocities of the records in the strike normal and strike parallel directions. This table can complement the extensive classification and evaluation of earthquake records using a range of ground motion parameters provided by Naeim and Anderson (1993; 1996).

The recorded time histories listed in Table 1 include a limited number of recordings at close distances to large earthquakes. Broadband simulation techniques which have been validated against recorded strong ground motions can be used to generate time histories for large magnitudes and close distances. For example, broadband time histories for hypothesized magnitude 7 earthquakes on the Elysian Park thrust beneath downtown Los Angeles (Somerville et al., 1995), and on the predominantly strike-slip Palos Verdes fault in the Long Beach area, were used by Somerville, Smith and Sun (1997) to complement recorded ground motions in a set of near fault recordings for use in Phase 2 of the SAC Steel Project. Both the recorded and simulated near-fault time histories can be accessed by anonymous ftp to "ftp.csn.net" in the directory wwclyde/SAC2, file NearFault. They are rotated into strike-normal and strike-parallel components.

We conclude this paper with some specific guidelines for the selection of appropriate time histories for the representation of near-fault rupture directivity effects.

Forward Rupture Directivity

Forward directivity occurs when the rupture propagates toward the site and the direction of slip on the fault is also toward the site. Most near-fault strike-slip recordings, and all near-fault reverse fault recordings, are influenced by forward directivity. Backward directivity occurs when the rupture propagates away from the site. Recordings near the epicenters of strike-slip earthquakes, a relatively small group, fall in the backward directivity category. None of the reverse faults in our data set ruptured in the downdip direction away from surface stations, so none have backward directivity. Recordings that do not clearly belong in either of these categories are grouped in a neutral category. This category includes sites located fairly close to the epicenters of strike-slip earthquakes, and sites located off the end of the updip projection of reverse faults.

Recordings Close to Epicenters

It is a common fallacy to assume that recordings close to the epicenters of strike-slip and oblique-slip earthquakes (such as Bond's Corner, 1971 Imperial Valley earthquake; Corralitos, 1987 Loma Prieta earthquake; and Joshua Tree, 1992 Landers earthquake) contain forward rupture directivity effects. On the contrary, these records contain neutral or backward directivity effects, produced when the rupture propagates away from the site, and are characterized by relatively low amplitudes of long period ground motions. Also, strong motion recordings above shallow thrust faults, such as the Cape Mendocino and Petrolia recordings of the 1992 Cape Mendocino earthquake, do not contain rupture directivity effects. The effects of rupture directivity are primarily manifested at the longer periods, so that large peak accelerations in near-fault recordings do not necessarily imply large long period ground motions.

Faulting Mechanism

If the seismic hazard at a site is dominated by a particular style of faulting of faulting mechanism (e.g. strike-slip or reverse), it is preferable to use time histories from that style of faulting. In the recorded data analyzed by Somerville et al. (1997), it was found that the relation between strike-normal and strike-parallel ground motions is similar for strike-slip and reverse earthquakes. However, differences between strike-slip and reverse faulting were found in the azimuthal variation of duration and response spectral amplification. Also, for larger earthquakes, there may be differences between strike-slip and reverse ground motions because the rupture directivity effect in reverse faulting builds up over a limited fault width, whereas for strike-slip faulting it can build up over a much larger fault length.

Duration

It is a common fallacy to assume that near-fault ground motion time histories close to large earthquakes should have a long duration. As shown in Figure 4b, the stronger the near-fault directivity effect, the shorter the duration. This is because the forward directivity effect causes nearly all of the seismic radation from the fault to arrive in a single brief pulse of motion. It does not make sense to sequentially combine several near-fault records containing brief pulses to make up for the short duration that is characteristic of forward rupture directivity effects.

REFERENCES

Abrahamson. N.A. and W.J. Silva (1997). Empirical response spectral attenuation relations for shallow crustal earthquakes, *Seismological Research Letters* 68, 94-127.

McGuire, R.K. (1995). Probabilistic seismic hazard analysis and design earthquakes: closing the loop. *Bull. Seism. Soc. Am.* 86, 1275-1284.

Naeim, F. (1995). On seismic design implications of the 1994 Northridge earthquake records, *Earthquake Spectra* 11, 91-110.

Naeim, F. and J.C. Anderson (1993). Classification and evaluation of earthquake records for design, *Earthquake Engineering Research Institute*, 287 pp.

Naeim, F. and J.C. Anderson (1996). Design Classification of Horizontal and Vertical Earthquake Ground Motion, *Report to the U.S. Geological Survey by John. A. Martin & Associates, Inc.., JAMA Report No. 7738.68-96, 427 pp.*

Salah-Mars, S., L.H. Mejia, P.G. Somerville, R.K. Green, R.O. Hamburger, and C.A. Cole (1994). Ground motions for base isolation seismic retrofit of a building near the Hayward fault, *Proceedings of the 5th U.S. National Conference on Earthquake Engineering,* Chicago, July 1994.

Silva, W. and G. Toro (1996). Verification of response spectral shapes and anchor points for different site categories for building design codes. SMIP96 Seminar on Seismological and Engineering Implications of Recent Strong Motion Data, p. 37-51.

Somerville, P.G., N.F. Smith, R.W. Graves, and N.A. Abrahamson (1997). Modification of empirical strong ground motion attenuation relations to include the amplitude and duration effects of rupture directivity, *Seismological Research Letters* 68, 199-222.

Somerville, P.G. (1996). Strong ground motions of the Kobe, Japan earthquake of Jan. 17, 1995, and development of a model of forward rupture directivity effects applicable in California. *Proceedings of the Western Regional Technical Seminar on Earthquake Engineering for Dams,* Association of State Dam Safety Officials, Sacramento, April 11-12, 1996.

Somerville, P.G., N.F. Smith, R.W. Graves, and N.A. Abrahamson (1995a). Representation of near-fault rupture directivity effects in design ground motions, and application to Caltrans bridges. *Proceedings of the National Seismic Conference on Bridges and Highways,* San Diego, December 10-13, 1995.

Somerville, P.G., R.W. Graves, and C.K. Saikia (1995b). Characterization of Ground Motions During the Northridge Earthquake of January 17, 1994. Report No. SAC 95-03 of the SAC Joint Venture.

Somerville, Smith and Sun (1997). Suites of ground motion time histories developed for Phase 2 of the SAC Steel Project. Unpublished draft report.

Table 1. Description of Rupture Directivity Effects in Near-Fault Strong Motion Recordings
(See Table 8 of Somerville et al., 1997 for a listing that includes directivity parameters X and θ for strike-slip faults, and ϕ and Y for dip-slip faults, in place of the general directivity descriptor [forward, neutral, backward] provided in this table).

EQK DATE	STAT. NO.	STATION	CLOSEST DISTANCE (km)	SITE CODE[1]	PEAK HORIZONTAL ACCEL (g)		PEAK HORIZONTAL VEL (cm/s)		DIRECTIVITY[3]
					FN[2]	FP[2]	FN[2]	FP[2]	
400519	117	IMPERIAL VAL IRRIG. DIST, EL CENTRO	10.0	SL	0.21	0.32	32.2	60.1	B
660627	014	CHOLAME, SHANDON, CA ARY 5	3.7	SL	0.33	0.36	26.1	23.6	F
660627	015	CHOLAME, SHANDON, CA ARY 8	8.0	SL	0.24	0.28	11.7	12.2	F
660627	097	TEMBLOR, CA, STATION 2	4.4	HR	0.36	0.25	23.5	12.6	F
671210	9001	KOYNA DAM	3.0	HR	0.51	0.45	32.9	21.9	B
710209	24207	PACOIMA DAM	3.3	HR	1.17	1.08	114.9	59.3	F
760517	9201	KARAKYR POINT, USSR	3.0	SR	0.65	0.67	63.7	59.8	N
780916	9101	TABAS	1.2	SR	0.90	0.98	110.2	106.7	N
791015	6616	AEROPUERTO MEXICALI	0.4	SL	0.28	0.36	27.1	42.7	B
791015	6618	AGRARIAS	0.8	SL	0.24	0.36	38.7	39.7	B
791015	955	EL CENTRO ARY 4, ANDERSON ROAD	7.1	SL	0.36	0.49	77.7	38.0	F
791015	952	EL CENTRO ARY 5, JAMES ROAD	4.1	SL	0.37	0.53	88.1	43.8	F
791015	942	EL CENTRO ARY 6, HUSTON ROAD	1.2	SL	0.43	0.35	106.2	62.9	F
791015	5028	EL CENTRO ARY 7, IMPERIAL VAL COLL.	0.2	SL	0.46	0.33	106.4	44.7	F
791015	958	EL CENTRO ARY 8, CRUICKSHANK RD	3.8	SL	0.47	0.61	50.1	52.7	F
791015	412	EL CENTRO ARY 10, HOSPITAL	9.0	SL	0.18	0.23	44.9	39.9	F
791015	5054	BONDS CORNER, EL CENTRO	2.4	SL	0.79	0.59	48.6	43.8	B
791015	5053	FIRE STATION, CALEXICO	10.1	SL	0.26	0.21	18.3	15.4	N
791015	6619	MEXICALI CASA FLORES	9.7	SL	0.23	0.43	19.3	28.8	B
791015	6622	COMPUERTAS	4.5	SL	0.15	0.15	9.7	13.7	B
791015	9301	EL CENTRO DIFFERENTIAL ARRAY 1	5.5	SL	0.73	0.74	119.8	111.8	F
791015	9302	EL CENTRO DIFFERENTIAL ARRAY 2	5.5	SL	0.62	0.77	121.6	110.4	F
791015	9304	EL CENTRO DIFFERENTIAL ARRAY 3	5.4	SL	0.61	0.68	120.8	109.5	F
791015	9305	EL CENTRO DIFFERENTIAL ARRAY 4	5.2	SL	0.83	0.73	117.9	104.4	F
791015	9306	EL CENTRO DIFFERENTIAL ARRAY 5	5.1	SL	1.19	2.07	131.4	135.7	F
791015	5165	DIFFERENTIAL ARRAY-DOGWOOD ROAD	5.2	SL	0.41	0.45	56.0	49.3	F
791015	5055	POST OFFICE, HOLTVILLE	7.5	SL	0.27	0.23	50.3	42.7	N
791015	335	IMPERIAL COUNTY FF	7.4	SL	0.18	0.22	52.1	41.3	F
840424	1652	ANDERSON DAM, DOWNSTREAM	4.5	SL	0.44	0.28	27.0	28.9	F
840424	57217	COYOTE LAKE DAM, SAN MARTIN	0.01	SR	0.85	0.93	66.5	68.3	F
840424	57191	HALLS VALLEY	2.5	SL	0.31	0.16	39.0	14.2	B
851223	6097	IVERSON, NW TERRITORIES (STA 1)	9.6	HR	1.24	1.20	45.3	44.1	N
851223	6098	SLIDE MOUNTAIN (STA 2)	6.1	HR	0.40	0.42	27.0	37.6	N

[1]HR-HARD ROCK; SR SEDIMENTARY AND CONGLOMERATED ROCK; SL-SOIL AND ALLUVIUM
[2]FN-FAULT NORMAL; FP-FAULT PARALLEL
[3]F-FORWARD; N-NEUTRAL; B-BACKWARD

Table 1 (cont.). Description of Rupture Directivity Effects in Near-Fault Strong Motion Recordings
(See Table 8 of Somerville et al., 1997 for a listing that includes directivity parameters X and θ for strike-slip faults, and ϕ and Y for dip-slip faults, in place of the general directivity descriptor [forward, neutral, backward] provided in this table).

EQK DATE	STAT. NO.	STATION	CLOSEST DISTANCE (km)	SITE CODE[1]	PEAK HORIZONTAL ACCEL (g)		PEAK HORIZONTAL VEL (cm/s)		DIRECTIVITY[3]
					FN[2]	FP[2]	FN[2]	FP[2]	
851223	6098	SLIDE MOUNTAIN (STA 2)	6.1	HR	0.40	0.42	27.0	37.6	N
860708	5073	CABAZON - POST OFFICE	8.4	SL	0.23	0.20	6.9	16.2	F
860708	12149	DESERT HOT SPRINGS	6.7	SL	0.34	0.29	29.7	22.9	N
860708	5997	DEVERS HILL SUBSTATION	4.1	SL	1.10	0.42	90.0	14.7	F
860708	5070	NORTH PALM SPRINGS POST OFFICE	4.0	SL	0.71	0.60	67.8	32.9	F
860708	12025	PALM SPRINGS AIRPORT	9.6	SL	0.16	0.15	14.7	10.3	F
860708	5072	WHITEWATER CANYON TROUT FARM	5.9	SL	0.50	0.58	39.6	29.9	F
891017	57007	CORRALITOS	3.4	SR	0.47	0.51	45.7	43.9	B
891017	47006	GAVILAN COLLEGE PHYS. SCI. BLDG.	9.5	SL	0.30	0.39	31.9	27.6	N
891017	47379	GILROY #1 - GAVILAN WATER TOWER	9.2	SR	0.42	0.41	39.5	29.8	N
891017	57180	LEXINGTON DAM - LEFT ABUTMENT	6.3	SR	0.45	0.39	118.0	45.6	F
891017		LOS GATOS PRESENTATION CNTR	3.5	HR	0.66	0.44	105.5	57.4	F
891017	58065	SARATOGA - ALOHA AVENUE	8.3	SL	0.37	0.35	57.0	44.8	F
920313	9401	ERZINCAN, TURKEY	2.0	SL	0.43	0.46	120.2	65.4	F
920628	22170	JOSHUA TREE - FIRE STATION	7.4	SL	0.28	0.19	42.7	30.0	B
920628		LUCERNE VALLEY	1.1	SL	0.76	0.73	127.5	95.3	F
940117	655	JENSEN FILTRATION PLANT	6.5	SL	0.38	0.62	45.4	100.1	F
940117	24088	PACOIMA; KAGEL CANYON	8.0	HR	0.53	0.24	55.5	36.8	N
940117	24279	NEWHALL; LA COUNTY FIRE STATION	6.7	SL	0.72	0.65	118.2	49.3	F
940117	24087	ARLETA; NORDHOFF FIRE STATION	9.5	SL	0.24	0.33	26.0	31.4	N
940117	24207	PACOIMA DAM - DOWNSTREAM	7.6	HR	0.50	0.24	48.5	18.9	F
940117	5968	RINALDI RECEIVING STATION - FF	7.5	SL	0.89	0.39	178.4	67.5	F
940117	306	SYLMAR CONVERTER STATION - FF	6.4	SL	0.59	0.80	130.1	89.3	F
940117	6273	SYLMAR CONVERTER STATION E - FF	6.2	SL	0.84	0.49	116.3	75.8	F
940117	637	SEPULVEDA VA HOSPITAL	9.3	SL	0.73	0.79	48.7	76.0	F
940117	24514	SYLMAR; OLIVE VIEW FF	6.2	SL	0.73	0.59	122.2	54.3	F
950117		KOBE UNIVERSITY (CEORKA)	3.8	RK	0.33	0.26	49.1	38.8	F
950117		KOBE (CEORKA)	6.2	SL	0.67	0.54	56.4	38.2	F
950117		KOBE (JMA)	3.4	SL	0.86	0.52	104.3	51.9	F
950117		KOBE PORT ISLAND, SURFACE	6.6	SL	0.43	0.14	95.9	30.3	F
950117		TAKATORI (JR)	4.3	SL	0.81	0.42	174.9	62.7	F

[1]HR-HARD ROCK; SR-SEDIMENTARY AND CONGLOMERATE ROCK; SL-SOIL AND ALLUVIUM
[2]FN-FAULT NORMAL; FP-FAULT PARALLEL
[3]F-FORWARD; N-NEUTRAL; B-BACKWARD

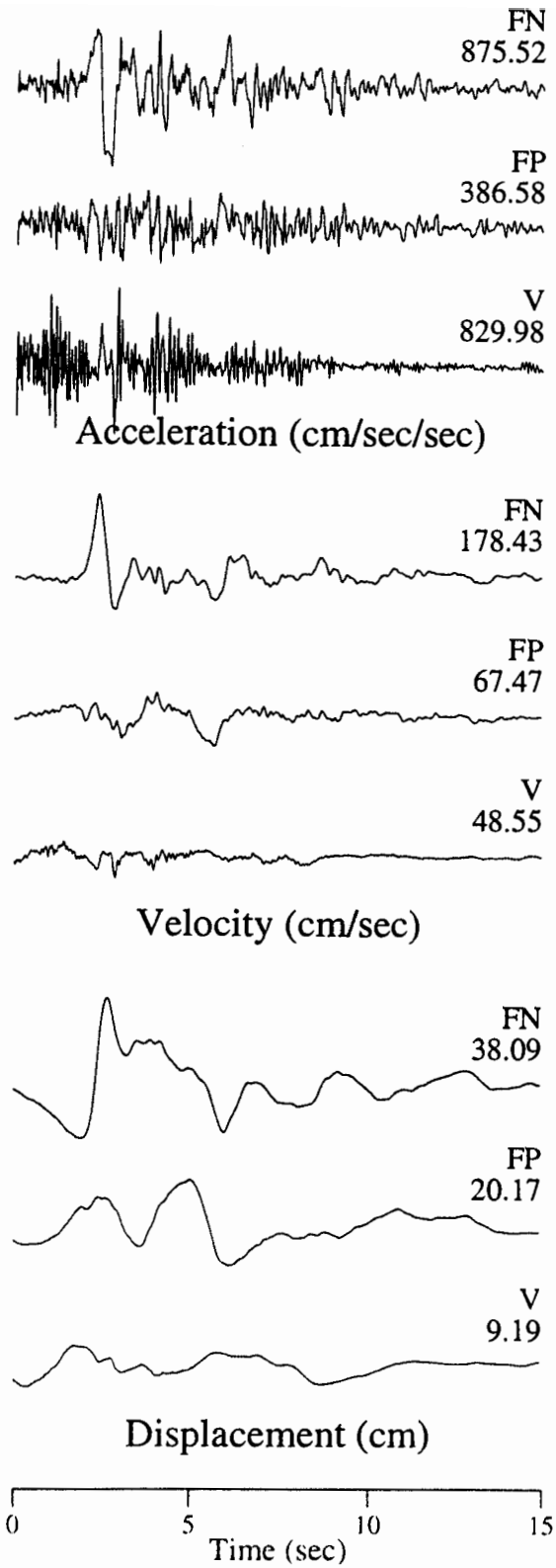

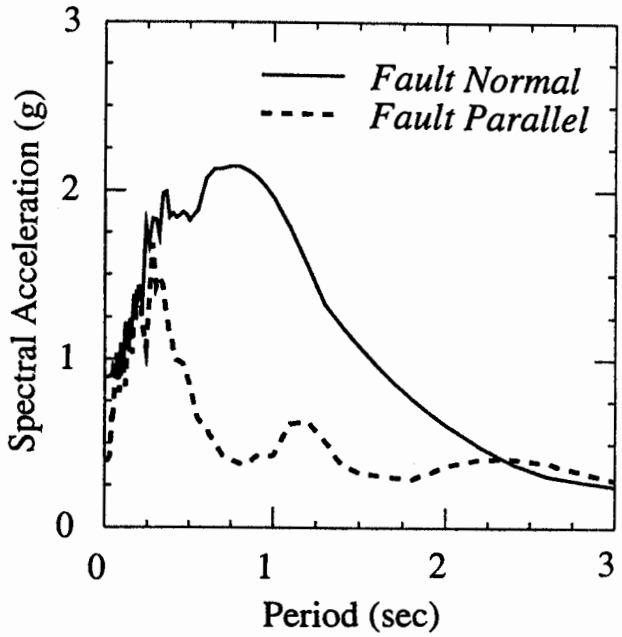

Figure 1. Acceleration and velocity time histories for the strike-normal and strike-parallel horizontal components of ground motion, and their 5% damped response spectra, recorded at Rinaldi during the 1994 Northridge earthquake.

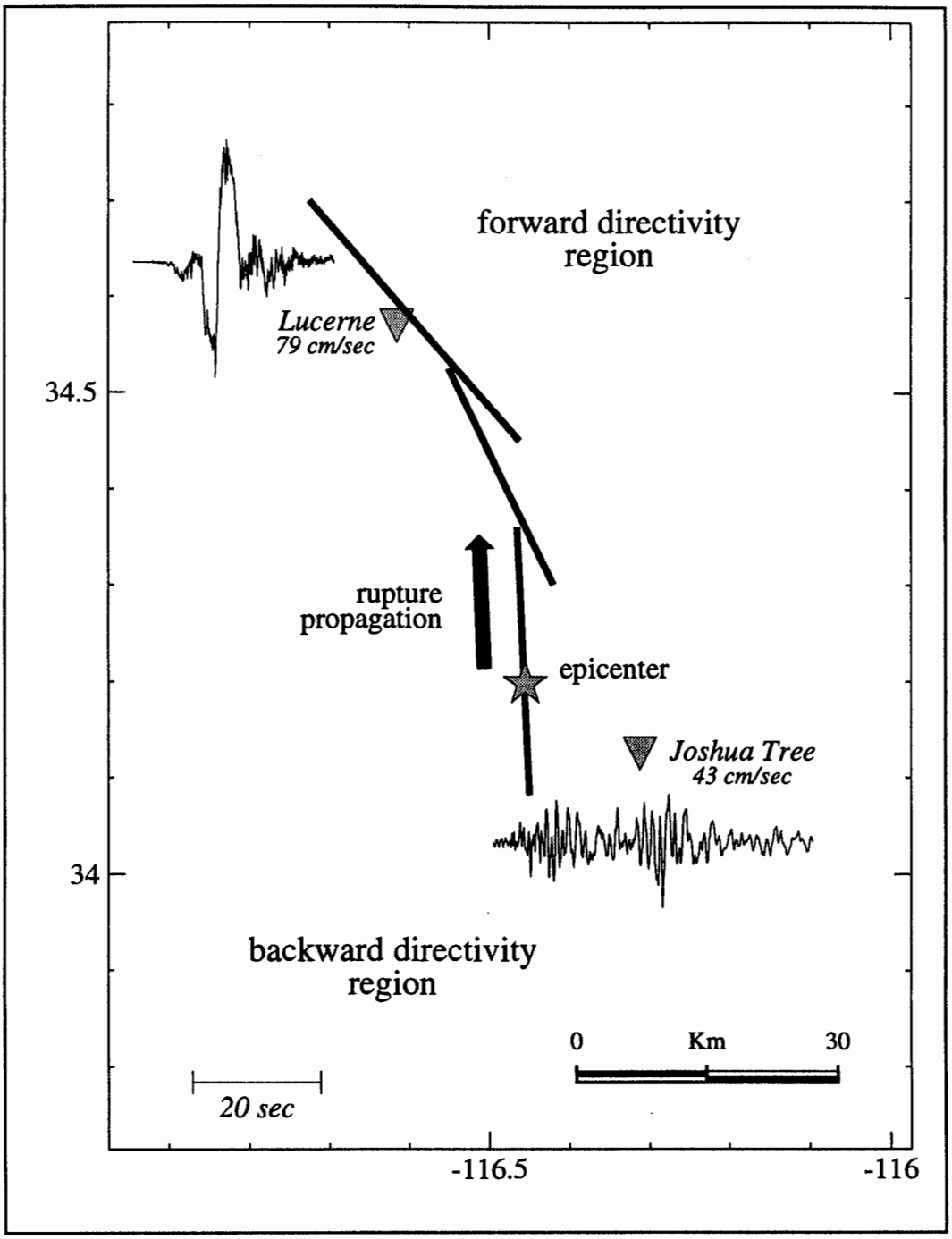

Figure 2. Map of the Landers region showing the location of the rupture of the 1992 Landers earthquake (which occurred on three fault segments), the epicenter, and the recording stations at Lucerne and Joshua Tree. The strike normal velocity time histories at Lucerne and Joshua Tree exhibit forward and backward rupture directivity effects respectively.

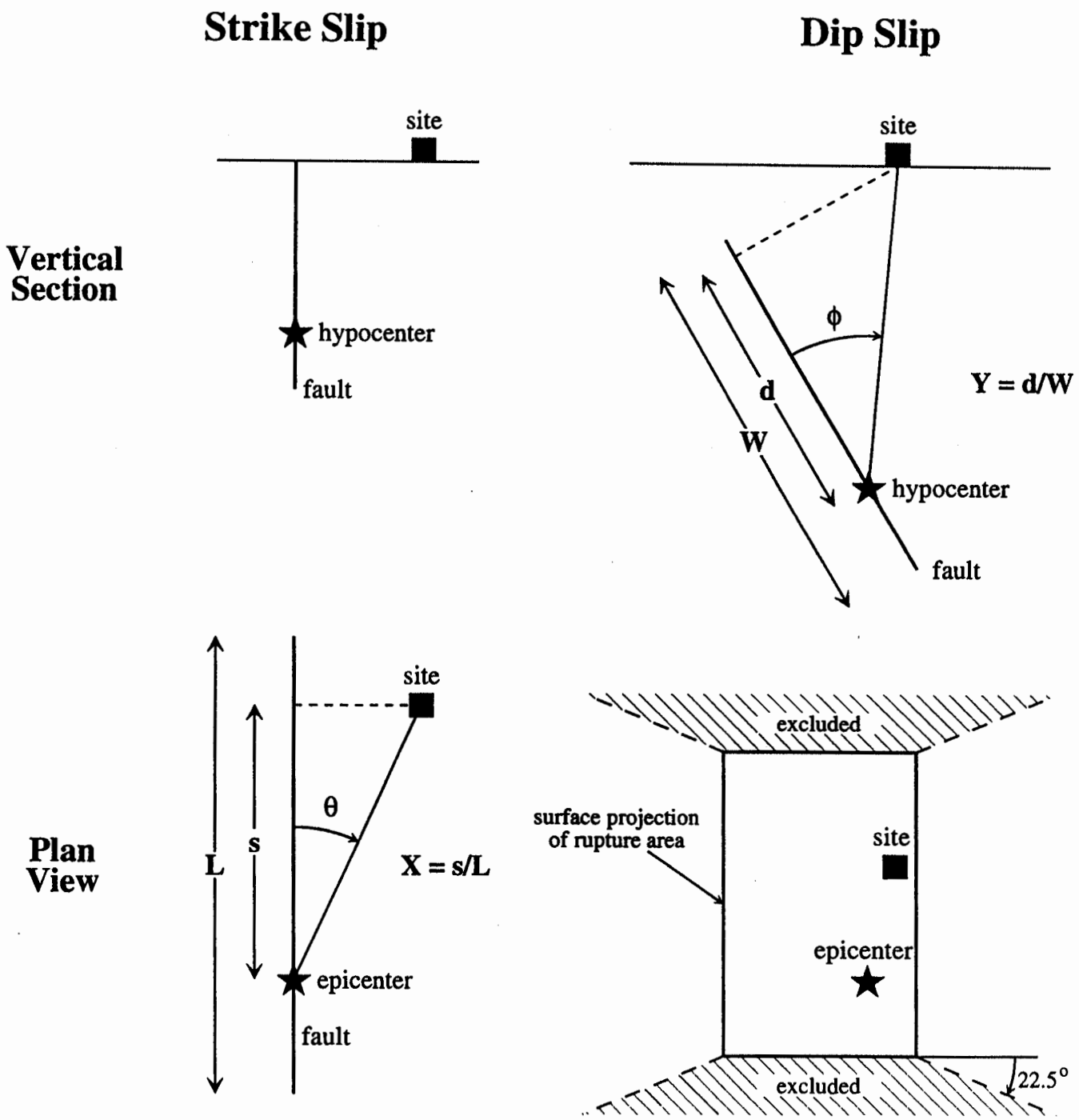

Figure 3. Definition of rupture directivity parameters θ and X for strike-slip faults, and ϕ and Y for dip-slip faults, and region off the end of dip-slip faults excluded from the model.

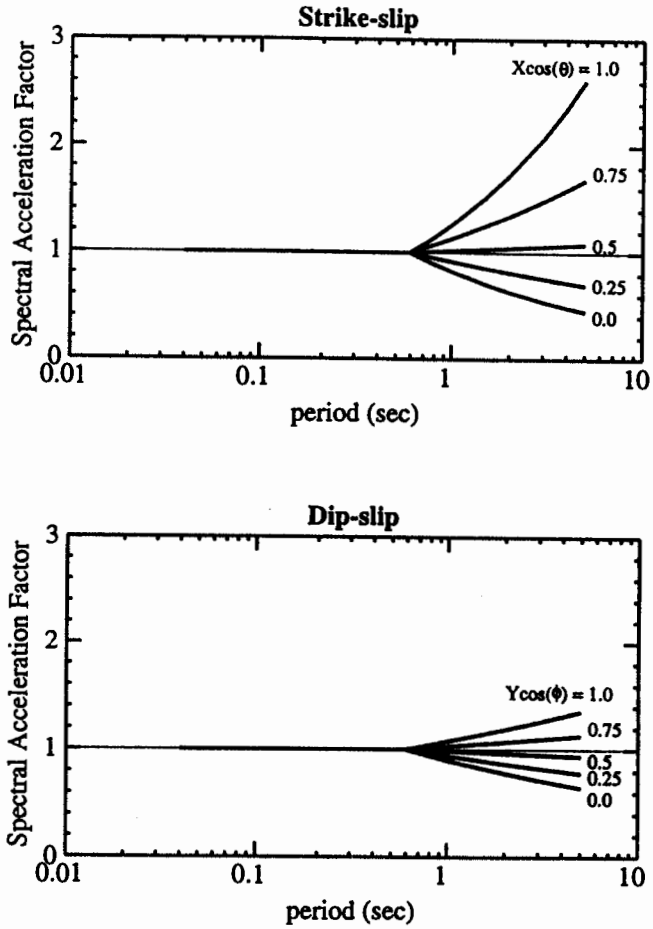

Figure 4a. Empirical model of the response spectral factor, showing its dependence on period and on the directivity function (X cos θ for strike-slip; Y cos ϕ for dip-slip)

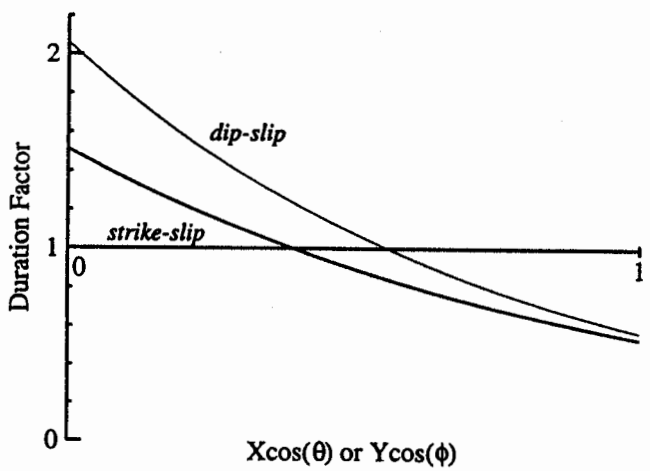

Figure 4b. Empirical model of the duration factor, showing its dependence on the directivity function (X cos θ for strike-slip; Y cos ϕ for dip-slip).

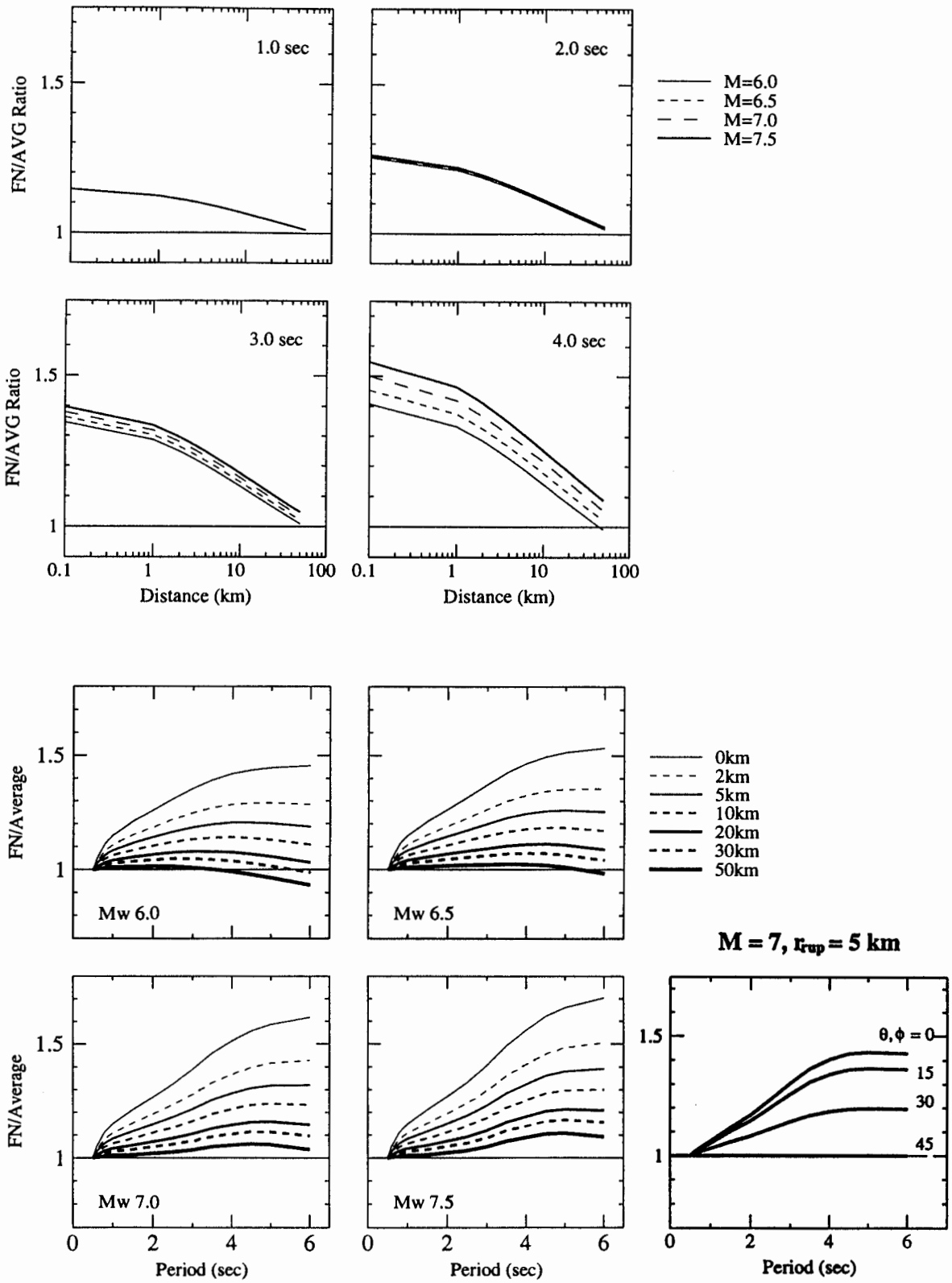

Figure 5. Empirical model of the strike-normal to average horizontal response spectral ratio excluding dependence on the angles θ or ϕ, shown as a function of period for various magnitudes and distances (top), and as function of distance for various magnitudes and periods (bottom). The dependence on angle θ or ϕ for M = 7 and r_{rup} = 5 km is shown as a function of period on the bottom right.

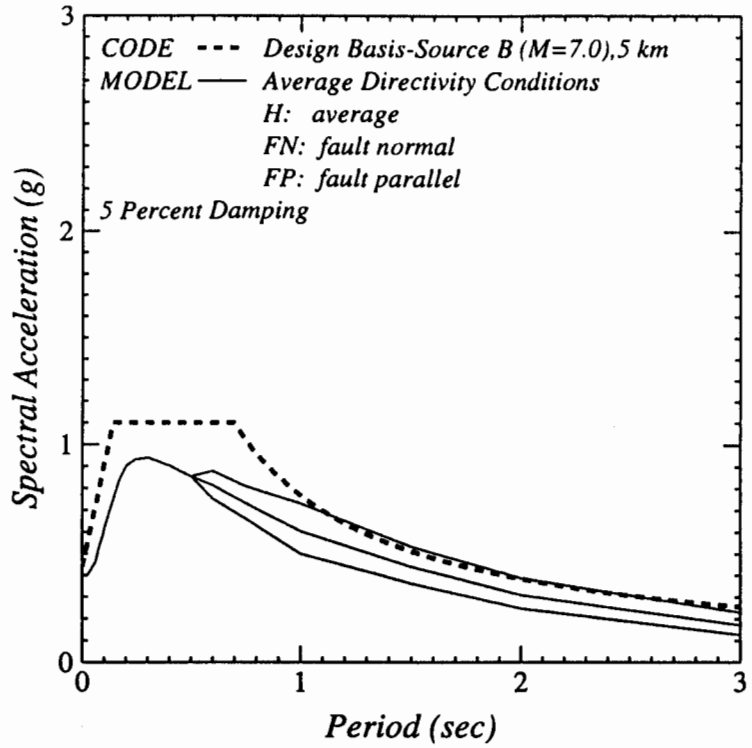

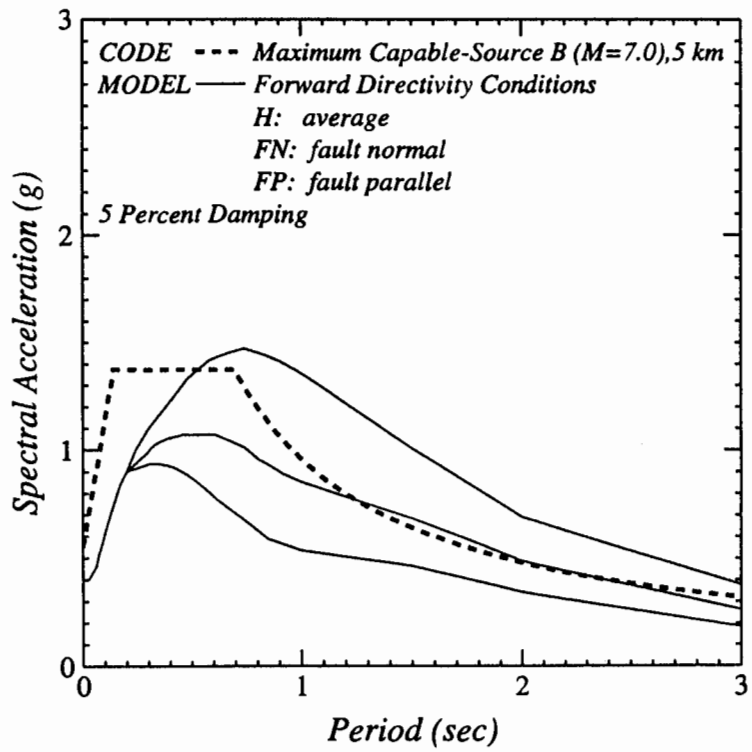

Figure 6. Response spectra for (top) average rupture directivity conditions and (bottom) forward rupture directivity conditions for a magnitude 7 earthquake at a distance of 5 km on soil. The response spectra are shown for the strike-normal, strike-parallel, and average horizontal components. Also shown for comparison are UBC spectra including the near-fault factor for design basis (top) and maximum capable (bottom) events.

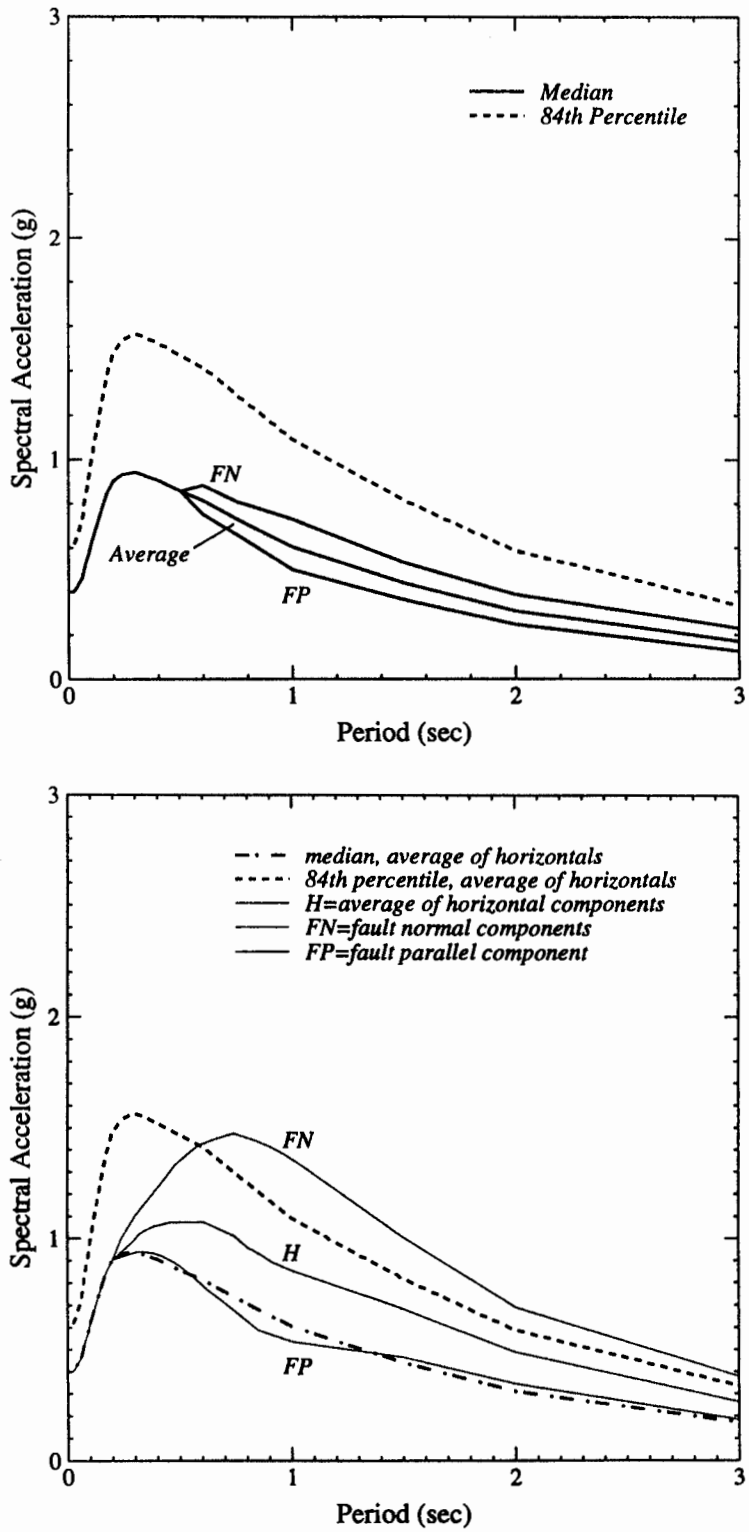

Figure 7. Response spectra for (top) average rupture directivity conditions and (bottom) forward rupture directivity conditions for a magnitude 7 earthquake at a distance of 5 km on soil. The response spectra are shown for the strike-normal, strike-parallel, and average horizontal components. Also shown for comparison are the median and 84th percentile spectra for the empirical attenuation relation (Abrahamson and Silva, 1997) on which the modifications for near-fault effects are based.

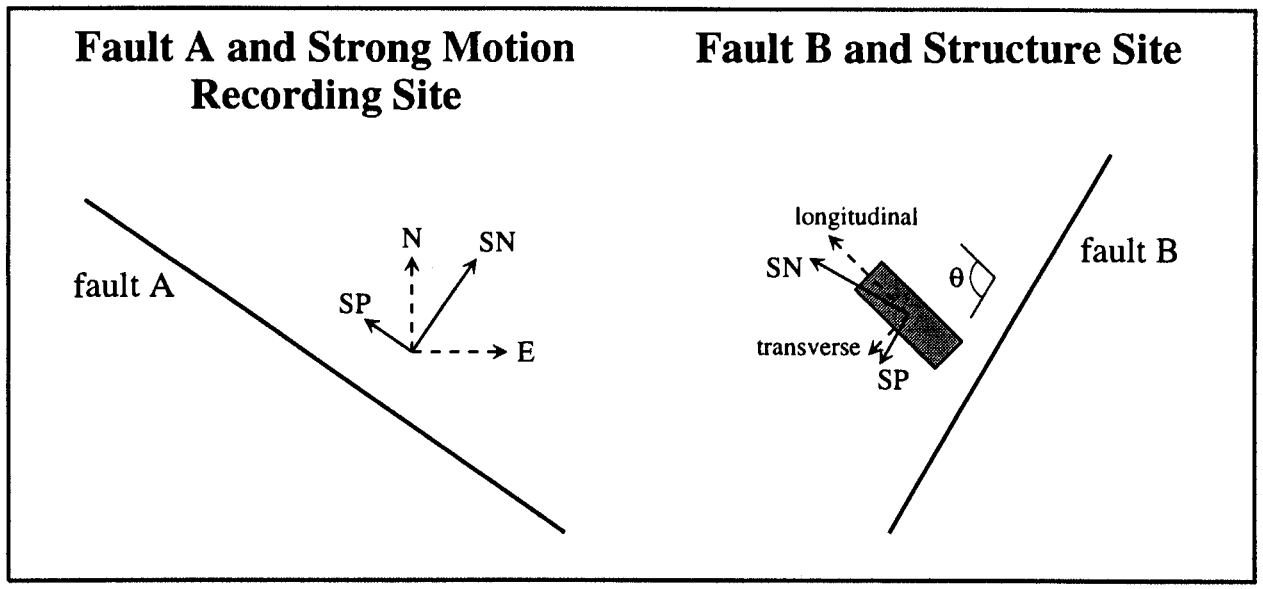

Figure 8a. Schematic diagram of the orientation of ground motion at a recording site, its rotation into strike-normal and strike-parallel components, transfer to a structure site in that orientation, and rotation into longitudinal and transverse components of the structure.

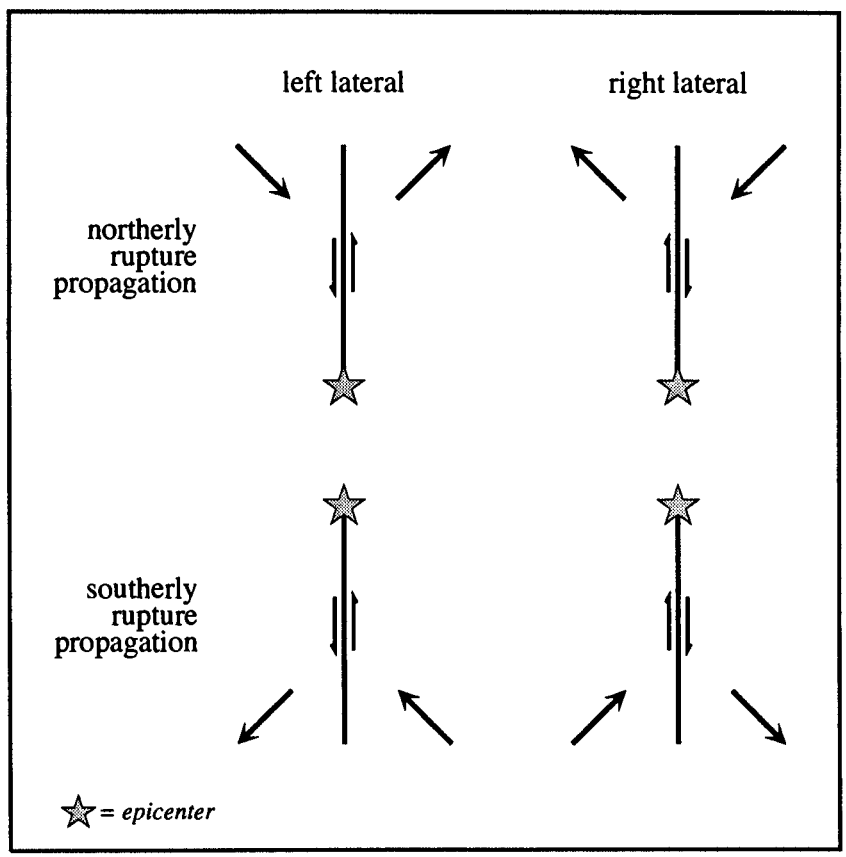

Figure 8b. Schematic diagram of the polarity of permanent ground displacement for strike-slip earthquakes. The motions are shown for both left-lateral and right-lateral unilateral faults, and for both northerly and southerly rupture propagation on north-striking faults.

1997 Uniform Building Code Ground Shaking Criteria

Charles A. Kircher, Ph.D.
Kircher & Associates, Palo Alto California
and
Robert E. Bachman, S.E.
Fluor Daniel, Inc. Irvine, California

Abstract

The recently published 1997 Uniform Building Code incorporates two significant changes to the ground shaking criteria which apply to all structures. The first change is a revision to soil types and soil amplification factors. The second change is the incorporation of near source factors in UBC seismic Zone 4. Together these changes result in the largest increases in code ground shaking criteria which has occurred in the past 30 years. Records obtained from the strong motion Instrumentation Program (SMIP) along with USGS records were the primary sources of data used to justify these code changes.

Soil Types and Soil Amplification Factors

The ground shaking basis for code design is reflected in the 5% damped elastic response spectra shown in Figure 1 (UBC Figure 16-3). The response spectra is defined in terms of two site seismic coefficients C_a and C_v. The site seismic coefficients are determined as a function seismic zone, soil type, and in Zone 4 near source factors. The soil profiles are subdivided into six types based on the average soil properties in top 100 feet of the soil profile. The types are identified as S_A through S_F are defined in accordance with Table 16-J (attached). The types are based on consensus deliberations from the USGS/NCEER/SEAOC workshop held at USC in 1992. These are identical to soil profile types that are found in 1994 NEHRP Provisions.

The site seismic coefficients C_a and C_V are determined from Tables 16-Q and Table 16-R (attached) based upon the soil profile type, seismic zone and in UBC Zone 4 the near source factors N_a and N_v. It should be noted that the value of the soil factors depart significantly from previous codes in that both short period and long period structures are effected by soil effects and that the amplifications increase significantly at lower ground acceleration levels. In previous codes soil effects were only considered for long period structures. . The amplification factors are consistent with the consensus from the previously referenced USC workshop and are identical to those found in the 1994 NEHRP provisions. These effects are consistent with observations in the Mexico City and the Loma Prienta earthquakes

Near Source Factors

The near source factors were developed by Ground Motion-Ad-Hoc-Committee of the SEAOC Seismology Committee to account for the effects of ground motions near the source of seismic events. The factors are a refinement of what was developed for seismically isolated structures included initially in the 1991 UBC. Near source ground motion records and observed damage from Northridge and Kobe have provided convincing evidence of significantly more intense ground shaking near the fault rupture than had been previously accounted for.

In order to establish, the near source factors, the first step is to identify and locate known active faults in UBC Zone 4 and classify them into one of three source type based on maximum moment magnitude and

slip rate in accordance with Table 16-U (attached). Faults are classified based on their maximum magnitude M and slip rate R. Type A sources are faults that have a moment magnitude potential of $M \geq 7.0$ and a slip rate SR equal to or greater than 5 mm/year. These types of faults are considered to be active and capable of producing large magnitutde events. Most segments of the San Andreas fault would be classified as a Type A fault. Type C sources are faults that have a moment magnitude potential of M less than 6.5 and a slip rate of SR less than or equal to 2 mm/year. Type C faults are considered to be sufficiently inactive and not capable of producing large magnitude events such that potential near-source ground shaking effects can be ignored. Most faults outside of California are Type C. Type B sources are all faults that are not either Type A or Type C and include most of the active faults in California. The 1997 UBC requires that the locations and characteristics of these faults be established based on approved geotechnical data from reputable sources such as the California Division of mines and Geology and the USGS.

Once faults are located relative to a site and the source type is established, the near source factors N_a and N_v are determined in accordance with Table 16-S and 16-T (attached). These factors were established by the Ad Hoc Ground Motion Committee and are based on the average increase, measured in the near field from Northridge and other earthquakes. The near source factors apply to both strike-slip and reverse-slip (thrust) fault mechanism although reverse-slip faults produce about 20% greater shaking on the average. The short period (acceleration domain) near source factor (N_a) is based on response at 0.3 seconds and long-period (velocity-domain) near source factor (N_v) based on 1.0 second response. Values of N_v are bumped upward by about 20% to account for the increase in average response in the fault-normal direction above that predicted by the attenuation function for the random component of horizontal ground shaking (ref. Somerville, 1996 7th US/Japan Workshop, Lessons learned from Kobe and Northridge). The commentary to the SEAOC bluebook notes ground shaking at "forward directivity" sites is likely to be 1.25 times the C_v and C_a coefficients based on average fault normal response. The values of N_a and N_v are used in Tables 16-S and 16-T to determine the values of C_a and C_v in UBC Zone 4 ($Z = 0.40$).

Distance from Faults and Fault Maps

The rules for measuring distance from a fault were also established by the Ad Hoc ground motion committee and are found in the code. The rules are illustrated in figure 2 for a variety of fault types and depths. It is interesting to note that for non-vertical faults a zero distance fault zone has been established as illustrated. The distance from a fault is measure from this zero distance fault zone.

Active fault near field maps are currently being developed for California Zone 4 for California Mines and Geology. The form of the maps will be like a Thomas Guide and will be at a scale of 1:150,000. The background will include street maps and freeways. An individual will be able to find their house on the maps. The USGS is providing fault information developed for Project 97 for maps outside of California and the maps will be developed by donated private sources. The maps will be published for sale by ICBO in fall of this year. Examples of the legend sheet is shown in Figure 3 and examples of expected near field maps are shown in Figures 4 and 5.

Conclusion

In conclusion, the inclusion of soil and near field effects in the 1997 UBC represent one of the most state-of-the-art, meaningful, and impactive changes in the code by the geoscience community in the history of seismic codes. The effects will continue to be improved in the new International Building Code which replaces the UBC begining in the year 2000.

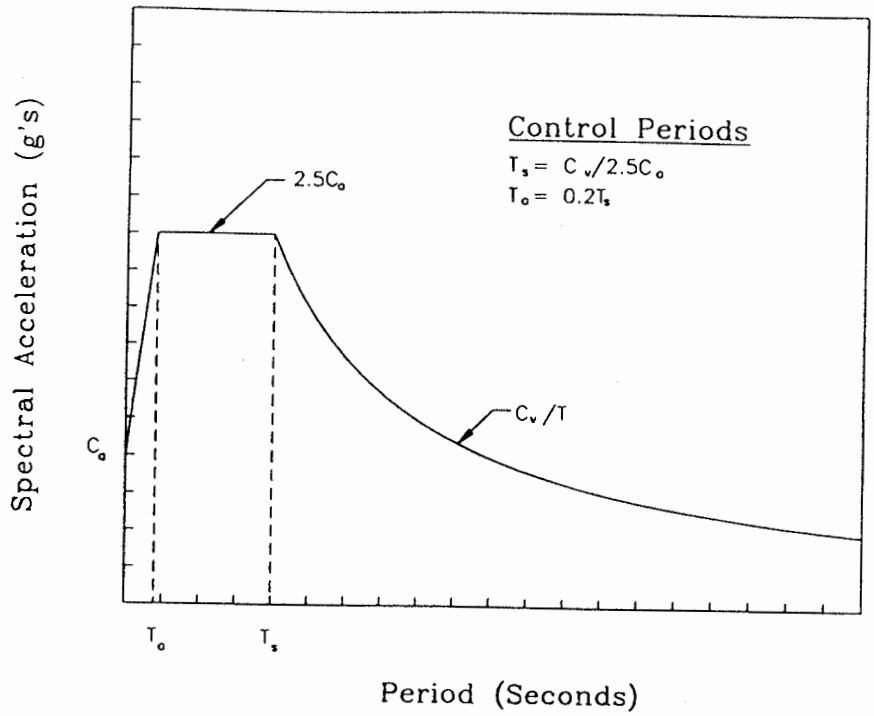

Figure 1: Design Response Spectra

Table 16-J. *Soil Profile Types*

Soil Profile Type	Soil Profile Name/Generic Description	Average Soil Properties for Top 100 Feet (30 480 mm) of Soil Profile		
		Shear Wave Velocity, $\overline{v}_s$ feet/second (m/s)	Standard Penetration Test, $\overline{N}$ (or $\overline{N}_{CH}$ for cohesionless soil layers) (blows/foot)	Undrained Shear Strength, $\overline{S}_u$ psf (kPa)
S_A	Hard rock	> 5,000 (1500)		
S_B	Rock	2,500 to 5,000 (760 to 1500)		
S_C	Very dense soil and soft rock	1,200 to 2,500 (360 to 760)	> 50	> 2,000 (100)
S_D	Stiff soil profile	600 to 1,200 (180 to 360)	15 to 50	1,000 to 2,000 (50 to 100)
S_E[1]	Soft soil profile	< 600 (180)	< 15	< 1,000 (50)
S_F	Soil requiring site-specific evaluation. See Section 1644.3.1			

1. Soil profile Type S_E also includes any soil profile with more than 10 ft (3048 mm) of soft clay defined as a soil with a plasticity index, $PI > 20$, $w_{mc} > 40$ percent and $\overline{S}_u < 500$ psf (25 *kPa*). The Plasticity Index, PI, the moisture content, w_{mc}, shall be determined in accordance with approved national standards.

Table 16-Q. Seismic Coefficient C_a

Soil Profile Type	Seismic Zone Factor, Z				
	Z=0.075	Z = 0.15	Z = 0.2	Z = 0.3	Z = 0.4
S_A	0.06	0.12	0.16	0.24	$0.32N_a$
S_B	0.08	0.15	0.20	0.30	$0.40N_a$
S_C	0.09	0.18	0.24	0.33	$0.40N_a$
S_D	0.12	0.22	0.28	0.36	$0.44N_a$
S_E	0.19	0.30	0.34	0.36	$0.36N_a$
S_F	See Footnote 1				

1 Site-specific geotechnical investigation and dynamic site response analysis shall be performed to determine seismic coefficients for Soil Profile Type S_F.

Table 16-R. Seismic Coefficient C_v

Soil Profile Type	Seismic Zone Factor, Z				
	Z=0.075	Z = 0.15	Z = 0.2	Z = 0.3	Z = 0.4
S_A	0.06	0.12	0.16	0.24	$0.32N_v$
S_B	0.08	0.15	0.20	0.30	$0.40N_v$
S_C	0.13	0.25	0.32	0.45	$0.56N_v$
S_D	0.18	0.32	0.40	0.54	$0.64N_v$
S_E	0.26	0.50	0.64	0.84	$0.96N_v$
S_F	See Footnote 1				

1 Site-specific geotechnical investigation and dynamic site response analysis shall be performed to determine seismic coefficients for Soil Profile Type S_F.

Table 16-U. Seismic Source Type[1]

Seismic Source Type	Seismic Source Description	Seismic Source Definition	
		Maximum Moment Magnitude, M	Slip Rate, SR (mm/year)
A	Faults that are capable of producing large magnitude events and which have a high rate of seismic activity	M ≥ 7.0 and	SR ≥ 5
B	All faults other than Types A and C		
C	Faults which are not capable of producing large magnitude earthquakes and which have a relatively low rate of seismic activity	M < 6.5 and	SR ≤ 2

1 Subduction sources shall be evaluated on a site specific basis.

Table 16-S. Near Source Factor N_a[1]

Seismic Source Type	Closest Distance to Known Seismic Source[2,3]		
	≤ 2 km	5 km	10 km
A	1.5	1.2	1.0
B	1.3	1.0	1.0
C	1.0	1.0	1.0

1 The near-source factor may be based on the linear interpolation of values for distances other than those shown in the table.

2 The location and type of seismic sources to be used for design shall be established based on approved geotechnical data (e.g. most recent mapping of active faults by the United States Geological Survey or the California Division of Mines and Geology).

3 The closest distance to seismic source shall be taken as the minimum distance between the site and the area described by the vertical projection of the source on the surface (i.e., surface projection of fault plane). The surface projection need not include portions of the source at depths of 10 km, or greater. The largest value of the near-source factor considering all sources shall be used for design.

Table 16-T. Near Source Factor N_v[1]

Seismic Source Type	Closest Distance to Known Seismic Source[2,3]			
	≤ 2 km	5 km	10 km	15 km
A	2.0	1.6	1.2	1.0
B	1.6	1.2	1.0	1.0
C	1.0	1.0	1.0	1.0

1 The near-source factor may be based on the linear interpolation of values for distances other than those shown in the table.

2 The location and type of seismic sources to be used for design shall be established based on approved geotechnical data (e.g. most recent mapping of active faults by the United States Geological Survey or the California Division of Mines and Geology).

3 The closest distance to seismic source shall be taken as the minimum distance between the site and the area described by the vertical projection of the source on the surface (i.e., surface projection of fault plane). The surface projection need not include portions of the source at depths of 10 km, or greater. The largest value of the near-source factor considering all sources shall be used for design.

Figure 2.

1997 UBC NEAR SOURCE FACTOR
RULES FOR DETERMINING PLOTTED FAULT LOCATION
AND DISTANCE FROM FAULT

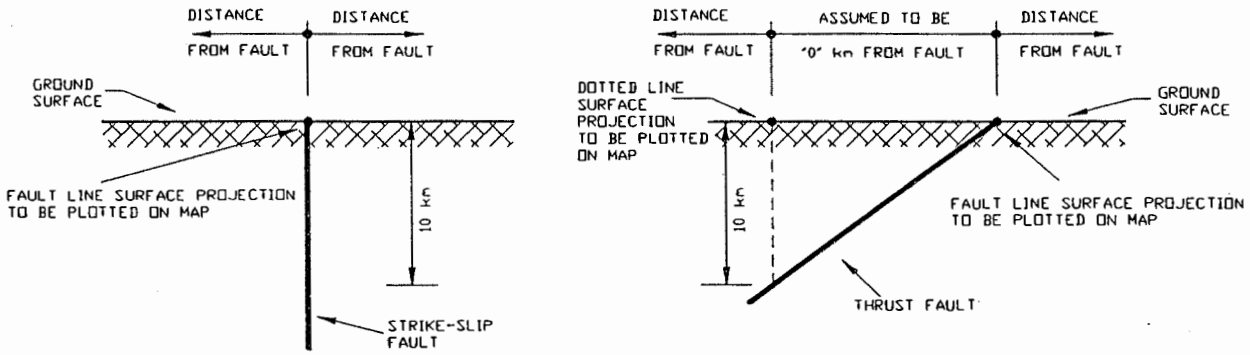

ACTIVE A & B SEISMIC SOURCES
WHOSE FAULT PLANE EXTENDS TO SURFACE

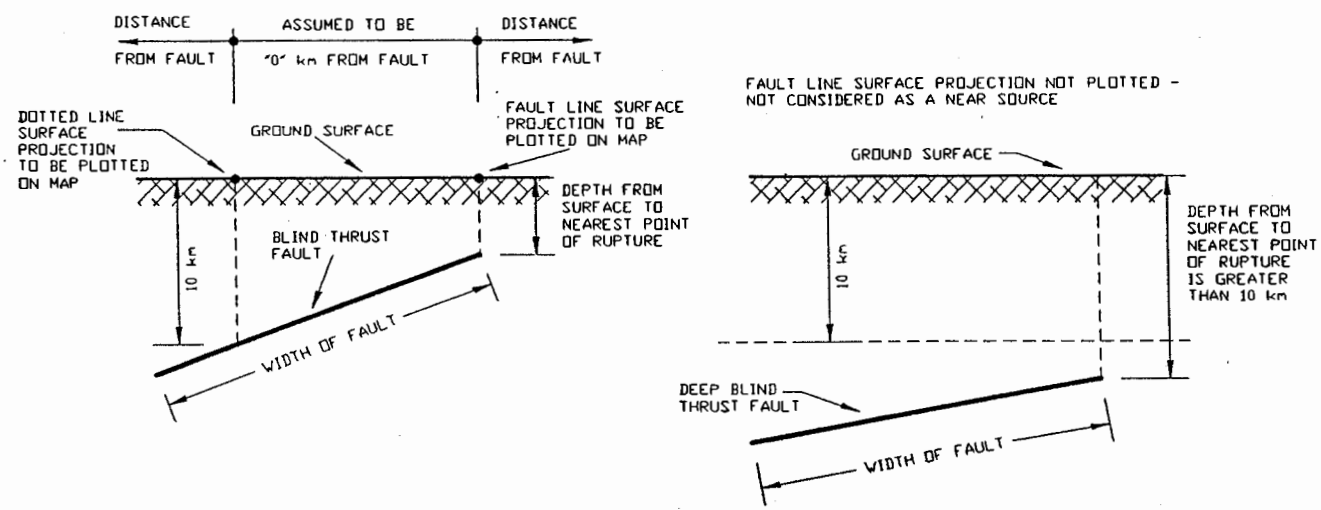

ACTIVE A & B SEISMIC SOURCES WHOSE
FAULT PLANE DOES NOT EXTEND TO SURFACE

EXPANDED LEGEND

The maps are intended for use with the 1997 Uniform Building Code (UBC), Tables 16-S and 16-T, to determine near fault seismic factors N_a and N_v.

The shaded areas are near field zones of active faults where the the near source factors are maximum (within 2 km of "zero" fault width zones).

Active faults are classified as A or B in accordance with Table 16-u of 1997 UBC.

The dotted lines indicate distances of 5, 10, and 15 km from the "zero" fault width zones.

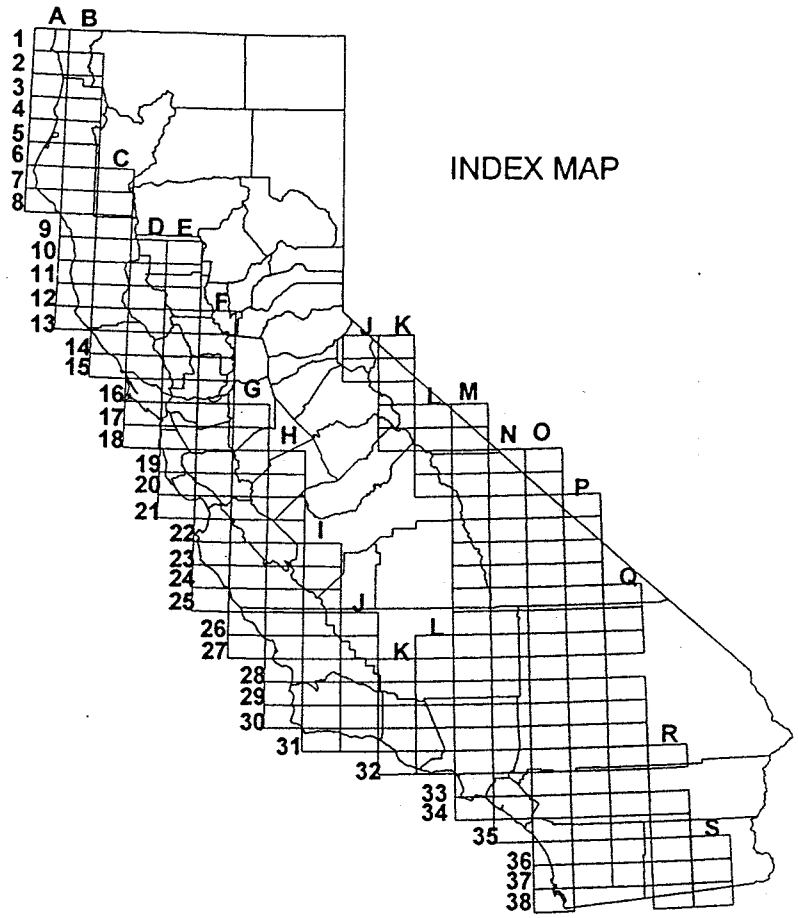

Figure 3: Example Legend Page for Near Field Fault Maps

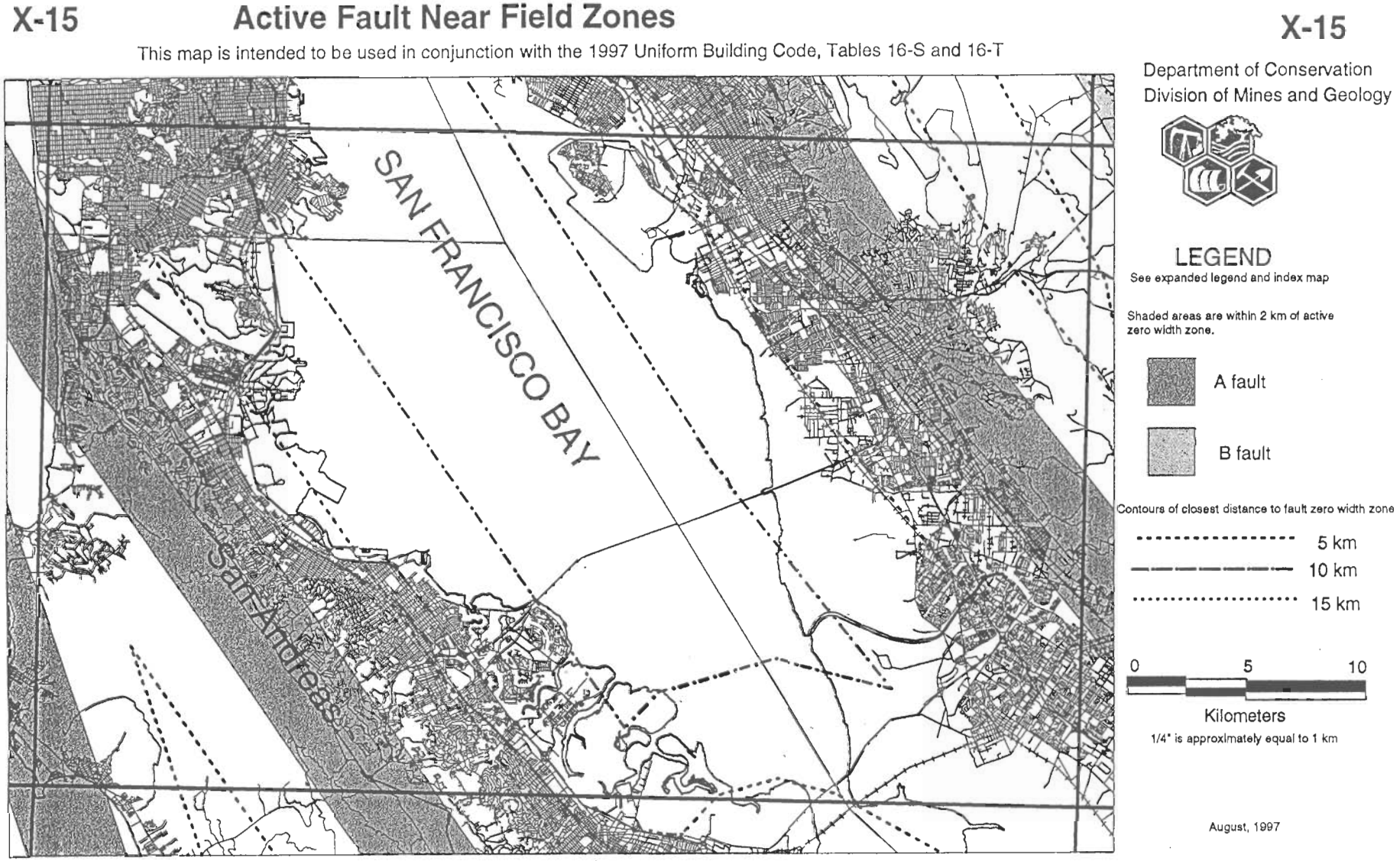

Figure 4: Example of Active Fault Near Field Map for San Francisco Bay Area

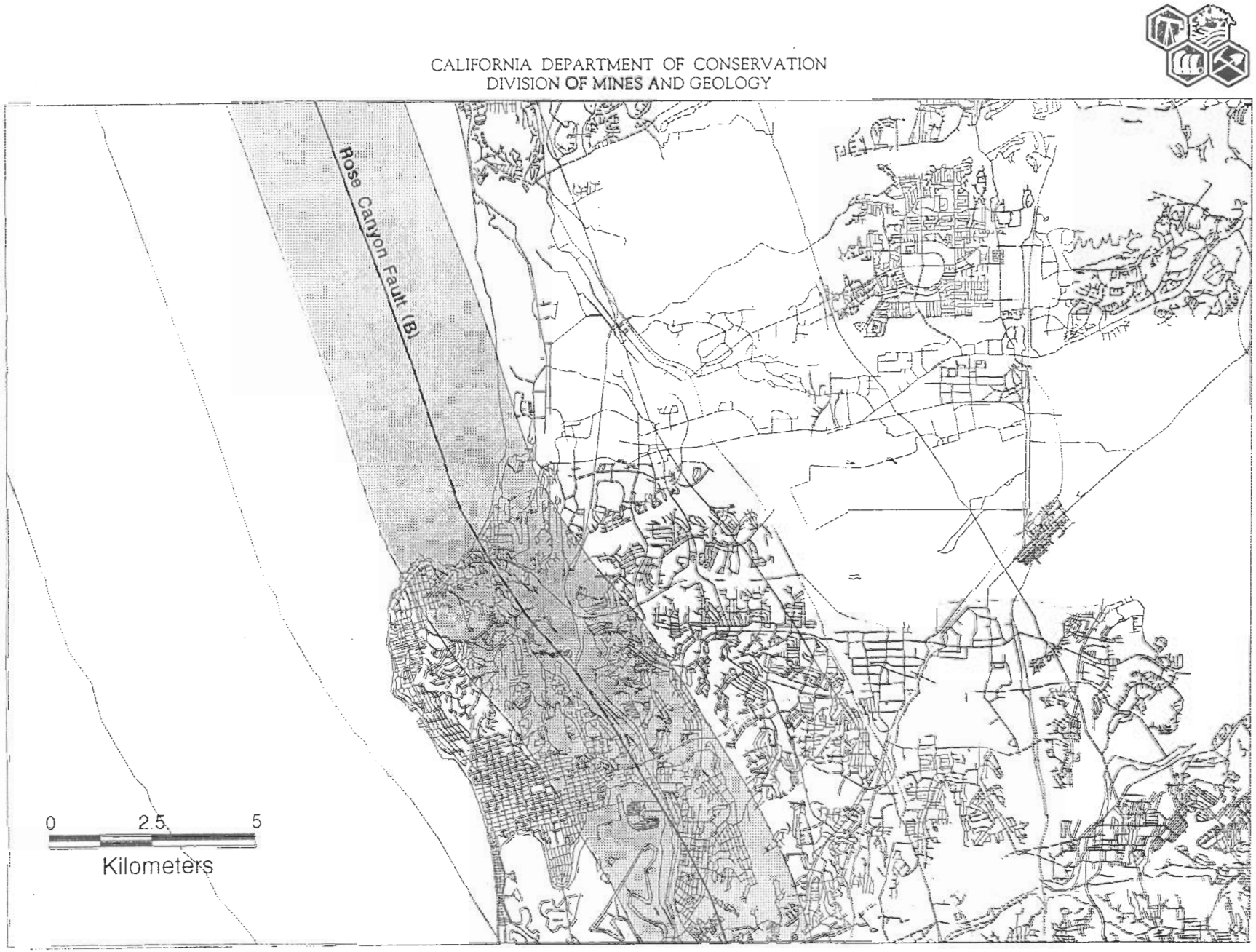

Figure 5: Example of Active Fault Near Field Map for La Jolla, City of San Diego

NEAR-REAL-TIME STRONG MOTION, TRINET DATA, AND DATA DISSEMINATION THROUGH THE INTERNET

A. Shakal, V. Graizer, C. Petersen and R. Darragh

California Division of Mines and Geology
Department of Conservation, Sacramento, CA

Abstract

Recent developments in near-real-time recovery of strong-motion data have been expanded to include new means to disseminate and rapidly utilize the data. The TriNet project, a cooperative project in southern California involving CDMG, Caltech and the USGS, will disseminate earthquake data and information rapidly for use by emergency responders. In another development, the release of strong-motion data by CSMIP will include simple descriptors of the shaking level (Light, Moderate, Strong and Extreme Shaking). These descriptors, designed to be easily understood by the non-specialist, will be complemented by more customary quantitative characterizations (time-history and spectral levels). To make strong-motion data widely available for use in earthquake engineering and engineering seismology, the data will be available for access by any current Web browser at the Internet site http://www.consrv.ca.gov/dmg/csmip. All strong-motion data released by CSMIP over the years are or will soon be available at this location. For future significant earthquakes, strong-motion data will also be available rapidly at the site.

Developments in Near-Real-Time Strong Motion

Near-real-time strong motion record recovery by the California Strong Motion Instrumentation Program (CSMIP) was first described at the SMIP95 conference (Shakal and others, 1995). The system has continued to evolve since then. A total of 70 stations are now configured with appropriate accelerographic and communication equipment to transmit strong-motion data automatically to a bank of computers in Sacramento. One new development is that summary parameters of the recorded motion (peak acceleration, etc.) are now being automatically uploaded to the Internet. In addition, the data recovery software and protocols in Sacramento have evolved to become increasingly robust, in order to withstand known error situations in a fail-safe mode. Experience has indicated that, for a successful automated strong motion communication system, developing fail-safe robustness is as challenging as initially establishing the capability. On a related front, a significant development in rapid utilizing near-real-time strong-motion data is the introduction of the data into the cooperative TriNet system.

TriNet: A Multi-Network Earthquake Measuring and Data Utilization Consortium

One outgrowth of the Northridge earthquake was an initiative to increase the measurement of ground shaking data and to accelerate the distribution and utilization of that information. This eventually led to a cooperative project in southern California among the principal agencies recording earthquake motion in the area. The California Institute of Technology (Caltech) and the Pasadena office of the U.S. Geological Survey operate the Southern California Seismic Network (SCSN), a weak-motion network well known for recording and rapidly determining the location of earthquakes in southern California, for magnitude 1 and larger events. The earthquake locations and magnitudes reported in newspapers and on radio or television after events in southern California are determined by this network. For larger earthquakes, the CSMIP network of the California Division of Mines and Geology (CDMG) is the primary strong motion network in the area, and it recovers and disseminates strong-motion data after moderate and larger earthquake (typically magnitude 5 and above).

TriNet, a cooperative project among these three institutions, was established with funding for 5 years from the Federal Emergency Management Agency (FEMA), co-sponsored by the California Office of Emergency Services (OES). One focus of the CSMIP part of TriNet is a data interpretation project which will fund studies to improve seismic design codes.

Joint products of the TriNet project will include rapid determination and characterization of the earthquake shaking. A map of the shaking, called ShakeMap, will be produced by TriNet that shows the areal distribution of shaking intensity. This can be used by emergency responders to direct their resources most effectively to areas of the greatest shaking and damage. A prototype of ShakeMap has been prepared for several recent small events by the USGS Pasadena Office. The ongoing processing and release of strong-motion data by CSMIP to the earthquake engineering and seismological community, in forms customary to them, will continue unaltered. In fact this will be improved, and more data will be available, more rapidly, since part of the TriNet project will include the upgrade of CSMIP instruments in southern California from analog (film) recorders to digital instruments with telephone communications, and they will become part of the near-real-time data recovery discussed above. Another aspect of the TriNet project is that new instruments to be installed at stations of the weak-motion seismographic network of Caltech and USGS will also be able to record strong shaking, and these data will be processed along with the CSMIP strong-motion data. Similarly, for smaller events of little engineering interest, any low-level records obtained by CSMIP will be provided to the Caltech/USGS network to improve their accuracy in locating the event and determining magnitude and other seismological characteristics.

The net effect of the TriNet project in terms of strong-motion data should be the provision of more data, more rapidly, for the earthquake engineering community, while also expanding the capability of the seismic networks in southern California to understand earthquake generation and shaking distribution. Caltech and the USGS also intend to develop a prototype warning system as part of the project. In northern California, an effort paralleling the southern California TriNet project is in the discussion stage among CDMG, UC Berkeley and the USGS at Menlo Park.

Shaking-Level Descriptors for Use in Response: Light, Moderate, Strong and Extreme Shaking

The customary use of strong-motion data is to quantitatively describe the level of shaking, in a precise and definite way. For example, the motion at the Arleta station during the Northridge earthquake had a peak horizontal acceleration of 0.34 g and a peak velocity of 40 cm/sec. There are several reasons to accompany this traditional characterization with short descriptive words. First, from a human factors perspective, rapid response to strong shaking information requires a more easily recognizable characterization than a series of quantities which must be interpreted and considered. Second, peak acceleration is known to correlate poorly with damage, in general. A striking example is the Tarzana station, which in the Northridge earthquake had a peak acceleration of over 1.8 g, and yet damage in the area was not great. Third and most importantly, most emergency responders are not accustomed to the usage of the technical quantities used by seismologists and engineers. However, conventional vernacular already includes well-understood descriptive words, that while normally applied to other phenomena or situations, can be brought forward to help make shaking levels more quickly understood by nonspecialists.

Since we wish to describe the shaking at a location it is natural to incorporate concepts from the Modified Mercalli Intensity scale. This scale was developed to characterize shaking and damage at various locations in the vicinity of an earthquake before instrumental measurements were available. Richter (1956) describes the scale and its evolution in detail. The MMI scale is also considered in the contemporary book Earthquakes by B.A. Bolt (1993). Bolt (1993) includes a correlation between the MMI Intensity level and instrumentally-measured acceleration and velocity. Other correlations are also available and can be considered for reference. With a tie between instrumental measurements and the effects of shaking embodied in the MMI scale, a useful set of descriptors can be used.

The descriptive words characterizing shaking levels are shown in Table 1, along with the MMI Intensity level range and the structural damage descriptions, ranging from none (Light Shaking) through significant destruction (Extreme Shaking). Although this approach capitalizes on an accepted, description-based system like Mercalli Intensity, it must be noted that the MMI scale has limitations because of its introduction before modern design and construction methods. However, it is still an effective scale to use, which may be improved as new events occur. This characterization will be used as part of the post-earthquake data released by CSMIP, accompanied by the customary quantities (time and spectral domain). These descriptors have been found to be very useful in quickly interpreting the pager messages described in Shakal and others (1995).

TABLE 1

SHAKING LEVEL DESCRIPTORS
STRONG MOTION MONITOR SYSTEM

Light Shaking
(Intensity V-VI MMI)

Structural Damage
- None or slight.

Other Aspects
- Felt by nearly everyone, some frightened.
- A few cases of cracked or fallen plaster and chimney damage.
- Unstable objects overturned, some heavy furniture moved and dishes/windows broken.
- Movement of trees, poles, etc. sometimes noticed.

Corresponding motion to be measured (at ground level)
- Sustained acceleration of .02 to .10 g, or velocity of 2 to 10 cm/sec.

Moderate Shaking
(Intensity VII MMI)

Structural Damage
- Buildings of good design and construction: Negligible
- Well-built ordinary structures: Slight to moderate
- Poorly built or badly design structures: Considerable

Other Aspects
- Everybody runs outdoors; some chimneys broken; noticed by people driving cars.

Corresponding motion to be measured (at ground level)
- Sustained acceleration of .10 g to .25 g, or velocity of 10 to 25 cm/sec.

Strong Shaking
(Intensity VIII-IX MMI)

Structural Damage
- Specially designed structures: Slight to considerable.
- Ordinary substantial buildings: Considerable to great, with partial collapse.
- Poorly built structures: Great.

TABLE 1 (Continued)

Other Aspects

- Fall of chimneys, factory stacks, columns, monuments, walls.
- Panel walls thrown out of frame structures.
- Heavy furniture overturned; people driving cars disturbed.
- Underground pipes may be broken; sand and mud ejected in small amounts.

Corresponding motion to be measured (at ground level)

- Sustained acceleration of .25 g to .60 g, or velocity of 25 to 60 cm/sec.

Extreme Shaking

(Intensity X-XII MMI)

Structural Damage

- Well-built wooden structures: Some destroyed.
- Masonry and frame structures: Destroyed.
- Bridges: Some destroyed.

Other Aspects

- Landslides considerable.
- Rails bent.
- Fissures in ground.

Corresponding motion to be measured (at ground level)

- Sustained acceleration greater than .60 g, or velocity greater than 60 cm/sec.

Rev. 2.0, 12/96

Accessing Strong-Motion Data Through the Internet

The most effective means for distributing the digital version of strong-motion records has evolved over the last 20 years. The traditional means was based on the nine-track computer tape; a particular tape would be requested, and shipped in a specified format. In the last decade, the most common means of distribution became the floppy disk. As personal computers became more common, people could now request records and load them into the computer at their own desk. The next step of evolution is the Internet and the World Wide Web, which can revolutionize the distribution and use of strong-motion data even more than floppy disks did.

CSMIP has developed a Strong Motion Data Center site on the Internet. The site allows a user to request specific records, as desired, without submitting request forms or waiting for package delivery. Usage of the Data Center is quite straightforward, as described below. The Web site is operational and available, although an improved phase is underway.

The home page of the Data Center is shown in Figure 1. The site, at address http://www.consrv.ca.gov/dmg/csmip, can be accessed by any of the current browsers, such as Netscape, America Online, or Microsoft Internet Explorer. Some of the earliest browsers (such as early Mosaics), may not portray the tables well, but should still work.

The Web site has two pathways for requesting data. The most common data request received by CSMIP is a request for the strong-motion record from a specific earthquake from one more stations. A similarly common request is for the records from a specific station, for several earthquakes. Accordingly, the Web site is designed so that these requests are the most convenient, and the flow path for the request is shown schematically in Figure 2. The first action button on the home page is "View/Download Strong Motion Data". Clicking on this button with a mouse brings up screen (2) in Figure 2, which allows the user to choose between requesting data for an earthquake or for a station. If the user wishes to request data for an earthquake, the left panel allows the selection of one of the listed earthquakes. After the cursor bar is moved to that selection, the "Submit Selection" button must be clicked to transmit that request to the server through the user's local Internet connection.

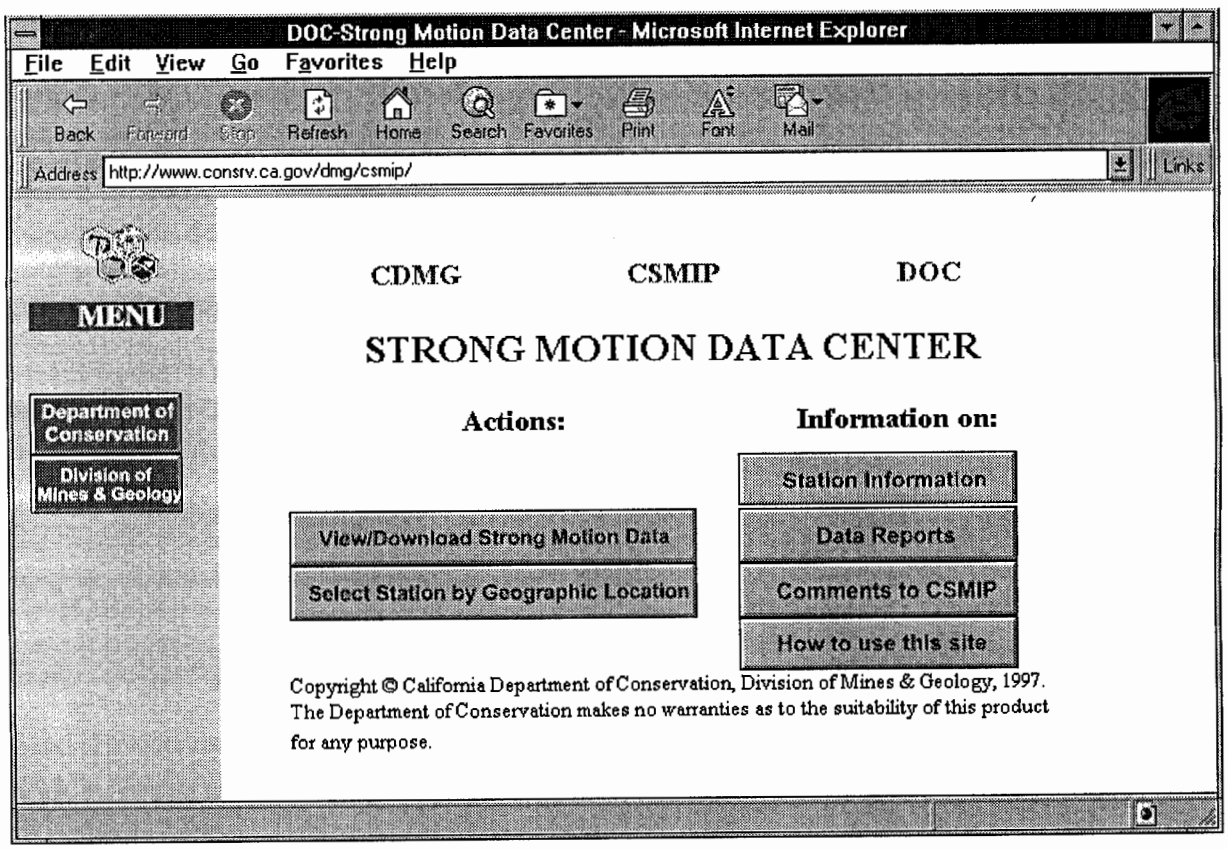

Figure 1. The Strong Motion Data Center home page on the Internet at http://www.consrv.ca.gov/dmg/csmip.

Selection of Records from a Specific Earthquake

Once the user selects an earthquake, Northridge for example, the following screen (3) lists all stations that have recorded data for that event in the database. These are listed alphabetically by station name in the left panel, and numerically by station number on the right, in case the user only knows the station number. The user may choose from either list, and then again "Submit" the selection. In the example, the user is about to request to view the data from the Obregon Park station in Los Angeles. Once that selection is submitted, the next screen (5) displays the retrieved time-history of the specified record, including the acceleration, velocity and displacement. This particular screen is long, and the user can scroll the display up to also obtain a display of the response spectra (screen 6). Other graphic representations of the data (additional spectral or time-history representations) will be added here in the future. If the user now desires, the record itself can be downloaded directly to his/her computer, simply by clicking on the "Download Record" button. The data files will be downloaded in a compressed format (PKZIP), and can be auto-uncompressed on PCs by simply executing the file. (A few users have Sun or other computers using Unix; a slightly different compression is needed, which can also be requested over the Internet). The format of these ASCII files is standard, conforming to the format CSMIP has adhered to for 15 years (Shakal and Huang, 1985). If the user does not wish to download at this point, he/she can just go back one screen and view other records in order to find one with the particular time-history or spectral properties desired.

Selection of Records from a Specific Station

A second pathway for obtaining data allows the user to request data from a particular station. In that case, the right panel of screen 2 in Figure 2 is used. There, the user can select from an alphabetical list of all stations in the network, statewide, scrolling down in the list as needed. Once a particular station is selected, the next screen (7) lists all earthquakes which were recorded at the station and are in the data base at the present time. In the example, Obregon Park has been selected, which has the recorded accelerogram from five earthquakes currently loaded into the Web site. The inset map on the left in screen (7) shows the locations of the station and the earthquake epicenters. At this point, the user can select the earthquake for which the record from this station is desired. This will result in screens identical to (5) and (6) discussed in the above example, and the same choice to download is available. (Note that the same station was used in these two examples simply to reduce the number of screens).

Searching for a Record from a Geographic Location

A very different application is provided by the option, "Select Station by Geographic Location" on the home page (Figure 1). This option ties to a second type of request from users, less common than the first. In this request, the user has an unfocused request, and may not be familiar with the data available. The user basically asks "Is there data from any station near my site (building, development, etc.)?" This can be a time consuming request for CSMIP staff to respond to. However, the example in Figure 3 shows the screen (2) that

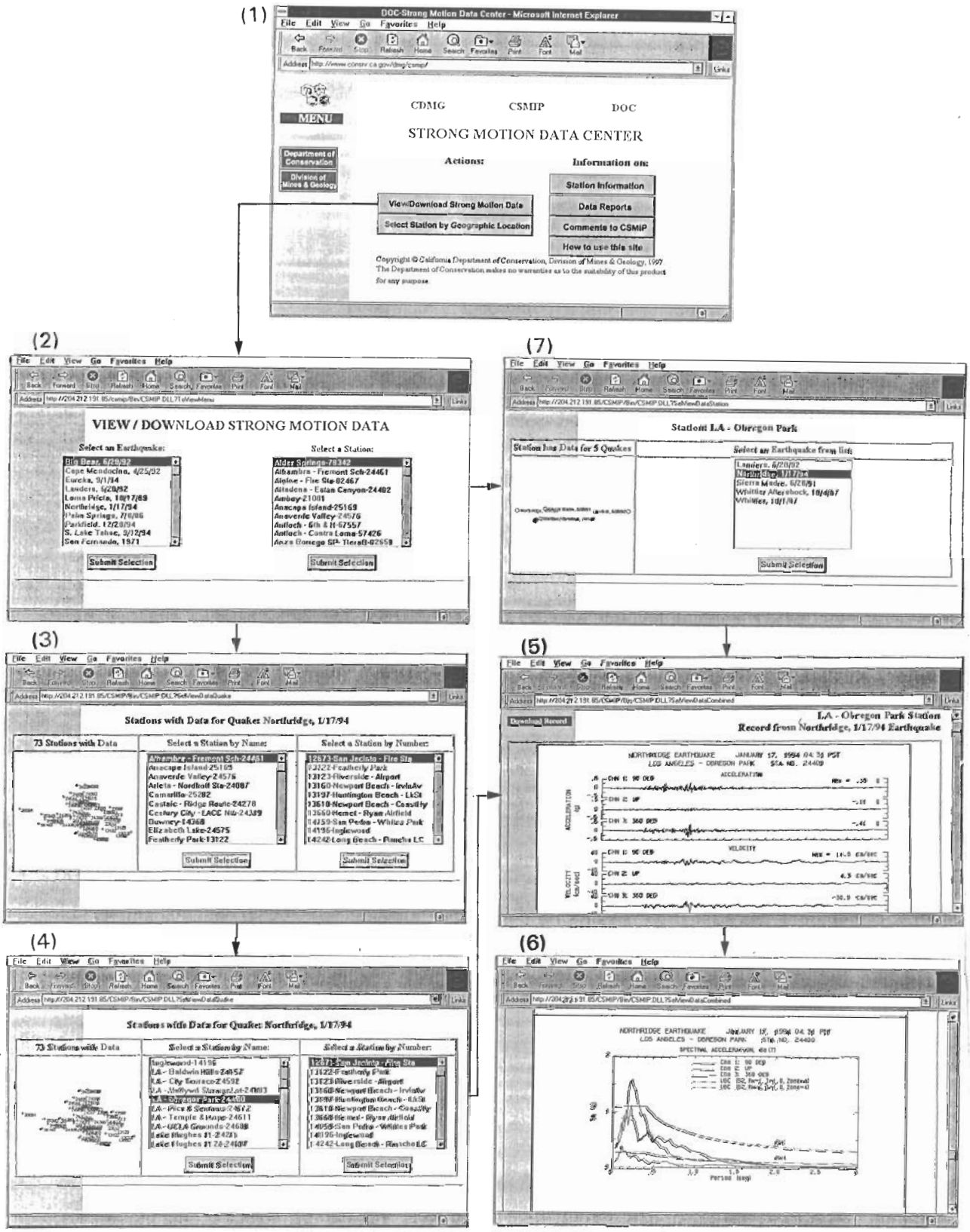

Figure 2. The flow path for accessing strong motion data using the upper action button "View/Download Strong Motion Data", as described in the text.

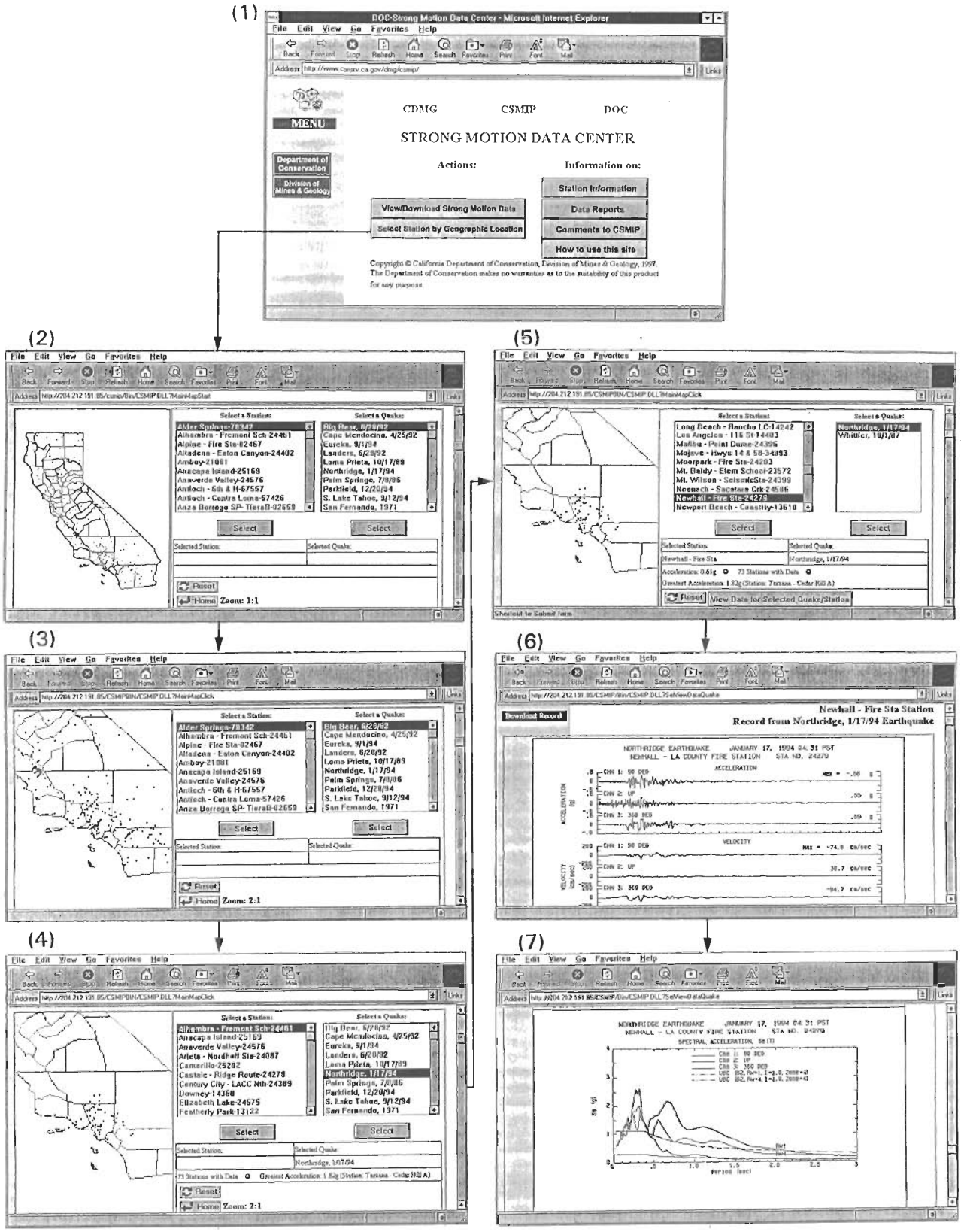

Figure 3. The flow path for accessing strong motion data using the lower action button "Select Station by Geographic Location", as described in the text.

the user is presented with if this option is selected. In this example, the user is interested in southern California stations, and so clicks on the southern California area to zoom in on the map (screen 3). If the user now restricts the request to data recorded in the Northridge earthquake, a map of just the stations that recorded Northridge appears (screen 4), which indicates that records from 73 stations are available on the Web site for this event. By studying the map, the users may localize their request further, zooming in again and again. (In the current version county boundaries are dropped at the third zoom level. Also, some intermediate re-zoom steps are necessary in going from screen 3 to 4 and 4 to 5). Finally, users may identify the station they want to know about the data for; and in this example the Newhall station has been selected (screen 5). The user learns that the station had a peak acceleration of 0.61 g in Northridge. If desired, the user then selects "View Data for Selected Quake/Station", and panels identical to screens 5 and 6 of the first application (Figure 2) appear, and the user may then elect to download the data after viewing the time-histories and spectra, or consider other stations in the vicinity of the user's building or site.

This application of Web site and database technology has recently been made operational. Dynamically creating screens, as in this application, is significantly more complex than presenting fixed screens with company logos, etc, which is most common on the Web. The present version is not as powerful as CSMIP desires, nor as powerful as some users will want once they begin using it regularly. The site is fully operational now, and additional data are being added weekly. CSMIP intends to discontinue the FTP site that has been maintained since 1994 once this site incorporates all the data. The site only includes data from freefield or ground reference stations at the present time, as these constitute the greatest volume of requests to CSMIP. Data from buildings and other structures data will be added in the next phase. Some improvements now being addressed include allowing the download of records without viewing under option 1, and improving the map-zooming operation under option 2 (which turns out to be significantly more complex over the Web than expected). Additional, non-CSMIP data will be added, always with full attribution of the data source, if the source network agrees to their data being added and it appears that there would be significant demand for the data. Old data, for example the 1971 San Fernando earthquake data collected by the Coast and Geodetic Survey and digitized by Caltech, are being added, with attribution, as the data are converted to standard format.

Distribution Policies and Security

There are no charges for downloading data from the Strong Motion Data Center site at this time. The only request of the Department of Conservation's Division of Mines and Geology is that appropriate credit of the source of the data be given in reports and citations so that the value of the data and its utilization can be demonstrated to the agencies funding the data collection and dissemination. Other Web sites, either commercial or private, may desire to download all the records from this site, and distribute the data from a site they set up themselves. Several aspects discourage that. First, only the data at this site will be maintained by CSMIP. As better instrument-correction algorithms or noise removal techniques become available, CSMIP will re-process and update the records in the data base as appropriate. If there were to be an error in sensor orientation or scaling constants for a

record, something that networks like CSMIP work hard to prevent but is still a possibility, the early data would be replaced by the corrected data. Any copies at other Web sites would still be the old version. (This ability to improve the data is an advantage of archiving data through the Web versus using CDROMs. Once a CDROM is made, it is permanent and files can not be changed.)

The second aspect is that the processed data at the Web site are copyrighted by the State of California as part of the quality assurance effort, and legal issues would probably need to be resolved before the data are copied for redistribution. Finally, from the user's perspective, data archived at the CSMIP Web site is virus-free, and anti-virus security programs are automatically run at frequently scheduled times to ensure that the data remain virus-free.

In general, an effective approach for an independent site is to develop and archive information about data and earthquakes, useful for users and reflecting the mission of the organization, but then to simply have an Internet link which passes the user through to this Data Center site when an actual record is desired.

Acknowledgements

The authors acknowledge the comments and input of the Strong Motion Instrumentation Advisory Committee (SMIAC) members regarding the shaking level descriptors. J. Torkelson of the Department of Conservation was instrumental in getting the Web site operational on the Department's Internet server, and Marotz Inc/M. Carry provided important programming support for the data system on the server. In addition, D. Beeby provided important institutional support.

References

Bolt, B.A. (1993). Earthquakes, W.H. Freeman, New York, 331 pp.

Richter, C.F. (1958). Elementary Seismology, W.H. Freeman, San Francisco, 768 pp.

Shakal, A.F. and M.J. Huang (1985). Standard Tape Format for CSMIP Strong-Motion Data Tapes, Report OSMS 85-03, California Division of Mines and Geology, Sacramento.

Shakal, A., C. Petersen, A. Cramlet, and R. Darragh (1995). CSMIP near-real-time strong motion monitoring system: Rapid recovery and processing for event response, in SMIP95 Proceedings, California Division of Mines and Geology, Sacramento.

FEMA-273 SEISMIC REHABILITATION GUIDELINES THE NEXT STEP - VERIFICATION

Ronald O. Hamburger, SE
Senior Vice President, EQE International, Inc.
San Francisco, California

ABSTRACT

FEMA-273/274, *Guidelines and Commentary for Seismic Rehabilitation of Buildings* (ATC, 1996a., b.) represents a landmark in the practice of structural/seismic engineering. In addition to providing a long-needed consensus basis for the design of building seismic upgrades, it also is a first major step towards the development of performance-based design procedures for seismic resistance. Under the *Guidelines*, design is performed with the expectation that for specified levels of ground motion intensity, building performance will remain within anticipated levels. Performance levels are defined in terms of permissible damage to individual structural and nonstructural components and are intended to provide specific defined margins of safety. In order to accommodate this performance-based approach new analytical procedures and acceptance criteria were developed. While the *Guidelines* represent a significant advance in the practice of earthquake engineering, calibration of the analysis procedures and acceptance criteria to real building performance is clearly needed. The use of strong motion data obtained from instrumented buildings experiencing strong earthquake ground shaking will be an essential part of this process.

INTRODUCTION

In the early 1980s, the Federal Emergency Management Agency (FEMA) committed to a plan to facilitate the mitigation of existing hazardous buildings in the United States. This plan included the development of guidelines and resource documents that would permit engineers and building officials to evaluate the existing hazards, estimate the range of costs required to mitigate these hazards through building upgrade programs, and to actually implement such programs. Under this plan, a series of guideline and resource documents were developed. These included ATC-14 (ATC-1987), a methodology for engineering evaluation of buildings to determine if they posed unacceptable risks to life safety; ATC-21 (ATC-1988) a handbook to allow rapid estimation of the probability of severe damage to buildings, based on consideration of building type, age, configuration and siting; FEMA-172 (URS - 1992) a guideline indicating alternative techniques that could be used to implement seismic rehabilitation of buildings; FEMA-178 (BSSC-1992) an update to the evaluation guidelines first presented in ATC-1986 and later modified in ATC-22 (ATC-1989); FEMA-157 (Englekirk & Hart - 1988) a guide to the probable range of costs to perform seismic rehabilitation in buildings; and most recently, FEMA-273/274 (ATC-1996a., b.) *Guidelines and Commentary for Seismic Rehabilitation of Buildings.*

As the program for the mitigation of hazards in existing buildings matured through the 1980s and 1990s, its goals evolved. Initially, the program intent was to encourage owners of hazardous

buildings to upgrade these structure so as to bring the earthquake posed risk to life safety to an acceptable level. The purpose of each of the earlier documents in the series including ATC-1986, ATC-1988, ATC-1990 and FEMA-178 was to permit the identification of buildings that would pose an undue risk to life safety either through collapse, generation of large falling debris or loss of ready egress capability. However, as engineers began to use these resource documents to evaluate buildings, and building owners contemplated programs to rehabilitate their buildings and reduce the existing seismic risk, these owners began to ask for alternatives with regard to the performance the rehabilitated buildings would provide. While some owners were most interested in protecting the safety of the occupants of their buildings, other owners were interested only in preventing their buildings from collapsing and still others, particularly institutions, utilities and large businesses, became interested in minimizing the risk of earthquake induced interruption of the use of their facilities. Therefore, when FEMA commissioned the development of the rehabilitation guidelines document, in 1991, it sought to produce a document which would permit engineers to address each of these performance goals that were commonly being requested by the public.

Although not originally intended as such, the development effort for the *Guidelines for Seismic Rehabilitation* was to become the vanguard for a long series of research and development efforts intended to develop performance-based seismic design procedures. FEMA turned to a partnership of the American Society of Civil Engineers (ASCE), the Building Seismic Safety Council (BSSC) and Applied Technology Council (ATC) to develop this document. ASCE was responsible for the development of a data base of pertinent research results from the literature for use by the Guideline writers, as well as to provide consultation on issues relating to archaic construction systems and historic preservation and to hold a series of workshops to obtain input on the development of the *Guidelines* from various stakeholder groups. BSSC managed the program and also provided a consensus balloting process for review and approval of the *Guidelines*. ATC was responsible for developing the actual *Guidelines* and *Commentary* documents, through the assembly of a large team of researchers and structural engineering practitioners.

The performance-based design approach adopted by the Guidelines has three basic components. The first of these is the specification of a performance objective, comprised of an anticipated performance level and the design earthquake ground motion at which this performance is to be achieved. Performance levels are defined in terms of permissible levels of damage to individual building components and were formulated with the intent of providing specific margins against failure. The second component of the performance-based design approach is structural analysis. Analysis predicts the demands (forces, deformations, etc.) on the individual components and is performed in order to determine if a design is capable of meeting the selected performance objectives. Acceptance criteria provide the third component of the performance-based design process. Acceptance criteria are limiting values of component forces and deformations, against which the component demands predicted by the structural analysis are evaluated, in order to determine design acceptability.

STRUCTURAL PERFORMANCE

Three discrete structural performance levels are defined in the *Guidelines*. These are respectively termed the Immediate Occupancy Level, the Life Safety Level and the Collapse Prevention Level. The Immediate Occupancy Level is a damage state in which the building has experienced only very limited damage, perhaps consisting of minor yielding and cracking of elements. Structures meeting this performance level would retain nearly all of their pre-earthquake strength and stiffness and would be structurally safe for immediate post-earthquake occupancy. Repairs, if required, could be performed at the convenience of the owner and occupants. The Life Safety Level is a damage state in which the building has experienced significant damage to its structural components including yielding, cracking, spalling, and buckling, and perhaps, limited fracturing. Buildings meeting this level have substantially reduced post-earthquake stiffness and may have somewhat reduced post-earthquake strength. Such structures will generally require structural repair and may be judged unsafe for post-earthquake occupancy until such repairs can be made or at least, temporary shoring and bracing is installed. The Collapse Prevention Level is a state in which extreme damage, short of collapse, has occurred to the structure. Buildings damaged to this extent may experience large permanent lateral drifts as well as extensive localized failures of structural components. The stiffness of such a structure would be substantially degraded and the lateral strength may also be significantly reduced. Such buildings would not be safe for post-earthquake re-occupancy and may not be economically practical to repair and restore to service.

Both the Collapse Prevention and Life Safety performance levels have associated with them, a target margin against collapse. Margin may be thought of as the inherent factor of safety between the loading that the structure is designed to resist and the loading that would produce failure. When buildings are subjected to strong earthquake ground shaking, they generally behave in an inelastic manner. Although the building code provisions for earthquake design have typically been based on providing minimum specified levels of lateral force-resisting capacity in a structure, force is not a particularly useful design parameter for predicting the margin of a structure that is responding within the inelastic range of behavior.

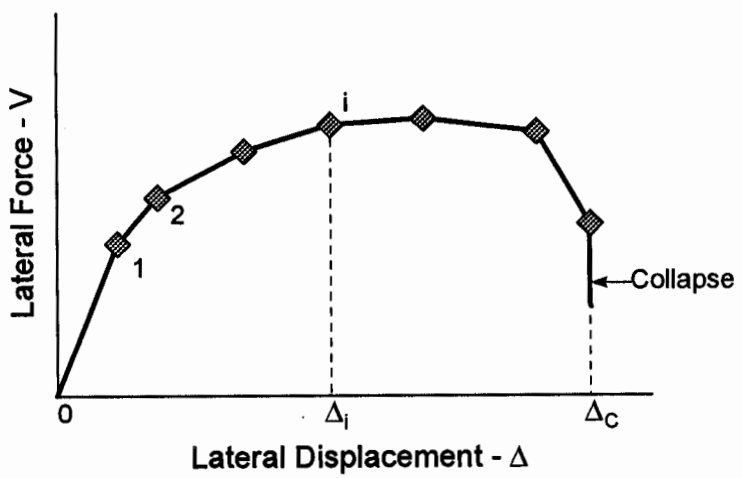

Figure 1 - Lateral Force - Displacement Curve

Figure 1 depicts the force-deformation behavior of a simple structure with the ability to respond to ground shaking in a non-linear, or inelastic manner. The vertical axis of this figure is the applied lateral force on the structure, V, and the horizontal axis is the resulting lateral displacement of the structure. At point "0" there is no lateral loading of the structure. The portion of the curve between points "0" and "1" represents the range of elastic behavior, in which no damage has occurred and the structure retains all of its strength and stiffness. As the structure is loaded beyond point "1" on the curve, damage events such as cracking, yielding, or buckling of elements, indicated by the symbol "◆" in the figure, start to occur. Each damage event results in a degradation of the structure's lateral stiffness and may also result in a degradation of lateral strength. As can be seen from the figure, once several damage events have occurred, lateral force becomes a relatively insensitive parameter by which to judge the structure's performance, since a wide range of different damage states can occur at a relatively constant level of applied lateral force. Because of this, FEMA-273 selected lateral displacement as the basic parameter by which structural performance is judged or controlled. In the figure, at any point "i" on the curve, the margin against failure can be defined as the ratio of the displacement at which collapse is likely to occur, Δ_c, to the displacement at point "i", Δ_i.

Figure 2 presents a curve similar to that of Figure 1, except that the FEMA-273 performance levels have been superimposed on the curve. As can be seen, the Collapse Prevention performance level is defined to have a margin of 1.0 against collapse. That is, the maximum lateral displacement induced in a structure meeting the Collapse Prevention performance level should not exceed the lateral displacement at which collapse is likely to occur. The Life Safety performance level is defined to have a margin of 1.33. This implies that the maximum lateral displacement induced into a structure meeting the Life Safety level is 1/1.33 or 3/4 of the lateral displacement at which collapse is likely to initiate. The Immediate Occupancy level does not have a specific margin associated with it, but instead, is achieved by maintaining damage to individual components of the structure to very low levels.

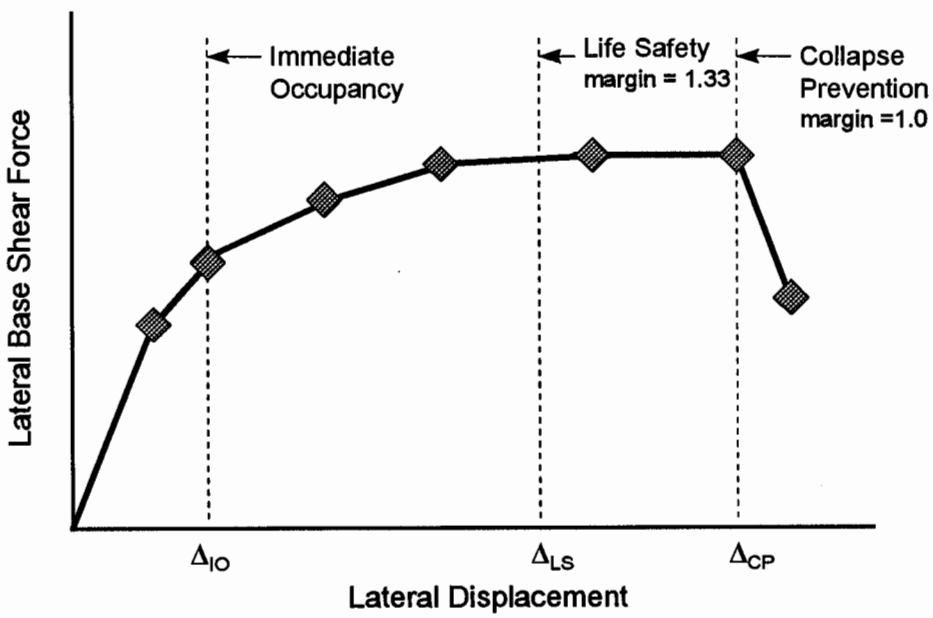

Figure 2 - FEMA-273 Performance Levels and Margins

STRUCTURAL RELIABILITY CONCEPTS

It is important to note that it is very difficult to predict a specific lateral displacement at which a structure will collapse, particularly in the case of earthquake induced collapse. There are a number of parameters that effect the displacement at which a structure will collapse. Some of these we can readily understand and predict, given the state of current engineering technology. For example, the amount of gravity load that a structure is supporting effects the amount of lateral displacement it can experience without developing P-Δ instabilities and collapsing. It is relatively easy for us to understand this relationship and also to predict the amount of gravity load a structure is supporting. There are other parameters that effect the likelihood of structural collapse at a given lateral displacement, the effect of which we can understand, but the actual values of which we have difficulty predicting. One such parameter is the yield or compressive strength of the actual materials present in the structure. We can understand that if the structural materials have relatively large strength, compared to the design values, that it will be less likely for the structure to collapse at a given displacement. However, without extensive testing of the properties of each of these materials, we have difficulty predicting what the actual strength of these materials in the structure is. There are still other parameters that affect the displacement at which a structure will collapse that we can neither understand nor predict, given today's technology and state of practice. As we continue to study the behavior of earthquakes and structures affected by them it is our hope that we can eventually understand all of the parameters that affect collapse and become better at predicting values for them.

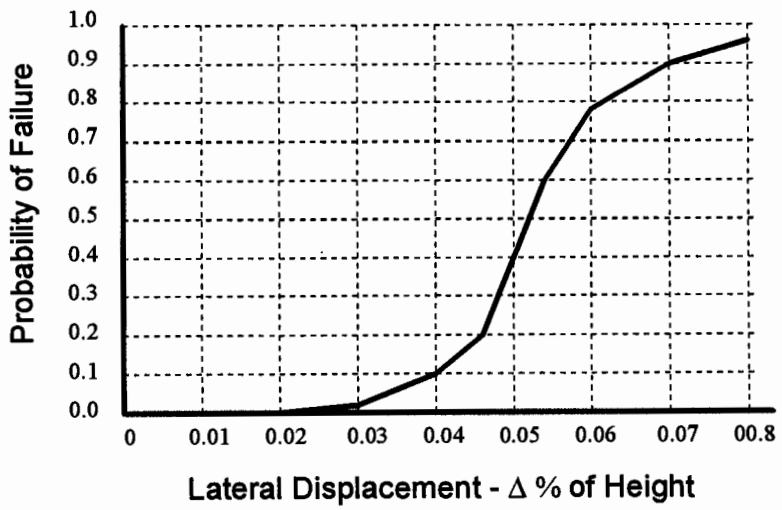

Figure 3 - Typical Structural Fragility

Since we do not currently have perfect knowledge of the parameters that control the displacement at which a structure is likely to collapse nor an ability to predict values for all of them, it is necessary to express the displacement at which collapse is likely to occur, Δ_c, in a probabilistic manner. In order to do this, reliability analysts typically use the concept of a fragility curve. A typical fragility curve is shown in Figure 3. As shown in the Figure, this curve expresses that at lateral displacements equal to approximately 2% of the story height, or less, there is a negligible probability of collapse for the structure represented by this curve while at lateral displacements equal to 8% of the story height, collapse is almost a certainty. This variation in the capacity of the

structure to resist collapse as predicted by lateral displacement, Δ, in this case ranging from 2% to 8%, is a measure of our lack of understanding and inability to perfectly predict the behavior and results in what appears to be behavioral randomness.

This randomness has commonly been observed in past earthquakes. For example, it is not uncommon to find discussion in earthquake reconnaissance reports of cases of two or more apparently similar structures, located near each other, and apparently having experienced similar ground motion, but exhibiting markedly different post-earthquake damage states.

In the previous discussion our current inability to perfectly predict the lateral displacements at which collapse will be induced in a structure were discussed and expressed as an apparent randomness in structural behavior. In addition to our inability to perfectly predict the displacement at which a structure will collapse, we also have an inability to perfectly predict the lateral displacement that an earthquake will induce in a structure. Prediction of the ground motion characteristics that will result from even a specific magnitude earthquake along a fault located a known distance from the site has associated with it a great deal of uncertainty. Further, given an estimate of the ground motion response spectrum or even time histories from a given earthquake, there is an uncertainty, or potential error, associated with our ability to estimate the lateral displacement induced in the structure by this ground motion.

In structural reliability analysis, the uncertainties associated with our ability to perfectly predict the behavior of a structure are often dealt with by establishing levels of confidence around our prediction. Figure 3 presented a fragility function for a typical structure, in which the randomness of structural behavior was represented. Figure 4 presents an expanded fragility function for this structure in which both this randomness and also the uncertainty inherent in our ability to predict failure are expressed. The uncertainties are represented by a family of fragility curves respectively representing the confidence associated with our prediction of structural behavior. In the Figure, three levels of confidence are indicated. One curve, representing our best estimate of the failure probabilities for the structure is labeled as a median confidence level. Located above the median curve is a curve representing a 90% confidence level of non-exceedance. That is every point on the 90% curve indicates a probability of failure, at a given lateral displacement, that we are 90% confident will not be exceeded. Similarly, the lower curve represents a 10% confidence level of non-exceedance. Though curves representing three specific confidence levels have been shown in the Figure, in reality an continuous spectrum of curves representing different confidence levels could be drawn.

The effect of considering uncertainty in evaluation of structural fragility is to further increase the variation in behavior already resulting from randomness. In the earlier discussion, related to Figure 3, it was indicated that there was a negligible probability of collapse of the structure if it experienced an earthquake induced lateral displacement equal to 2% of its height. If we add in uncertainties, such as our ability to predict the lateral displacement induced in the structure, then Figure 4 tells us that once our prediction of lateral displacement demand exceeds about 1.5% of story height, there starts to be a non-negligible probability of collapse. Similarly, Figure 3 indicated a near certainty of collapse at a lateral displacement demand of 8% of story height, while Figure 4 indicates that a significant potential for collapse not to occur at predicted lateral displacement demands in excess of 8%.

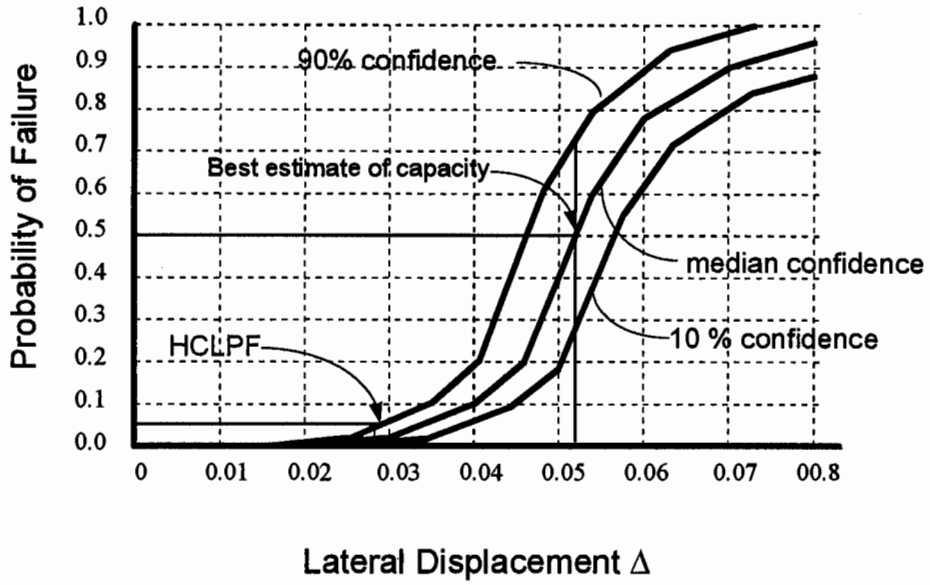

Figure 4 - Randomness and Uncertainty in Structural Fragility Evaluation

Two important points are represented in Figure 4. One of these occurs on the curve for a median confidence level, at a 50% probability of failure. This represents the best estimate of the lateral displacement demand at which collapse will occur, in this case, a lateral displacement of 5.2% of the structure's height. Although this may be our best estimate of the loading that would actually produce collapse, it would be an inappropriate point upon which to base a design since half of our structures would collapse if designed to this performance. The second point occurs at a somewhat arbitrarily selected 90% confidence level of less than a 5% chance of failure. This point, which in the figure has a value of 2.8% of structural height as a lateral displacement demand, is termed the point of High Confidence of Low Probability of Failure or HCLPF. The HCLPF is a more reasonable point upon which to base a design in that only a very few structures would actually be expected to fail when subjected to HCLPF loading.

In previous discussion, structural margin was described as the ratio of lateral drift demand at collapse, Δ_c, to that produced by a given design demand level, Δ_i. At this point, it is possible to redefine this margin as being the ratio of the HCLPF lateral drift demand to the demand, Δ_{HCLPF}, to that produced by a given design demand level, Δ_i. Although this concept was not specifically expressed in this manner, it was clearly considered in the development of the FEMA-273 *Guidelines* and accompanying *Commentary*. The *Commentary* notes that there are no guarantees that a structure rehabilitated using the procedures contained in the *Guidelines* will actually meet the expected performance levels when subjected to the design earthquake ground motions and that perhaps, one or two such structures out of every hundred, may fail to meet the expected performance.

The randomness and uncertainties inherent in the prediction of structural behavior are specifically dealt with in the *Guidelines*. Uncertainty is evaluated with the use of adjustment factors, selected based on the type of analysis performed and the engineer's knowledge of the way in which the structure was actually constructed. Randomness is evaluated in the selection of ground motion

loading criteria and in the evaluation of component capacities. These issues are discussed in the following sections.

STRUCTURAL ANALYSIS

Once a target performance level has been selected for a structure and a preliminary design developed, the Guidelines require that an analysis be performed to determine the structural demands and their acceptability. Four analytical procedures are contained within the Guidelines. These include a linear static procedure (LSP), a linear dynamic procedure (LDP), a nonlinear static procedure (NSP) and a nonlinear dynamic procedure (NDP).

Linear Static Procedure. The LSP is the least accurate of the four procedures, and therefore, introduces the greatest amount of uncertainty into the process of predicting performance. It is also the simplest procedure. It was developed to provide a counterpart to the equivalent lateral force (ELF) procedure commonly used by designers of new buildings under the code provisions. Though the LSP resembles the ELF procedure in many ways, there are significant differences. Both the ELF and LSP are simplified applications of the response spectrum analysis technique in which the dynamic properties of the structure (structural period, mode shape, modal participation) are taken based on simple default values rather than being calculated through rigorous analysis. However, while the ELF is used to proportion structures with a minimum lateral force-resisting strength, the LSP is used to predict the amount of lateral displacement demand that the structure will experience from a design earthquake motion.

The LSP starts with estimation of the structural period, T, for the building. This may be calculated using principles of structural mechanics, such as the Rayleigh equation, by performing a dynamic analysis, or by using simple approximate period formulae, similar to those contained in the building code. Once the building's period has been estimated, the spectral acceleration, from a 5% damped acceleration response spectrum, S_a, is obtained. If real buildings were simple single degree of freedom systems, it would be possible to obtain the spectral displacement, and consequently, the lateral displacement demand directly from the known values of the spectral response acceleration, S_a and the structural period, T, using the relationship:

$$S_d = \frac{T^2}{4\pi^2} S_a \qquad (1)$$

Then, it would be possible to adjust the calculated spectral displacement demand, which represents the response the structure would experience if it remained elastic, to the displacement that it will experience when it exhibits inelastic behavior. This adjustment is possible because over the years, a number of researchers have performed a series of analyses in which they have compared the predicted response for a simple, elastic, single degree of freedom system, to that obtained from more complex models using nonlinear time history analyses. These studies have permitted the development of a series of correlation coefficients that relate the displacement predicted by elastic response spectrum analysis to that predicted by the inelastic time history analyses. These coefficients are a function of the modal properties of the structure (period, and mode shape), the effective damping inherent in the structure (a function of the ductility demand

and the fullness of the hysteretic loops for the structure), and the extent to which strength degrades with increasing repeated cyclic motion. To account for these effects, FEMA-273 adopts a modified form of equation (1) expressed as follows:

$$\Delta = C_0 C_1 C_2 C_3 \frac{T^2}{4\pi^2} S_a \qquad (2)$$

In equation (2), Δ is the lateral drift demand induced in the structure by the ground motion, C_0 is a coefficient to adjust spectral displacement to structural displacement, based on the modal shape properties of the structure; C_1 is a correlation coefficient that relates the response of a perfectly elastic structure, to a structure that has elastic-perfectly plastic inelastic response characteristics; C_2 is a correlation coefficient that adjusts the estimated inelastic displacement demand for the effects of pinching in the hysteretic behavior of the structure; and C_3 is a correlation coefficient that adjusts the inelastic displacement demand for the effects of strength degradation in the structure. These effects are illustrated in Figure 5.

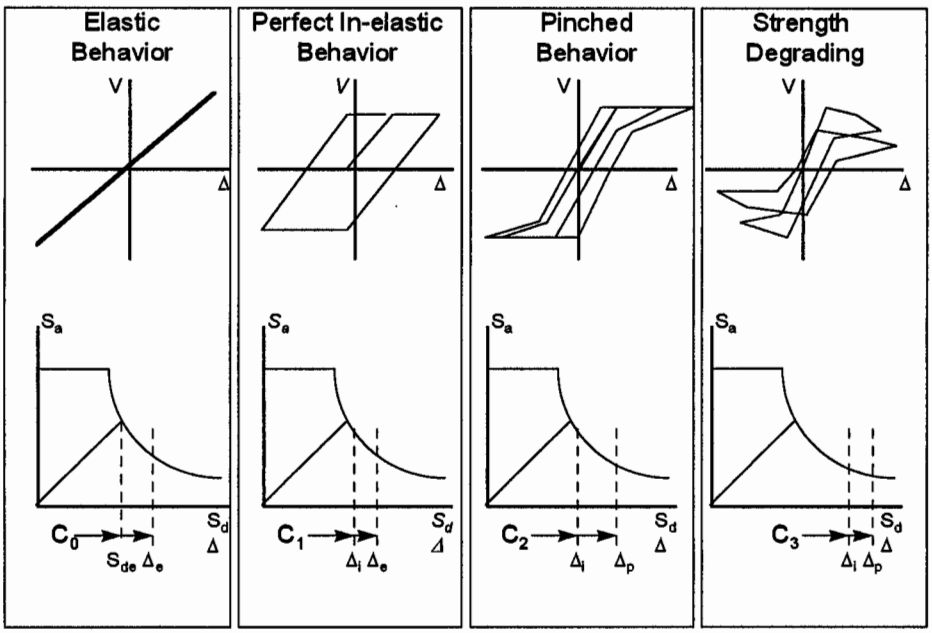

Figure 5 - Correlation of Elastic and Inelastic Behaviors

Structures are complex assemblies of components, including walls, diaphragms, braces, frames, etc., each of which has different capacity to resist earthquake induced lateral displacement. This assembly is made even more complex when new components, provided to increase the building's earthquake resistance are added, since these will typically be detailed in accordance with contemporary practice and will have often have significantly larger lateral displacement capacity than do the brittle elements of many existing buildings. Therefore, the use of a single lateral displacement, Δ, as implied by equation (2) was found not to be useful for real existing buildings. Instead it was decided to evaluate structural performance based on the effects of lateral displacement demand on the individual elements.

In order to do this, an equivalent lateral force, V, is calculated, which when applied to an elastic model of the structure, will provide the same displacement in the structure as predicted by equation (2). This force is calculated from the equation:

$$V = C_0 C_1 C_2 C_3 S_a W \qquad (3)$$

where the terms C_0, C_1, C_2, C_3, and S_a have the same meaning and use as in equation (2), and W is the effective weight of the structure. This equivalent lateral force is applied to a mathematical model of the structure, which is then analyzed for static response under this force to determine the total lateral displacement as well as the individual forces and deformations on the various structural components. Two basic assumptions are made at this point. One is that the distribution of deformation demands in the real structure, which is behaving in an inelastic manner is the same as the distribution of deformation demands predicted by this elastic static analysis. For structures that are reasonably regular, and in which the inelastic behavior is distributed throughout the structure, this is a reasonable assumption. The second assumption is that the ratio of the force calculated in each of the structural components from this elastic, static analysis, to the yield capacity of the component, can be used as a direct measure of the inelastic ductility demand on the component. The accuracy of this assumption was not explored in depth by the developers of the Guidelines, but was felt to be a necessary simplification for the LSP.

With the above two assumptions in place, the ability of a design to satisfy the intended performance is judged by comparing the computed force demands on each structural component to a permissible strength capacity. For components capable of significant ductility, the permissible strength capacity is taken as a value that is greater, by a factor m, than the expected yield strength of the component. The *Guidelines* provide tabulated values for these m factors, for different types of structural components and for each of the various performance levels. For components that are not capable of significant ductility and instead are subject to brittle failure if excessively loaded, the forces predicted by the linear analysis are adjusted, by a coefficient C_4, to account for the fact that forces in a structure that responds in-elastically are lower than those in a structure of similar stiffness but that has adequate strength to respond elastically. These adjusted forces are then evaluated against a lower-bound estimate of the probable strength of the component. Further discussion of these issues is contained in the discussion on acceptance criteria, below.

If a structure is very irregular and has large ductility demands, the use of the LSP introduces a great deal of uncertainty into the prediction of demands on the various components. Also, since the LSP is based on the response of a single degree of freedom system, it can be quite inaccurate (introducing uncertainty) when the response of the structure has significant participation by higher modes. Therefore, the Guidelines prohibit the use of the LSP in highly irregular structures, subjected to large ductility demands and strongly recommend that it not be used for structures with significant higher mode participation.

Linear Dynamic Procedure. The LDP is very similar to the LSP, except that instead of performing an elastic static analysis, using lateral forces intended to represent the inertial forces that would be calculated in a dynamic analysis, a dynamic analysis is actually performed. The dynamic analysis can consist either of an elastic response spectrum analysis or of a suite of elastic time history analyses. In a manner similar to the building code, if time history analyses are used at

least three analyses, using different time histories, scaled to match the design response spectrum must be performed, and the maximum of each of the member forces and structural displacements calculated from the three analyses are used to check acceptability of performance. If as many as seven analyses are performed, using different time histories scaled to match the design spectrum, then the average of the member forces and structural displacements predicted by the suite of analyses may be used to evaluate design acceptability. This approach is taken as a means of dealing with the uncertainty inherent in the use of any single ground motion record to represent the effects of a future earthquake. Due to the complexity involved in performing these multiple analyses, as well as the difficulty of reviewing and interpreting the results of a time history analysis, most designs employing the LDP will use the response spectrum method of analysis.

Just as with the LSP, when an LDP is performed it is necessary to adjust the results of the analysis to correlate with the probable behavior of the structure when it behaves in-elastically. Therefore, the member forces and structural displacements predicted from the elastic dynamic analysis are scaled by the combined term $C_1C_2C_3$, with each of these coefficients having the same value and same intent previously described for the LSP. It is not necessary to modify the results of an LDP by the coefficient C_0 because the effects of modal participation are directly accounted for by the dynamic analysis. The acceptability of structural performance is evaluated in the same way previously described for the LSP.

Nonlinear Static Procedure. The NSP is a type of analysis commonly known as a push-over analysis. It is intended to reduce the uncertainty inherent in both of the linear analysis procedures, by directly accounting for the non-linear behavior of the structure. It is performed as a series of linear static procedures, using sequentially modified versions of the mathematical structural model to represent the degradation in stiffness that the structure experiences as it is subjected to larger lateral deformations and becomes damaged. In the process of performing these analyses, a push-over curve, similar to those shown in Figures 1 and 2 is plotted for the structure, allowing direct evaluation of the structure's performance.

To perform an NSP a mathematical model of the structure is developed. The model must include the effects (stiffness and strength) of all elements that are significant to the behavior of the building. An element is significant if it contributes a significant amount of stiffness or strength to the overall structure, or, if it is likely to be damaged as a result of earthquake induced lateral deformation of the structure. This initial structural model is analyzed for an arbitrary static lateral force. The forces induced in each member of the model due to this lateral force is determined and compared against a best-estimate of the yield capacity of the various members, to provide demand-capacity ratios (DCRs). These DCRs are reviewed to determine the largest value. The member with the largest DCR is the one that will first experience damage or yielding, when the structure is subjected to an increasing lateral displacement. The entire analysis is scaled by a factor such that the largest value of the computed DCRs for the members has a value of 1.0, indicating that at the lateral displacement predicted by this scaled analysis, yielding in the structure initiates. The forces in each member are at this load step are recorded and the value of the total applied lateral force and corresponding displacement are plotted as the first damage event on the pushover curve.

To obtain the next point on the pushover curve, the mathematical model is modified to reduce the stiffness of the member that has yielded to an appropriate post-yield value. Again, a static lateral force is applied to this modified mathematical model and an analysis is performed to determine the various member forces. These demand forces are compared to the residual capacities of each of the various members. The residual capacities are simply obtained by subtracting from the initial member capacity, the demand force obtained at the previous load step. DCRs are again computed for all of the members, using these residual capacities. Again, a scale factor is determined such that the largest DCR from this analysis will have a value of 1.0. The analysis is then scaled by this factor and the resulting forces and displacements from the scaled analysis are added to those obtained from the first analysis step. The total applied lateral force (force in the first scaled analysis plus the force in the second scaled analysis) and the total lateral displacement (lateral displacement form the first scaled analysis plus the lateral displacement from the second scaled analysis) are then plotted as the second damage event on the push-over curve.

This entire process is repeated, with the mathematical model revised each time to represent the reduction in stiffness that occurs with each successive damage event until it is found that the structure has become unstable, predicting the onset of collapse. This pushover curve represents one estimate of the capacity of the structure. One of the uncertainties inherent in this analysis approach is that the actual pattern of inertial forces, that will drive the real structure during an earthquake are being estimated. In order to bound the effects of this uncertainty, the Guidelines specify that when the NSP is used, two independent analyses should be performed, each using a different assumption as to the vertical distribution of lateral forces in the structure. One loading pattern is the inverted triangular distribution of forces, used in the ELF procedure in the building codes. The second pattern is that which results from a uniform inertial acceleration of the structure (rectangular distribution of loading). The triangular distribution is a reasonable approximation of the lateral forces that will occur when a building is responding in the elastic range, while the rectangular distribution is representative of the loading that will occur on a structure that has formed an inelastic soft story. Together, these analyses should bound the capacity of the structure.

The next step is to predict the demand produced by the design earthquake. In order to do this, the pushover curve obtained from the analyses are represented by an equivalent elastic-perfectly plastic curve. The stiffness of the elastic portion of this equivalent curve is obtained by drawing a line from the origin of the curve, through the point on the pushover curve that occurs at a lateral force that is 60% of the maximum lateral force obtained in the analysis. This is illustrated in Figure 6. The slope of the elastic portion of the idealized pushover curve is next determined. This slope represents the stiffness of an idealized single degree of freedom structure, having dynamic characteristics similar to that of the structure. The period of this idealized structure, T_e, is determined from the equation:

$$T_e = T_i \sqrt{\frac{K_i}{K_e}} \qquad (4)$$

where T_i is the initial elastic period of the actual structure, K_i is the initial elastic stiffness of the actual structure, obtained as the slope of the initial segment of the push-over curve and K_e is the effective stiffness of the idealized elastic-perfectly plastic structure, as shown in Figure 6.

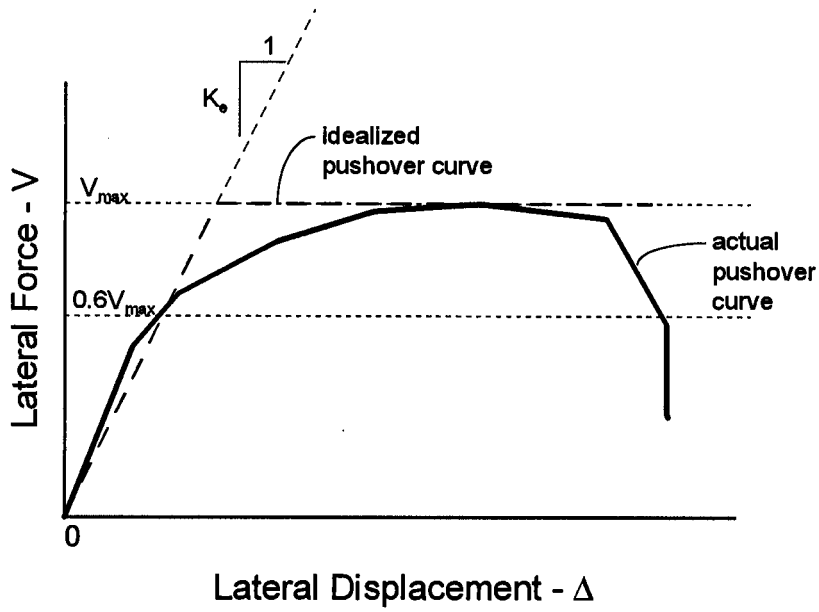

Figure 6 - Use of Pushover Curve to Determine Demand

Once the effective period, T_e, for the structure has been determined, the displacement demand is determined from equation (2), substituting T_e for T and evaluating S_a at period T_e. The coefficients C_0 and C_1 are evaluated in the same manner as for the linear procedures. The coefficients C_2 and C_3 are determined using the actual characteristics of the pushover curve.

Following determination of the demand, Δ, termed the target displacement in the *Guidelines*, it is necessary to determine the acceptability of the structural performance. This is performed by comparing the actual deformation demands for the various members at lateral displacement Δ, against the acceptance criteria presented in the *Guidelines* for the various performance levels.

The NSP entails a significant reduction in uncertainty, with regard to the prediction of building behavior, than do either of the linear procedures, except when the effects of higher modes are significant to the structure. If higher mode effects are significant, the NSP can introduce a significant error into the estimated performance. Therefore, for structures with significant higher mode response, the NSP is not recommended unless an LDP is also performed. Alternatively, an NDP analysis can be performed.

Nonlinear Dynamic Analysis. A nonlinear dynamic analysis is potentially the most accurate (least uncertain) of all of the various analysis procedures contained in the *Guidelines*. In this procedure, a non-linear mathematical model of the structure is developed and subjected to a series of time-history analyses. To the extent that it is possible to accurately model the building and the ground motion, many of the analytical uncertainties inherent in the other analysis procedures are eliminated with this approach. However, in reality it is not practical at the current time to reliably implement this approach for complex structures. There are currently few consensus models

available to represent the behavior of the many of types elements that are found in our existing structures. Since relatively small changes in the way elements are modeled can have significant effect on the results predicted by such analyses, use of this technique can create the impression of highly certain results without actually providing such accuracy. Therefore, the Guidelines recommend that when this approach is employed, independent third party review of the assumptions and approach should be performed by a knowledgeable expert. As with the LDP, suites of several different ground motion time histories should be used in the analyses to account for the variation and uncertainty inherent in the prediction of the ground motion. Analysts employing this approach should also consider running sensitivity studies and suites of analyses to explore the uncertainty inherent in various modeling assumptions employed in the analysis.

When the NDP is employed, the analysis directly predicts maximum values of member forces and deformation demands. These are compared against the acceptance criteria provided in the *Guidelines* to evaluate the predicted performance of the structure.

ACCEPTANCE CRITERIA

The acceptability of structural performance is evaluated on a structural component basis. In the *Guidelines*, structural components are classified as being force controlled or deformation controlled. Deformation controlled components are those that have significant ductility while force controlled components do not. In order to develop acceptance criteria for the document, an extensive literature search was conducted to determine typical hysteretic curves for the various types of structural components common in our existing buildings, based on past research. Where research data could be found for an element type, it was represented by a "backbone" curve. The backbone curve, illustrated in Figure 7, is an envelope of the hysteretic behavior of the component, taking into account the degradation that occurs under repeated cycles of motion to the same displacement level.

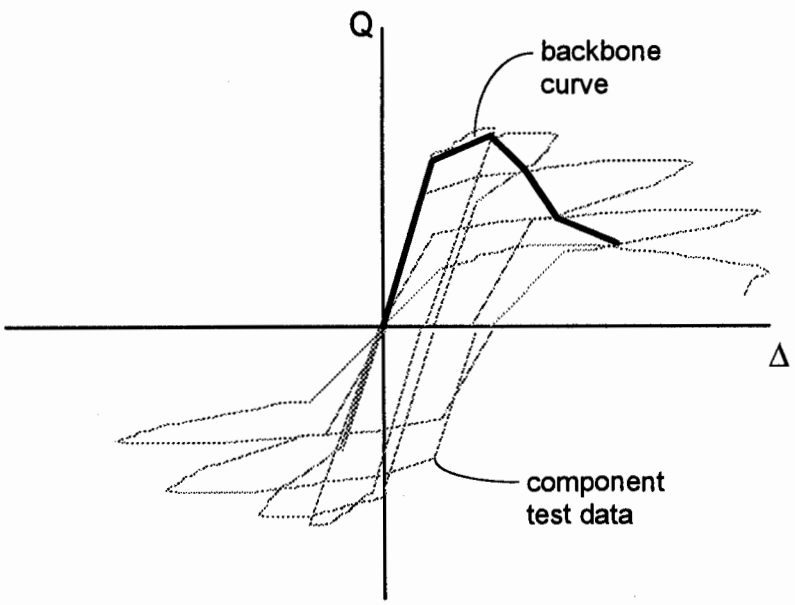

Figure 7 - Development of Backbone Curve from Hysteretic Data

Each of the backbone curves obtained from the available research data were represented by one of three idealized shapes, represented in Figure 8. The type 1 curve represents a ductile behavior in which there is an elastic range (points 0-1), a plastic range (points 1-2), and a strength degrading range (points 2-3). An example of a structural component that exhibits this type of behavior are steel beam-column connections with partially restrained joints. The Type 2 curve represents components with ductile behavior but a rapid degradation of strength after a limiting ductility is reached. Steel braces loaded in compression would be represented by such behavior. The type 3 curve represents a non-ductile or brittle behavior, such as may occur in an unconfined concrete element beam or column. Where specific research data could not be found on the behavior of a particular type of structural component, the developers of the *Guidelines* developed a "best-estimate" of such behavior based on judgment, thus introducing another source of uncertainty in the document.

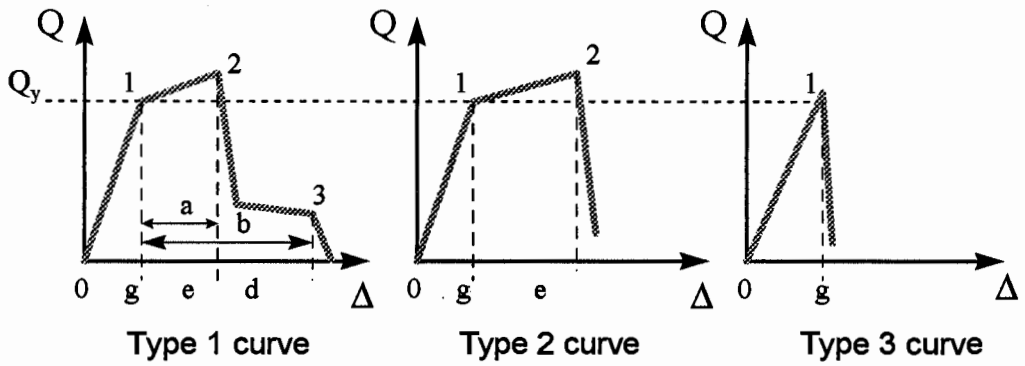

Figure 8 - Idealized Backbone Curves

The acceptance criteria (permissible forces and deformations) for the various structural components and performance levels were determined from these idealized backbone curves. As stated earlier, for Collapse Prevention performance, the intent is that there be a margin of 1.0 against failure. Therefore, for deformation controlled components, the acceptance criteria is that the predicted member deformation not exceed point "2" on the corresponding backbone curve. For force controlled components, the computed force on the component can not exceed a lower bound estimate of the yield (or ultimate) capacity of the component. For Life Safety performance, the desired margin has a value of 1.33. Therefore, the acceptance criteria for Life Safety performance is that the member deformation for deformation controlled elements not exceed 75% (1/1.33) times the deformation at point "2" of the corresponding backbone curves. For force controlled components, the total force on the component can not exceed 75% of a lower bound estimate of the yield (or ultimate) strength of the component. These permissible values are tabulated in the Guidelines, categorized by component type.

When either an NSP or NDP is performed, the component deformation demands and forces predicted by the analyses can directly be compared against the acceptance criteria obtained from the backbone curves and discussed above. However, when an LSP or LDP is performed, the analysis does not directly predict component deformation demands. Instead the analysis provides estimates of member forces, which often will exceed the member yield strength. In order to determine the acceptability of the behavior of deformation controlled components, the following equation is used when a linear procedure has been performed:

$$Q \leq m\kappa Q_{CE} \qquad (5)$$

In equation (5), Q is the value of the total computed strength demand on the component from the analysis, including the effects of dead and live loads. Q_{CE} is the expected, or median, value of the yield strength of the component, Q_y in Figure 8. The coefficient κ is intended to reduce the permissible capacity of the structure to account for uncertainty resulting from a lack of knowledge as to how the structure is actually constructed. It has a minimum value of 0.75 when relatively little knowledge is available as to the construction of the structure to a maximum value of 1.0 when extensive knowledge of the structure's construction has been obtained. The coefficient "m" is a ductility coefficient, obtained from the equation:

$$m = 0.75\delta_i \qquad (6)$$

where δ_i is the acceptable deformation for the component and performance level if a nonlinear analysis procedure is used, as has previously been described. The purpose of the 0.75 factor in equation (6) is to account for the additional uncertainty inherent in the prediction of component demands when a linear analysis procedure is used as opposed to a nonlinear procedure and also to account for the uncertainty inherent in the assumptions that a demand/capacity ratio computed on the basis of forces is an accurate representation of inelastic deformation demands.

For force controlled components, acceptance is evaluated using the equations:

$$Q_G + \frac{Q_E}{C_0 C_1 C_2 C_3 C_4} \leq Q_{CL} \qquad (7)$$

In the above equation Q_G is the force in the component due to gravity loads, Q_E is the computed force due to earthquake demands and the coefficient C_0 through C_4 have the meaning previously described. The quantity on the left side of equation (7) is intended to represent a best estimate of the actual force that can be delivered to a brittle component by the structure, considering its inelastic behavior. This is a very approximate estimation with a significant inherent uncertainty. Q_{CL} is a lower bound estimate, taken at a mean minus one standard deviation level, of the yield strength of the component.

THE NEED FOR VERIFICATION

The *Guidelines* represent a significant advancement in the state of practice for earthquake-resistant design of structures. The procedures take into account the actual nonlinear behavior of building structures, in a far more realistic manner than do the building codes, and also attempt to directly account for the randomness and uncertainties inherent in the evaluation process. However, because the *Guidelines* represent such a significant departure from past practice and also because the uncertainties have been accounted for in only a very approximate way, there is a real need to perform verification of the ability of the procedures to actually predict structural performance within the variance previously discussed, i.e., the expectation that when subjected to the design ground motions only 1% to 2% of the affected structures would experience worse performance than predicted.

The uncertainties inherent in the prediction of performance by the procedures contained in the *Guidelines* can be attributed to a number of different sources. Principal among these are our inability to accurately predict the character of ground motion that the structure will experience and our inability to accurately model the behavior of the structure when subjected to such ground motion. There is also significant uncertainty with regard to our ability to predict the capacity of components and of the structure itself. In addition to these uncertainties, there is a considerable apparent randomness in both the demand produced on structures and the capacity of structures to resist these demands. In developing the *Guidelines*, a conscious attempt was made to bound this randomness and these uncertainties by attempting to estimate the biases inherent in the various assumptions made in structural modeling and capacity evaluations and also by estimating the levels of confidence associated with various analytical procedures. However, these treatments of the variation were largely performed in a judgmental and qualitative manner, rather than as a result of rigorous reliability investigations. As a result, the procedures may currently contain significant biases, meaning that they may either significantly under-predict or over-predict the performance of buildings in a systematic matter.

If the *Guidelines* systematically over-predict building performance, than an undesirably large number of buildings rehabilitated in accordance with the *Guidelines* will fail to meet the intended performance objectives. Conversely, if the *Guidelines* systematically under-predict performance, than rehabilitation programs designed in accordance with the *Guidelines* will not be optimal in terms of the amount of rehabilitation work that is performed. Neither condition is particularly desirable. If actual performance is poorer than predicted, than a number of buildings may remain hazardous despite being rehabilitated. If the actual performance is better than predicted, then the excessive cost of implementing the *Guidelines*, relative to a more optimal approach will result in the mitigation of relatively fewer structures, and again a greater than desired risk. Clearly there is a need to verify the reliability actually provided by the procedures, with regard to the intended goals.

The use of strong motion data to test and calibrate the *Guidelines* is an essential part of this verification process. Ideally, in order to perform this verification there is a need for strong motion data from arrays that include both free-field and in-structure response recordings for a large number and wide variety of building types and site conditions, together with detailed documentation of the actual performance of the buildings from which this data is obtained. This data, if made available to the structural engineering community, will permit investigators to compare the performance predicted by the *Guidelines* to that actually experienced by real structures. It will also enable the accuracy and variation inherent in each of the individual steps followed in the *Guidelines* to be evaluated. In its simplest form, a comparison of the strong motion data with predicted response obtained from structural analyses can be used to determine the randomness and uncertainty introduced by the four analysis techniques with regard to prediction of lateral displacements. Such investigations can also be used as the basis for modifying the analytical technique so as to reduce the inherent variations as well as to determine the adequacy of limitations currently placed on each analysis technique based on the apparent limitations of reliability.

Strong motion data can also be used to verify the adequacy of acceptance criteria contained in the *Guidelines*. The acceptance criteria are based on values of acceptable deformation in various

structural components. Where hysteretic data from laboratory investigations was available, it was used as the basis for determining acceptance criteria. Unfortunately, no data was available for many of the types of structural components commonly found in existing buildings. Consequently, the developers of the Guidelines were forced to rely on estimates of the probable behavior rather than actual laboratory data. To the extent that strong motion data permits the cyclic deformation demands on elements of real instrumented buildings to be understood, the behavior of these elements in response to these demands can serve to greatly supplement the existing laboratory data and provide a method to benchmark and adjust the acceptance criteria as appropriate.

It is important to note that a large number of analyses of buildings for which strong motion data is obtained must be performed to be useful in this verification process. As previously discussed, the prediction of structural capacity to resist earthquake ground motion inherently includes great variation and apparent randomness. Therefore the ability of a few strong motion data sets to either confirm or apparently call to question the validity of the *Guidelines*, is not by itself meaningful. It is anticipated that some buildings will not perform as well as predicted by the Guidelines and that many buildings will perform better than predicted. In order to provide true verification, it will be necessary to perform a statistically significant series of analyses of buildings for which strong motion data is available so that relative reliability of the *Guidelines* can be appropriately judged.

SUMMARY

FEMA-273/274, *Guidelines and Commentary for Seismic Rehabilitation of Buildings*, is a landmark document that breaks new ground in the practice of performance-based seismic engineering of buildings. It employs new analytical techniques that are far more rational than those employed in standard building code procedures as well as acceptance criteria tied directly to laboratory test data on typical components. However, the complexity of this document as well as the radical extent to which it has departed from previous structural engineering practice suggests that it is likely to need considerable verification and adjustment in order to provide the desired level of economy in structural rehabilitation projects while maintaining acceptable levels of reliability. Application of the *Guidelines* to instrumented buildings from which actual strong motion data has been obtained should be a key part of this verification and adjustment process.

REFERENCES

Applied Technology Council. 1987. *Evaluating the Seismic Resistance of Existing Buildings Report No. ATC-14*. Redwood City, CA.

Applied Technology Council. 1988. *Rapid Visual Screening of Buildings for Potential Seismic Hazards Report No. ATC-21*. Redwood City, CA.

Applied Technology Council. 1989. *A Handbook for Seismic Evaluation of Existing Buildings Report No. ATC-22*. Federal Emergency Management Agency. Washington, D.C.

Applied Technology Council. 1996a. *NERHP Guidelines for Seismic Rehabilitation of Buildings Ballot Draft FEMA 273.* Building Seismic Safety Council. Washington, D.C.

Applied Technology Council. 1996b. *NERHP Commentary on the Guidelines for Seismic Rehabilitation of Buildings Ballot Draft FEMA 274.* Building Seismic Safety Council. Washington, D.C.

Building Seismic Safety Council. 1992. *NEHRP Handbook for the Seismic Evaluation of Existing Buildings FEMA-178.* Building Seismic Safety Council. Washington, D.C.

Engelkirk & Hart. 1988. *Typical Costs for Seismic Rehabilitation of Existing Buildings FEMA-157.* Federal Emergency Management Agency. Washington, D.C.

URS Corp. 1992. *NERHP Handbook for Seismic Rehabilitation of Existing Buildings FEMA-172.* Federal Emergency Management Agency. Washington. D.C.

SHEAR-WAVE VELOCITIES AND DESIGN RESPONSE SPECTRA - AN EXAMINATION USING STRONG-MOTION DATA FROM THE GILROY ARRAY: PRELIMINARY RESULTS

Robert B. Darragh
EERI/FEMA Professional Fellow at the
Department of Civil and Environmental Engineering
University of California at Davis

and

I. M. Idriss
Department of Civil and Environmental Engineering
University of California at Davis

ABSTRACT

Borcherdt (1994) proposed that the short- and mid-period amplification factors used to scale the estimate of site-dependent response spectra could be calculated as a continuous function of shear-wave velocity averaged in the upper 30 m for various input ground-motion levels. This proposal appears to be an improvement for estimating design response spectra over site classifications defined by soil descriptions (e.g., SEAOC, 1988) or by ranges of average shear-wave velocity (e.g., NEHRP, 1991).

However, it is not clear that the accuracy available in current measurements of shear-wave velocity is sufficient to support their use directly in design calculations of motion. For example, at Gilroy #2 there are differences of about 300 m/sec in the shear-wave velocity measurements in the upper 30 m (EPRI, 1993). In this paper, we analyze the effect of variations of shear-wave velocity in the upper 30 m for design applications including the effects of nonlinear soil response using an equivalent-linear site response formulation (Schnabel et al., 1972). The analysis uses the extensive geotechnical site characterization and shear-wave velocity measurements at Gilroy #2, a stiff soil site that has been characterized to a depth of 240 m (EPRI, 1993). Response spectral accelerations from the recorded strong motions are compared to calculated values from the equivalent-linear analyses with several shear-wave velocity profiles in the top 30 m.

The preliminary analyses suggest that the Borcherdt (1994) methodology works well at this stiff-soil site for design levels of motion near 0.4 g, appropriate for many parts of California, even though there is a difference of 60% in the measured average of the shear-wave velocities in the upper 30 m.

INTRODUCTION

The use of the average of the measured shear-wave velocities to a depth of 30 m (100') below the surface was incorporated by Boore et al. (1993, 1994) as a site effect term in the estimation of peak accelerations and response spectral ordinates from earthquake ground motion

attenuation relations. Borcherdt (1994) proposed this average in a methodology to directly estimate the site specific response spectra for design purposes. Thirty meters is selected since in many applications this is the typical depth of geotechnical site investigations that include borings, detailed sample testing and occasionally shear-wave velocity measurements. An ideal parameter may be the average of the shear-wave velocity to a depth of one-quarter wavelength for the period of interest as proposed by Joyner et al. (1981) and used by Joyner and Fumal (1984). However, only soils with an average shear-wave velocity of 120 m/sec or less would be properly characterized with a 30 m boring for a period of 1.0 second. Unfortunately, the necessary velocity measurements to a depth of one-quarter wavelength are not common.

Studies by Day (1996) and Anderson et al. (1996) have found that the response of the upper 30 m of material has a greater influence on surface strong ground motions than might be expected based on total thickness alone. The upper 30 m represents only 0.3% of the seismic wave travel path for an earthquake located directly underneath a site with a typical focal depth of 10 km. The peak acceleration and velocity recorded at the surface were found to be relatively independent of the properties below 30 m in these studies.

In this paper, we analyze the effect of variations of shear-wave velocity in the upper 30 m for design applications including the effects of nonlinear soil response. This variability may limit the use of velocity in design calculations of spectra and time histories. The recorded earthquake response data at Gilroy #2 are compared to those calculated by an equivalent-linear response analysis using the computer program SHAKE91 (Idriss and Sun, 1992) which is a recently modified edition of the original SHAKE program (Schnabel et al., 1972). The motion recorded at Gilroy #1 was used as the input rock outcrop motion in these analyses. The extensive geotechnical site characterization at Gilroy #2 (Fumal et al., 1982; Fumal, 1991; EPRI, 1993) includes shear-wave velocity measurements from several methods to a depth of 240 m. These velocity measurements show considerable variation in the upper 30 m and at greater depths.

The intent of this study is to evaluate the usefulness of the average of the measured shear-wave velocities in the upper 30 m. It is planned to conduct a series of ground response analyses at the Gilroy #2 site for earthquake ground motions recorded during several events to make this evaluation. The best estimate of the measured shear-wave velocities at this site will first be used to compare the calculated with the recorded motions. Such evaluations were done for many sites following the Loma Prieta earthquake and have indicated that this method of analyses provides a reasonable estimate of the recorded motions (e.g., Idriss, 1993; Dickenson and Seed, 1991; Chin and Aki, 1991; Schneider et al., 1991; EPRI, 1993). This study will include calculations for the Gilroy #2 site during the Loma Prieta earthquake and two of its aftershocks in addition to the 1979 Coyote Lake and the 1984 Morgan Hill earthquakes.

These studies are underway and the final results are expected in the summer of 1997. This paper provides preliminary results from the initial parts of the study and should be considered a progress report.

GILROY STRONG-MOTION ARRAY

The Gilroy array is an alignment of six strong motion stations that extends across the alluvial Santa Clara Valley in northern California. This array is a cooperative effort of the

California Strong Motion Instrumentation Program (SMIP) and the U. S. Geological Survey (USGS). The array is currently instrumented and maintained by SMIP. For this analysis, only the earthquake records from Gilroy #1 and Gilroy #2 are used because they are the closest rock and stiff-soil station pair (Fig. 1). Gilroy #1 is located just west of the western edge of the Santa Clara Valley and Gilroy #2 is located 2 km to the east. The soil depth varies from 0 m at Gilroy #1 to about 170 m at Gilroy #2 and deepens considerably to the east across the valley.

GEOTECHNICAL CHARACTERIZATION OF THE GILROY #2 SITE

The Gilroy #2 site has been well characterized to a depth of 240 m (790') during an Electric Power and Research Institute study (EPRI, 1993). In summary, Gilroy #2 is underlain by stiff soil to a depth of 168 m (550'). Loams, sands and clays of Holocene and Pleistocene age are present in the upper 46 m. Extensive deposits of Pleistocene gravels with sands and some clays are found beneath this depth. Bedrock is at a depth of 168 m and is a deeply weathered siltstone of the Monterey Shale Formation. The bottom of the hole is in serpentinite that has been deeply weathered to sandy clay.

EPRI (1993) performed an extensive series of geophysical surveys in the borehole to measure low-strain in-situ P- and S-wave velocities (Fig. 2) to a depth of 240 m. The seven measurements made in the top 122 m (400') show the variability in estimates of shear-wave velocity at this site. For example, in the top 30 m velocity measurements may differ by up to 300 m/sec (1000 ft/sec). In contrast, in the Pleistocene lake deposits all measurements cluster tightly around 305 m/sec. At greater depths, differences in shear-wave velocity of nearly 600 m/sec (2000 ft/sec) are shown.

Table 1 is an interpretation of the velocity structure at Gilroy #2 modified from EPRI (1993). Surface shear-wave velocities of about 230 m/sec more than double to 475 m/sec near 14 m. Beneath this depth the profile contains two low-velocity-zones. The upper zone, with shear-wave velocities ranging from 305 to 375 m/sec, extends from 22 to 42 m and consists of mainly Pleistocene lake deposits and the top of the Pleistocene alluvium. Between these two zones is a thick (40 m) soil with a velocity of 640 m/sec composed of primarily gravels and gravelly sands. The lower zone extends from 82 to 98 m. Shear-wave velocities range from 475 to 525 m/sec and reflect the increased proportion of clay in the soil at these depths. The velocity in the soil from 98 m to bedrock is 700 m/sec again reflecting the presence of gravels at these depths. The bedrock velocity is 1190 m/sec. Profiles of the site geology and the P- and S-wave velocities at Gilroy #2 and #1 are also given in Fumal et al. (1982) and Fumal (1991).

The average shear-wave velocities in the top 30 m and in the entire soil profile at Gilroy #2 are 302 and 578 m/sec, respectively. Using the site classification of Borcherdt (1994), the top 30 m is SC-III (stiff clays and sandy soils), while the entire profile is SC-II (gravelly soils) reflecting the presence of gravels at depths greater than 46 m. The bedrock is also appropriately classified as SC-Ib (firm rock). For comparison, Gilroy #1 is underlain by moderately weathered sandstone at the surface, with thin beds of shale at depth as determined in a 20 m borehole (Fumal et al., 1982; Fumal, 1991). The average shear-wave velocity in the top 20 m is 1230 m/sec and would be classified as SC-Ib (firm rock) by Borcherdt (1994).

In addition, nine undisturbed soil samples were collected for laboratory testing to determine modulus-reduction and damping curves. From the testing sets of curves were

developed for the depth range 0 to 12 m (40'), 12 to 24 m (80'), 24 to 40 m (130') and for deeper than 40 m (Table 2). The effect of gravels in the profile below 40 m produces increased damping and lower modulus-reduction at greater depths. This effect is counter to the effects of increasing confining pressure. Low-strain damping values of 3% (Q=17) were measured in the EPRI (1993) study (Table 2). An extensive discussion of the measurements and testing results are given in EPRI (1993).

EARTHQUAKE RECORDS

The Gilroy array has recorded a large range of earthquake response (Table 3). The recorded earthquakes range in local magnitude (M_L) from 4.3 to 7.0. Peak horizontal accelerations are from 0.04 to 0.37 g at Gilroy #2 with corresponding accelerations of 0.08 to 0.49 g at Gilroy #1. Peak velocities range from 2.2 to 39.2 cm/sec at the soil site with corresponding velocities ranging from 2.7 to 33.8 cm/sec at the rock site (Table 3).

In this preliminary study only the records from the north-south component from the Loma Prieta mainshock are used in the equivalent-linear analyses. The north-south base-line corrected and band-pass filtered acceleration, velocity and displacement time histories for Gilroy #1 and Gilroy #2 are shown in Figure 3. The peak accelerations are 0.43 and 0.37 g on the north-south component of Gilroy #1 and Gilroy #2, respectively. The 5% damped response spectral accelerations for the north-south component at Gilroy #1 and #2 are shown in Figure 4. This component was selected to facilitate comparison with an input level of acceleration of 0.4 g in Borcherdt (1994).

SITE RESPONSE ESTIMATION METHOD

The north-south component of the Loma Prieta mainshock ground motion and spectrum recorded at Gilroy #2 (Figs. 3 and 4) are modeled using the equivalent-linear method to calculate the seismic response of horizontally layered soil deposits that was implemented in the computer program SHAKE (Schnabel et al., 1972; Idriss and Sun, 1992). The program computes the response of a semi-infinite horizontally layered soil deposit over a uniform half-space subjected to vertically propagating shear waves. The analysis is done in the frequency domain, and therefore, for any set of properties is a linear analysis. An equivalent-linear procedure (Idriss and Seed, 1968; Seed and Idriss, 1970) is used to account for the nonlinearity of the soil using an iterative procedure to obtain values for modulus and damping that are compatible with the equivalent uniform strain induced in each sublayer. The recorded north-south accelerations at Gilroy #1 from the Loma Prieta earthquake (Fig. 3) are assumed to be the input motions in the equivalent-linear analysis.

The initial values for shear-wave velocity, modulus-reduction and damping used in the equivalent-linear analysis are from a geotechnical model given in EPRI (1993). Tables 1 and 2 are the low-strain shear-wave velocity, modulus-reduction and damping curves used for the best-fit model, respectively. The shear-wave velocity profile from EPRI (1993) has been slightly modified to obtain a response spectrum from the equivalent-linear analysis that reasonably matches the recorded response spectrum from the Loma Prieta mainshock (Fig. 4).

Figure 4 compares the recorded spectrum at Gilroy #2 with the best-fit spectrum from the equivalent-linear site response analysis. Also shown on the figure is the spectrum of the north-

south acceleration recorded at Gilroy #1 during the Loma Prieta earthquake. The high-frequency energy content in the Gilroy #1 spectrum has been reduced in the equivalent-linear analysis. Over the usable data bandwidth from 0.04 to 7.35 seconds the fit is generally quite good. The predicted peak acceleration value is 0.47 g within 30% of the observed value of 0.37 g.

The low-strain and strain-compatible shear-wave velocities are compared in Figure 5. The low-strain in-situ shear-wave velocity has been reduced significantly in the equivalent-linear analysis. The average velocity in the upper 30 m is reduced 21% from 302 to 249 m/sec. The average low-strain shear-wave velocity in the 170 m profile is reduced 25% from 578 to 465 m/sec. The fundamental period of the soil profile has correspondingly increased from 1.18 to 1.47 seconds.

VARIATION OF SHEAR-WAVE VELOCITY IN THE TOP 30 M

The shear-wave velocity above 30 m at Gilroy #2 is varied in the equivalent-linear model using the measured velocities (Fig. 2). The low-strain shear-wave velocities are not varied from the best-fit model for depths greater than 30 m (Table 1 and Fig. 5). The low-strain modulus-reduction and damping curves are also not varied (Table 2) in the equivalent-linear analysis.

Five velocity profiles for the top 30 m (100') and the low-strain velocity profile used in the best-fit equivalent-linear analysis are shown in Figure 6. The lower and upper shear-wave velocity profiles are from the bounds on the measured velocities (Fig. 2). The average shear-wave velocity in these profiles is 220 (720 ft/sec) and 355 (1165 ft/sec) m/sec, respectively. Three profiles with constant velocities of 200 (660 ft/sec), 300 (990 ft/sec) and 375 m/sec (1230 ft/sec) in the upper 30 m are also shown. One of the constant velocity profiles is the average velocity (300 m/sec) from the low-strain shear-wave velocity used in the best-fit equivalent-linear model. The other two constant velocity profiles are the minimum (200 m/sec) and the maximum (375 m/sec) mean shear-wave velocity from Borcherdt (1994) for site classification, SC-III (stiff clays and sandy soils). These two profiles increase the range of mean shear-wave velocity beyond the measured range at Gilroy #2 (Fig. 2). They are included in the analysis to bracket the range of response for this site classification.

The calculated response spectra from these five velocity profiles (Fig. 6) are compared to the spectrum from the best-fit model and the recorded data (Fig. 7). The recorded peak acceleration at Gilroy #2 was 0.37 g. The peak acceleration from the best-fit equivalent-linear model was 0.47 g. Peak accelerations from the five additional velocity profiles range from 0.36 to 0.56 g. The profile with the lower bound shear-wave velocity (Fig. 6) produced the largest peak acceleration of 0.56 g and the largest spectral response at most periods. The calculated response spectral acceleration is similar at periods greater than 2 seconds for the six soil profile models.

SUMMARY AND DISCUSSION

Borcherdt (1994) proposed that the short- and mid-period amplification factors used to scale design spectrum could be calculated as a continuous function of mean shear-wave velocity in the top 30 m (100'). However, there are large differences in the measured shear-wave velocity at Gilroy #2, a stiff-soil site. In the top 30 m shear-wave velocity differences of 300 m/sec are

observed (Fig. 2). The measured mean shear-wave velocity in the top 30 m varies from 220 to 355 m/sec, an increase of 60%.

An equivalent-linear site response analysis was performed using the site characterization at Gilroy #2 (EPRI, 1993) to determine the significance of these measured velocity variations in calculations of design spectrum in the Borcherdt (1994) methodology. The variation in spectral acceleration, over a broad range of periods from 0.04 to 7.35 seconds, are compared to the spectrum computed for soil models with variation of nearly a factor of 2 in the mean shear-wave velocity in the upper 30 m. For input levels near 0.45 g the spectrum calculated in the several equivalent-linear analyses match the recorded spectrum at Gilroy #2 reasonably well in this period range. At high frequencies, the peak acceleration computed in the analysis is from 0.36 to 0.56 g, on average about 14% larger than the observed peak acceleration of 0.37 g at the stiff-soil site.

A preliminary observation is that the proposed methodology to compute design spectrum from the average of the shear-wave velocity in the upper 30 m works well for input levels of motion near 0.4 g. These levels are appropriate for many parts of California. This preliminary analysis will be updated with the results from an equivalent-linear analysis of the other four earthquakes with input motions near 0.1 g (Table 3).

ACKNOWLEDGEMENTS

The first author is grateful for support from the Earthquake Engineering Research Institute and the Federal Emergency Management Agency that funded the 1997 EERI/FEMA NEHRP Professional Fellowship. The use of facilities and resources in the College of Engineering, Department of Civil and Environmental Engineering at University of California at Davis are gratefully acknowledged. The first author is on a leave-of-absence from the California Strong Motion Instrumentation Program.

The processed strong-motion records analyzed in this report were made possible through the efforts of SMIP and USGS technicians who installed and maintained these stations, and the SMIP and USGS seismologists who digitized and processed the analog film records. SMIP extends its appreciation to the site owners for their long-term cooperation with strong-motion instrumentation.

REFERENCES

Anderson, J. G., Y. Lee, Y. Lee and S. Day (1996). Control of strong motion by the upper 30 meters, Bull. Seism. Soc. Am., 86, 1749-1759.

Boore, D. B., W. B. Joyner, and T. E. Fumal (1993). Estimation of response spectra and peak accelerations from western North American earthquakes: An interim report, U. S. Geological Survey Open File Report 93-509, 72 pp.

Boore, D. B., W. B. Joyner, and T. E. Fumal (1994). Estimation of response spectra and peak accelerations from western North American earthquakes: An interim report, Part 2, U. S. Geological Survey Open File Report 94-127, 40 pp.

Borcherdt, R. D. (1994). Estimates of site-dependent response spectra for design (methodology and justification), Earthquake Spectra, 10, 617-653.

Brady, A. G., P. N. Mork, V. Perez, and L. D. Porter (1981). Processed data from the Gilroy array and Coyote Creek records from the Coyote Lake earthquake of 6 August 1979, California Division of Mines and Geology, Preliminary Report 24, 171 pp.

Chin, B-H., and K. Aki (1991). Simultaneous study of the source, path and site effects on strong ground motion during the 1989 Loma Prieta earthquake: A preliminary result of pervasive nonlinear site effects, Bull. Seism. Soc. Am., 81, 1859-1884.

Darragh, R. B., and A. F. Shakal (1991). The site response of two rock and soil station pairs to strong and weak ground motion, Bull. Seism. Soc. Am., 81, 1885-1899.

Day, S. D. (1996). RMS response of a one-dimensional half-space to SH, Bull. Seism. Soc. Am., 86, 363-370.

Dickenson, S. E. and R. B. Seed (1991). Correlations of shear wave velocity and engineering properties for soft soil deposits in the San Francisco Bay region, Earthquake Engineering Research Center, University of California at Berkeley, UCB/EERC 91-, 110 pp.

EPRI (1993). Guidelines for determining design basis ground motions, Electric Power Research Institute Report TR-102293s.

Fumal, T. E., J. F. Gibbs, and E. F. Roth (1982). In-situ measurements of seismic velocity at 10 strong motion accelerograph stations in Central California, U. S. Geological Survey Open File Report 82-407, 76 pp.

Fumal, T. E. (1991). Shear-wave velocity estimates and site geology for strong-motion recording sites of the Loma Prieta earthquake of October 17, 1989, U. S. Geological Survey Open File Report 91-311, 163 pp.

Idriss, I. M., and H. B. Seed (1968). Seismic response of horizontal soil layers, Journal of the Soil Mechanics and Foundations Division, American Society of Civil Engineers, 94, No. SM4, 1003-1031.

Idriss, I. M., and J. I. Sun (1992). User's manual for SHAKE91: A computer program for conducting equivalent-linear seismic response analyses of horizontally layered soil deposits, Center for Geotechnical Modeling, University of California at Davis, 71 pp.

Idriss, I. M. (1993). Assessment of site response analysis procedures – A report to the National Institute of Standards and Technology, Department of Civil and Environmental Engineering, University of California, Davis.

Joyner, W. B., R. E. Warrick, and T. E. Fumal (1981). The effect of Quaternary alluvium on strong ground motion in the Coyote Lake, California of 1979, Bull. Seism. Soc. Am., 71, 1333-1349.

Joyner, W. B. and T. E. Fumal (1984). Use of measured shear-wave velocity for predicting geologic site effects on strong ground motion, Proceedings of the Eighth World Conference on Earthquake Engineering, 2, 777-783.

NEHRP (1991). Recommended provisions for the development of seismic regulations for new buildings, prepared by the Building Seismic Safety Council for the Federal Emergency Management Agency, 1, 199 pp.

Schnabel, P. B., J. Lysmer, and H. B. Seed (1972). SHAKE: A computer program for earthquake response analysis of horizontally layered sites, Earthquake Engineering Research Center, University of California at Berkeley, UCB/EERC 72-12, 102 pp.

Schneider, J. F., W. J. Silva, and C. L. Stark (1993). Ground motion model for the 1989 M 6.9 Loma Prieta earthquake including effects of source, path and site, Earthquake Spectra, 9, 251-287.

SEAOC (1988). Recommended lateral force requirements and tentative commentary. Seismology Committee of the Structural Engineers Association of California, San Francisco.

Seed, H. B., and I. M. Idriss (1970). Soil moduli and damping factors for dynamic response analysis, Report NO. UCB/EERC 70-10, Earthquake Engineering Research Center, University of California, Berkeley, 48 pp.

Shakal, A. F., M. J. Huang, D. L. Parke and R. W. Sherburne (1986). Processed data from the strong-motion records of the Morgan Hill earthquake of 24 April 1984, California Division of Mines and Geology, Office of Strong Motion Studies, Report No. OSMS 85-04, 249 pp.

SMIP (1991). Plots to accompany tapes: Loma Prieta 1989 ground-response stations, California Division of Mines and Geology, Office of Strong Motion Studies, Report No. OSMS 91-06.

TABLE 1
Shear-Wave Velocity and Lithology for Gilroy #2 (modified from EPRI, 1993)

Thickness (ft)	Vs (ft/sec)	Thickness (m)	Vs (m/sec)	Lithology
35	750	10.7	229	Holocene Alluvium
10	1000	3.1	305	Late Pleistocene Alluvium
30	1560	9.1	476	Pleistocene Lake Deposits
31	1000	9.5	305	
20	1140	6.1	348	Pleistocene Alluvium
12	1230	3.7	375	
132	2100	40.2	640	
23	1550	7.0	473	
29	1730	8.8	527	
238	2300	72.6	701	
	3900		1189	Monterey Shale

TABLE 2
Modulus-Reduction, Damping and Q (attenuation) Values for Gilroy #2
(modified from EPRI, 1993)

Strain (%)	G/Gmax (0-12 m) (0-40')	G/Gmax (12-24 m) (40-80')	G/Gmax (24-40 m) (80-130')	G/Gmax (>40 m) (>130')
1.0E-4.0	1.00	1.00	1.00	1.00
1.0E-3.5	1.00	1.00	1.00	1.00
1.0E-3.0	1.00	1.00	1.00	1.00
1.0E-2.5	0.99	0.99	1.00	0.95
1.0E-2.0	0.91	0.93	0.95	0.81
1.0E-1.5	0.72	0.76	0.80	0.57
1.0E-1.0	0.47	0.51	0.56	0.32
1.0E-0.5	0.24	0.27	0.31	0.14
1.0E-0.0	0.09	0.11	0.14	0.05

Strain (%)	Damping % (0-12 m)	Damping % (12-24 m)	Damping % (24-40 m)	Damping % (>40 m)
1.0E-4.0	3.0	3.0	3.0	3.0
1.0E-3.5	3.0	3.0	3.0	3.0
1.0E-3.0	3.0	3.0	3.0	3.0
1.0E-2.5	3.0	3.3	3.2	3.3
1.0E-2.0	3.5	4.4	4.1	4.1
1.0E-1.5	4.7	6.9	6.3	10.0
1.0E-1.0	7.5	11.2	10.1	15.9
1.0E-0.5	12.1	17.3	16.0	22.2
1.0E-0.0	24.4	23.5	22.3	27.5

Strain (%)	Q (0-12 m)	Q (12-24 m)	Q (24-40 m)	Q (>40 m)
1.0E-4.0	16.7	16.7	16.7	16.7
1.0E-3.5	16.7	16.7	16.7	16.7
1.0E-3.0	16.7	16.7	16.7	15.2
1.0E-2.5	14.3	15.2	15.6	12.2
1.0E-2.0	10.6	11.4	12.2	8.2
1.0E-1.5	6.7	7.2	7.9	5.0
1.0E-1.0	4.1	4.5	5.0	3.1
1.0E-0.5	2.7	2.9	3.1	2.3
1.0E-0.0	2.1	2.1	2.2	1.8

TABLE 3
Strong-Motion Data at Gilroy #1 and Gilroy #2 (Notes 1 and 2)

		Peak Parameters									
		Gilroy #2 (stiff soil)					Gilroy #1 (rock)				
Earthquake Name	M_L (UCB)	Comp (deg)	Acc (g)	Vel (cm/sec)	Disp (cm)	Dist* (km)	Comp (deg)	Acc (g)	Vel (cm/sec)	Disp (cm)	Dist* (km)
Coyote Lake	5.9	050	0.20	10.2	2.2	14	320	0.12	10.3	1.7	16
		140	0.26	31.9	5.3	(7)	230	0.10	4.0	0.7	(8)
Morgan Hill	6.1	360	0.16	5.0	1.1	38	320	0.10	2.7	0.5	39
		090	0.21	12.5	2.0	(17)	230	0.07	2.5	0.3	(18)
Loma Prieta	7. 0	360	0.37	33.3	6.7	30	360	0.43	31.9	6.5	29
		090	0.33	39.2	10.9	(16)	090	0.49	33.8	6.3	(15)
Loma Prieta (Note 3)		360	0.04	2.2	0.2		360	0.08	2.7	0.1	
Aftershock #1		090	0.03	1.6	0.1		090	0.06	1.4	0.1	
Loma Prieta	4.3	360	0.17	4.0	0.2	23	360	0.11	2.1	0.1	22
Aftershock #2		090	0.10	3.0	0.2		090	0.07	1.3	0.1	

* The distances given are epicentral (top) and when appropriate the distance to the nearest point on the surface projection of the fault inferred from the aftershock distribution (bottom, in parenthesis).

Notes:

1) The processed data are from Brady et al. (1981), Shakal et al. (1986) and SMIP (1991) for the Coyote Lake, Morgan Hill and Loma Prieta mainshocks, respectively. The Loma Prieta aftershock data are discussed in Darragh and Shakal (1991). These processed records are distributed by SMIP.

2) The filter corner frequencies and the Usable Data Bandwidth vary for each of these earthquakes. The corner frequencies used for the processed data are:
   Coyote Lake: 0.05-0.25 Hz, 23-25 Hz
   Morgan Hill: 0.20-0.40 Hz, 23-25 Hz (Gilroy #1); 0.08-0.16 Hz, 23-25 Hz (Gilroy #2)
   Loma Prieta: 0.14 to 23.6 Hz (0.04 to 7.35 sec)
   Loma Prieta (aftershock #1): 0.40-0.80 Hz, 23-25 Hz
   Loma Prieta (aftershock #2): 0.40-0.80 Hz, 23-25 Hz.
   The Usable Data Bandwidth for the Loma Prieta earthquake is from 0.14 to 23.6 Hz (0.04 to 7.35 sec).

3) The U.C. Berkeley Seismographic Stations did not estimate the epicenter and magnitude for the first Loma Prieta aftershock because the motions occurred during the coda of the mainshock that occurred 86 seconds earlier.

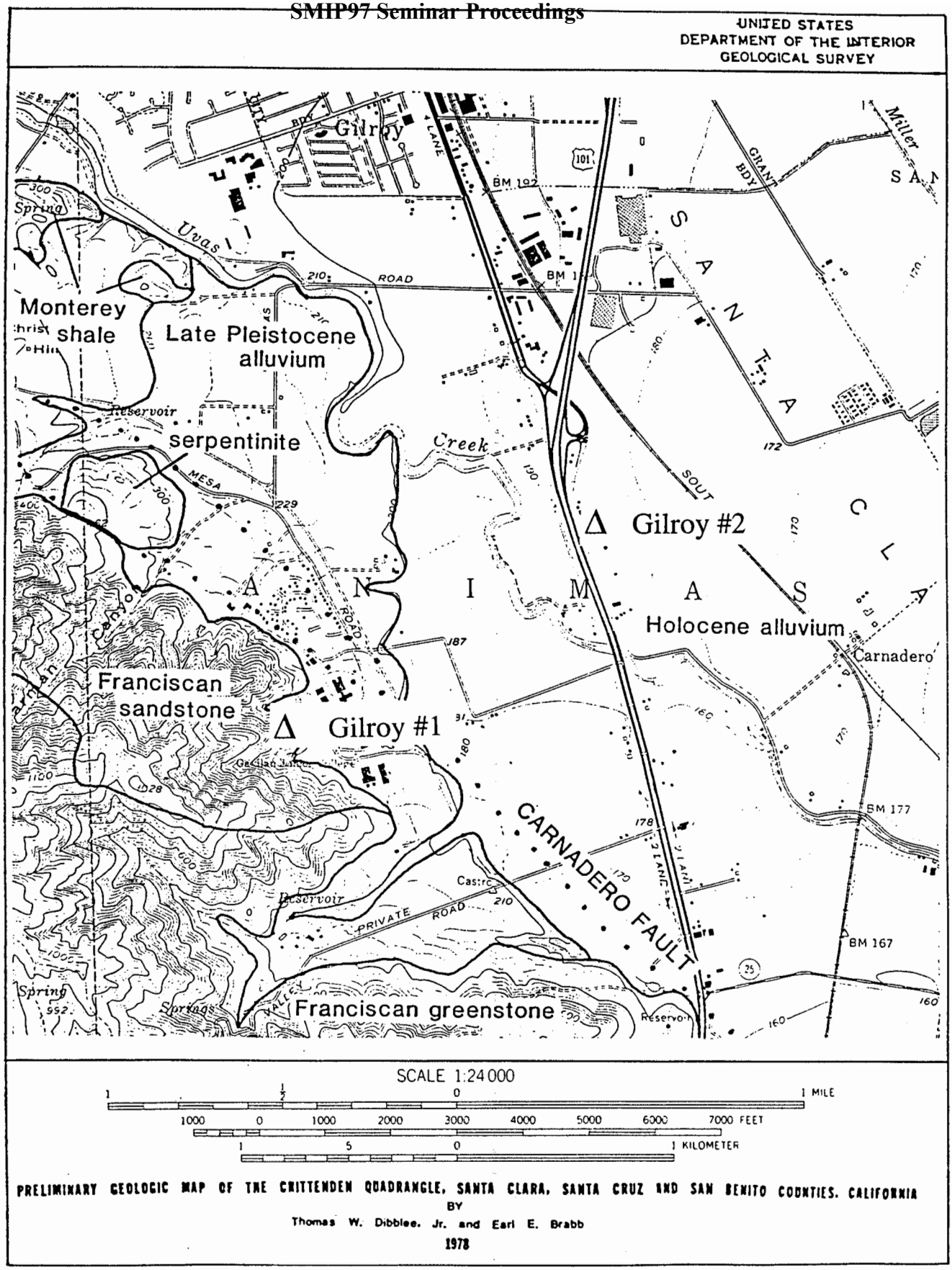

Fig. 1. Site location map for Gilroy #1 and Gilroy #2. The geology of the southern Santa Clara Valley region in California is also shown (modified from Fumal, 1991).

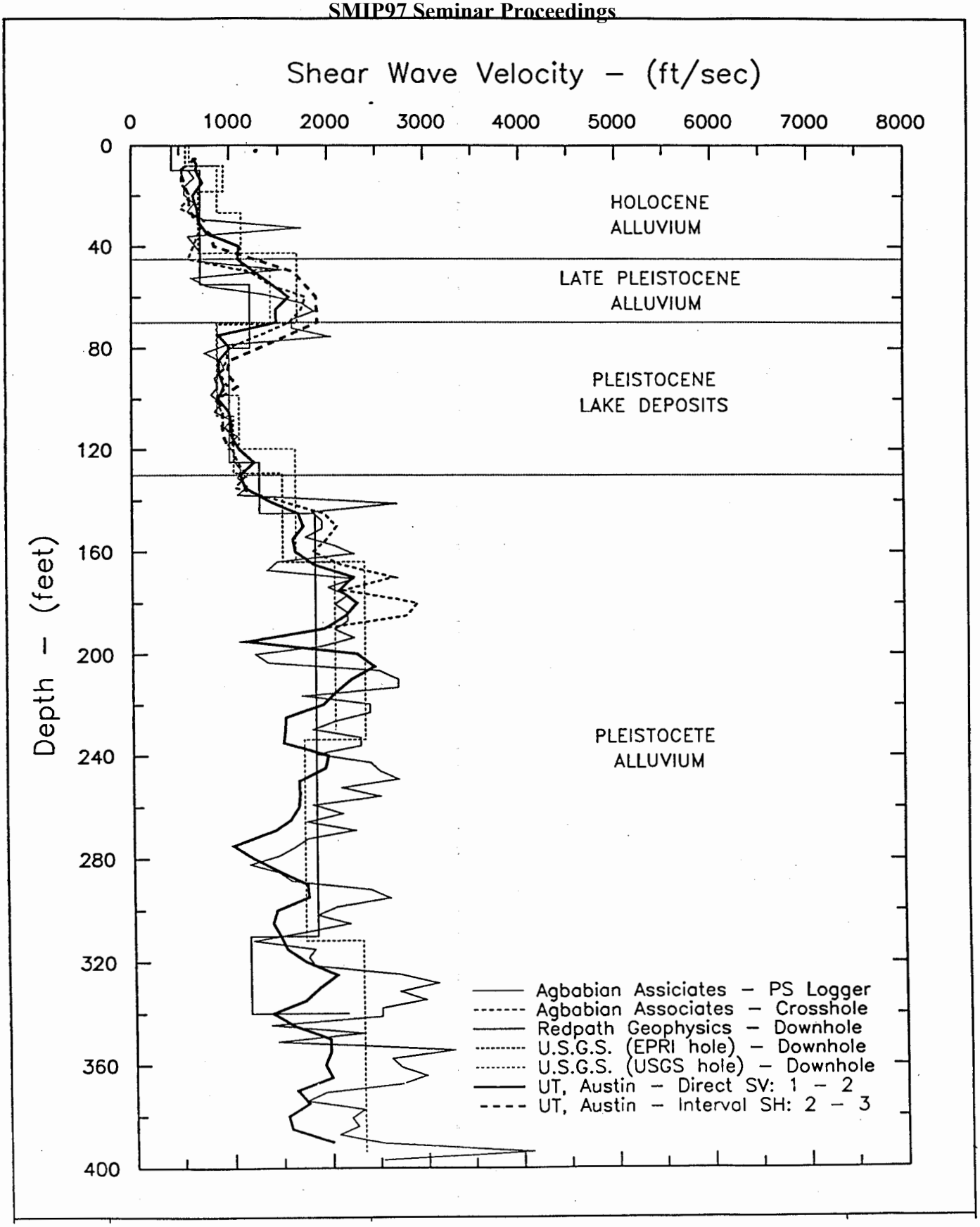

Fig. 2. Shear-wave velocity measurements at Gilroy #2 (modified from EPRI, 1993).

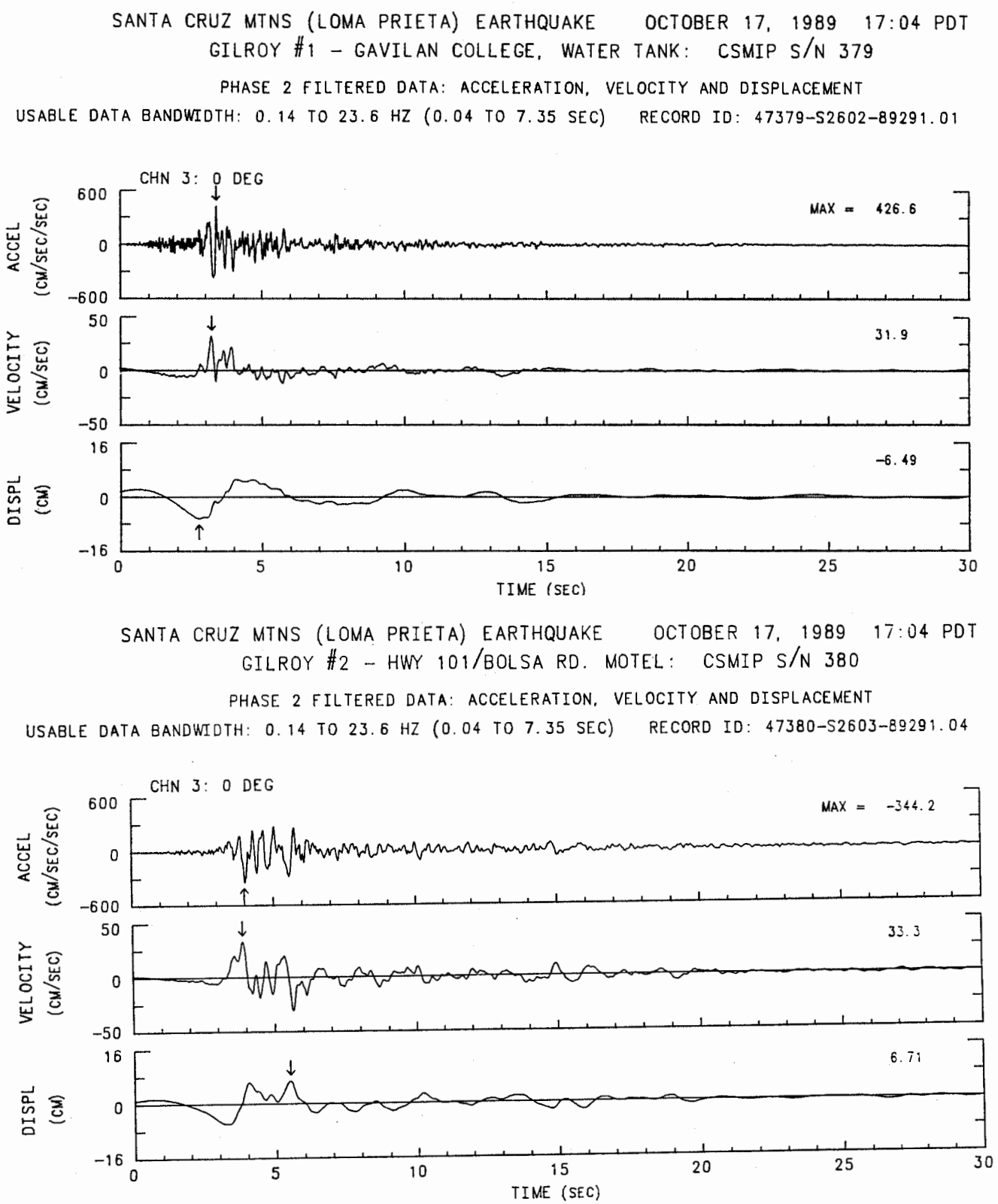

Fig. 3. The base-line corrected and band-pass filtered acceleration, velocity and displacement for the north-south component of Gilroy #1 (top) and Gilroy #2 (bottom) from the Loma Prieta mainshock. The Usable Data Bandwidth of the processed data is from 0.14 to 23.6 Hz (0.04 to 7.35 sec) (modified from SMIP, 1991).

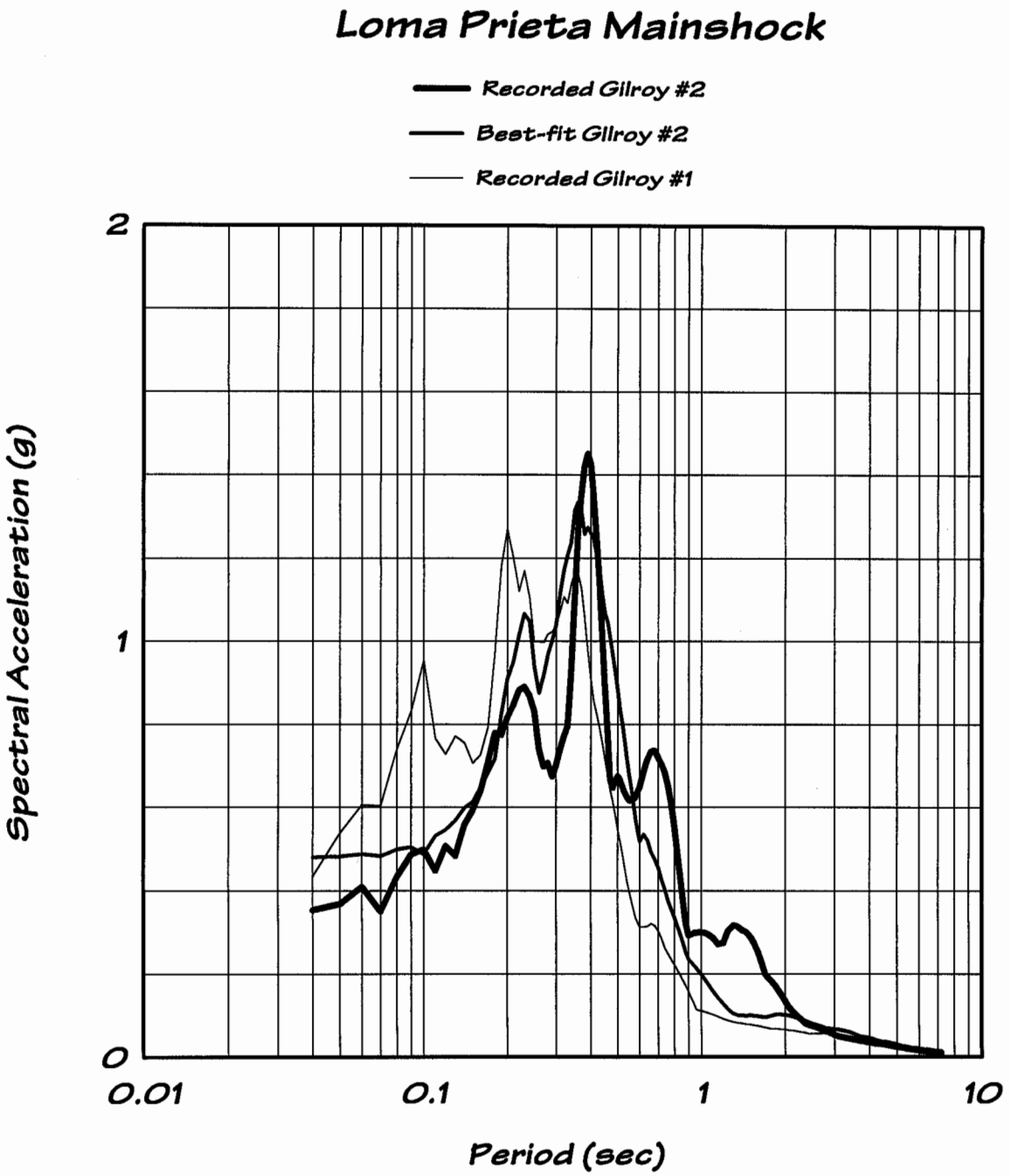

Fig. 4. Response spectra (5% damped) for the north-south component of the Loma Prieta mainshock at Gilroy #1 and #2. Also, the best-fit spectrum at Gilroy #2 from the SHAKE analysis.

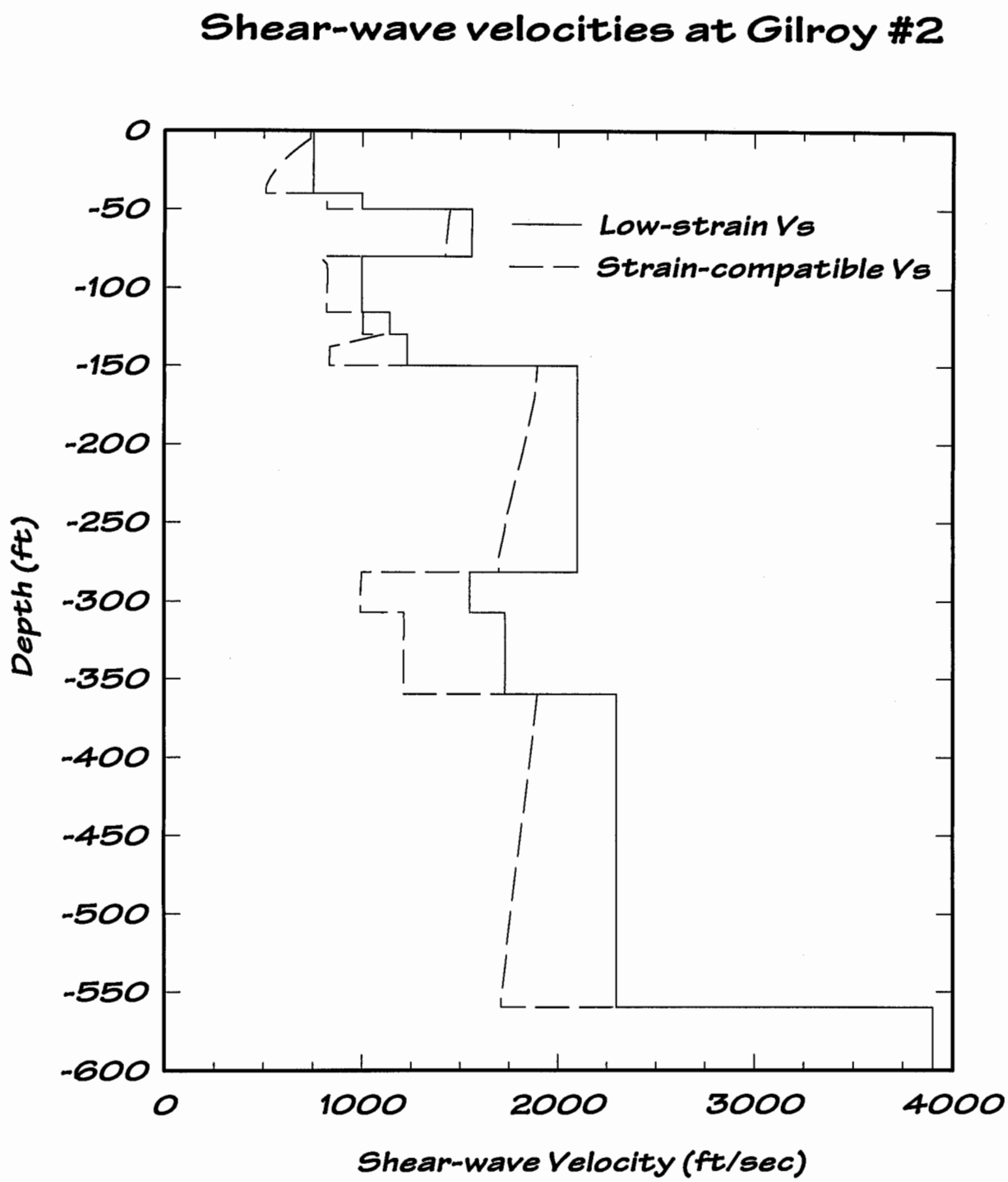

Fig. 5. Low-strain and strain-compatible shear-wave velocities at Gilroy #2. The low-strain and strain-compatible velocities are from EPRI (1993) and the best-fit SHAKE analysis, respectively.

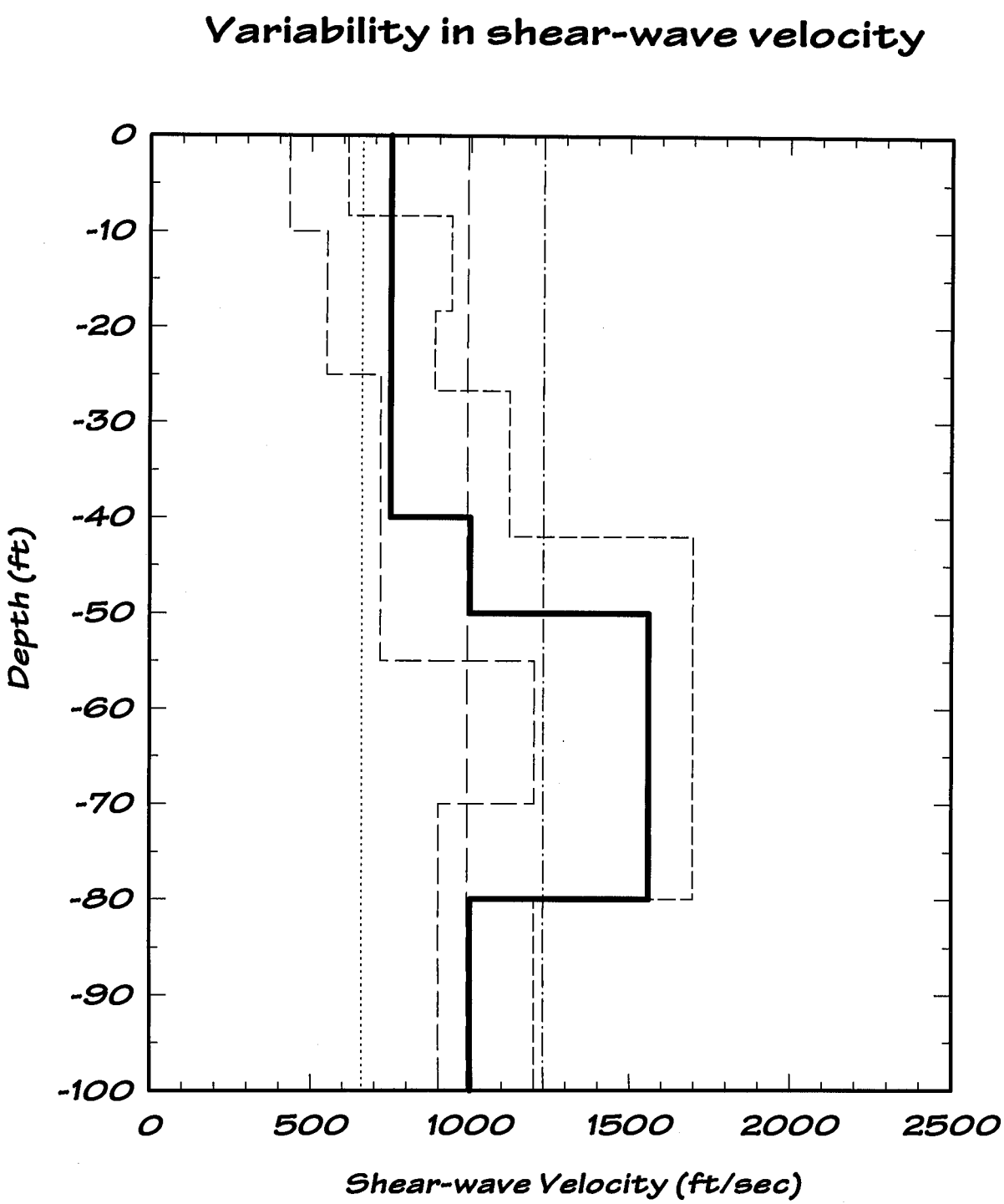

Fig. 6. Variability in the shear-wave velocity in the top 100 ft (30 m) at Gilroy #2. The low-strain velocity is shown with a thick solid line. Other velocity profiles are shown with thinner lines.

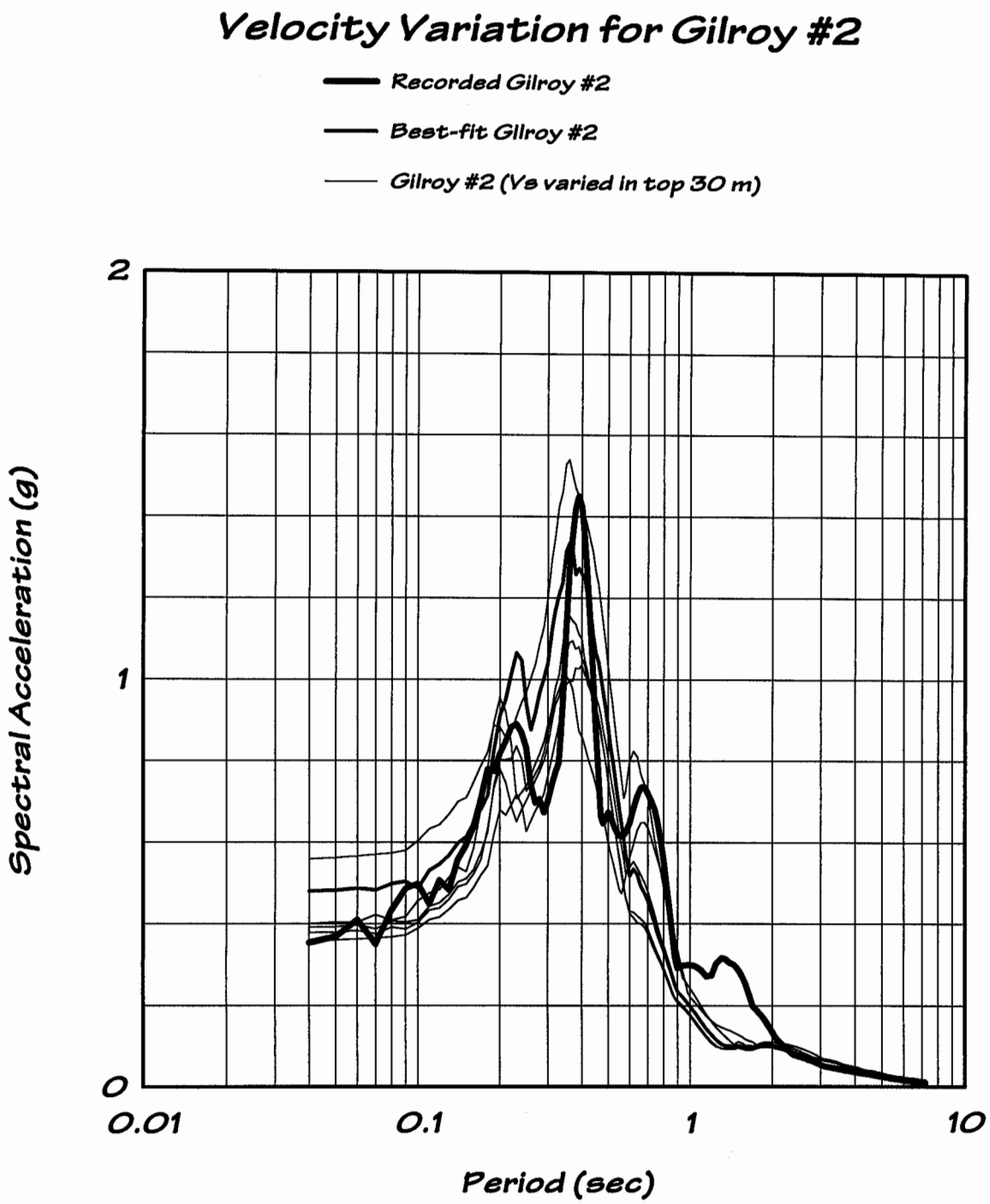

Fig. 7. Response spectral accelerations (5% damped) from the north-south component of the Loma Prieta mainshock at Gilroy #2. The spectrum from the best-fit and other models with variable Vs in the upper 30 m.

IMPORTANCE OF MEASURED FULL-SCALE BUILDING RESPONSE IN THE COMPUTER MODELING OF BUILDINGS

by

Gary C. Hart
Professor of Engineering and Applied Science
Department of Civil and Environmental Engineering
University of California, Los Angeles

ABSTRACT

This paper presents a perspective on the importance of developing accurate computer models of constructed buildings and the role that measured earthquake response records play in advancing this area of structural engineering research and practice.

INTRODUCTION

I wish to express my sincere appreciation to the Strong Motion Program of the California Division of Mines and Geology for inviting me to speak on this most important topic. This part of my research has spanned almost 30 years and I have many, many special memories. One such special memory was doing research relating to developing a computer model for a high-rise building in San Diego. This research on full-scale response started in 1969 when I was a new UCLA Assistant Professor. I helped drag the cables up and down the San Diego Gas and Electric Building as my leaders, the late UCLA Professor R.B. "Fritz" Mathieson and Professor Paul Jennings of Cal Tech, vibrated the building with shakers and measured the building's natural periods of vibration, damping, and mode shapes.

Perhaps the single most important reason for measuring full-scale building response is that it records the real motion of the building, and therefore, documents what really happened and not just what the computer model says happened. I remember as if it were yesterday, walking up and down the stairs of the San Diego Gas and Electric Building as it was being vibrated at one of its higher mode natural frequencies. I could feel the decrease in motion as I moved toward the nodal points in the mode shape and the increase in motion at the locations of greatest modal displacement. This was a real high-rise building and it really did have mode shapes!

I learned in the 1970s from Professor Ray Clough of UC Berkeley that the purpose of an experiment is to serve as a reality check, or verification, of a computer model of the structure being tested. Therefore, the past and future acquisition of measured full-scale response of buildings and the study of this response is an essential part of the development of performance based design criteria. The need for accurate computer models of buildings that are used by structural engineers has never been greater than it is now. The economic loss incurred by the

urban community during the Northridge earthquake was not acceptable. Unfortunately, the computer models that are used by most structural engineers for designing buildings do not have a high credibility rating when they are used to estimate building performance. Without a strong consensus on the risk and probable loss in future earthquakes based on good computer models of buildings, the "stoppers" within the business and structural engineering community will block any serious spending of money now to prevent future loss of life and dollars. My hope is that this paper will present some insight into the importance of measured response and the barriers that must be removed to help utilize the full potential of measured full-scale building response.

THE EVOLUTION OF COMPUTER MODELING OF BUILDINGS

The evolution of the computer modeling of buildings and other civil structures can be viewed as a journey down a very long and winding "technical load path." Imagine the following sections of this path:

Section 1: Buildings and bridges needed to be built (e.g., roman time) and unfortunately no mathematics tools or IBM Aptiva computers existed to develop a computer model of the structure. Therefore, without the benefit of a stiffness method of analysis or the Newmark-β numerical solution routine, the focus of the structural engineer was on the loads imposed on the structure (e.g., 200 soldiers on a bridge). The attempt by the structural engineer was to address the reality of the loading on the structure and then to develop a "structural design" for a building based on "professional experience" and hope that the building does not fail in the next large load experience.

Section 2: A beautiful baby called applied mathematics was then born and this birth was followed by the birth of children, grandchildren, and great-grandchildren that all became members of a structural engineering family called Structural Mechanics. The early members of this structural mechanics family (e.g., pre-1950s) helped develop analytical models of structures that followed a systematic and traceable computational path. However, this development was only possible after the structural engineer made the assumption that the materials were linear and the deformations were small. Therefore, the structural engineering world transformed itself from the reality of the loads to the new and improved world of linear elastic analysis. The flaw in this new world was that when the best estimate of real loads was applied to this new world linear elastic building model, the result was that the element deformations that were calculated exceeded the elastic limit of the element. What to do? The approach that was followed by the structural engineer was simple and it was to use a "fake" set of loads and earthquake ground motions. These "fakes" were loads much smaller than real loads, but they were winners because they produced element response in the linear elastic response domain. This approach was justified on the grounds that we really do not know the real loads on the building with any real accuracy. It also was justified on the grounds that if we did not use this new linear elastic approach we would be "technical dinosaurs." Of course this entire linear elastic world expanded beyond the sphere of civil and military structures when the aerospace program and the cold war started in the 1960s. Spacecraft and airplanes were expected to

respond to their real loads in the elastic response domain and thus the analysis made sense. However, buildings are not expected to response to "the big one" in the elastic response domain.

Section 3: The desire to understand and use real loads and earthquake ground motions emerged in the 1970s like spring flowers. During this time, earthquake ground motion recording units were introduced at first on the ground and then later in buildings. The extra special efforts of the USGS, the Building of Safety Department of the City of Los Angeles, and the Strong Motion Program of the CDMG, have brought Structural Engineers back to where their focus is on trying to address the reality of the loads and the real earthquake ground motions. The refocus on loads and the climb up the real world learning curve started with the recording of a few relatively strong earthquake time history records on the ground away from all structures. Then the 1972 San Fernando earthquake produced records of motion at numerous ground locations throughout southern California and also in several buildings. More recently the Whittier, Loma Prieta, and Northridge earthquakes have provided many records of earthquakes ground motion and building response. The existence of these full-scale building response records has made clear the real need to develop an accurate model of the real building. A linear elastic analysis alone just does not cut it! Therefore, nonlinear computer models of buildings must be developed and these computer models must seek to estimate the response and performance of the specific building that is the focus of the attention of the structural engineer to the site specific ground motion description that is provided by the Geotechnical Engineer. Of course, the entry of the computer age (i.e., the PC age, not the mainframe age) has offered computational tools that could not have been imagined by most structural engineers just a few years ago. However, when all is said and done, the new world is one where for a particular new or existing building, the Structural Engineer and the Geotechnical Engineer work together as a team to develop and use the best real estimates of earthquake ground motions with the best possible computer model of the real building, to estimate the performance of the building and its probability of responding beyond defined performance limit states.

LINEAR ANALYSIS MODELS

Performance Based Design requires computer models of buildings that are both linear and nonlinear. Consider first the two types of linear analysis models.

A **RESPONSE SPECTRUM COMPUTER MODEL** is today the most common building computer analysis model used by structural engineers. This type of computer model is really a static response model because the response is not calculated as a function of time. However, this model has its foundation in structural dynamics and specifically with an analysis procedure called the Normal Mode Method. In the normal mode model analysis procedure, the matrix equation of motion of the building system in its physical coordinates, $\{X\}$, are transformed into a set of coordinates called normal mode coordinates, $\{q\}$. These normal mode coordinates

when used transform the matrix equation of motion into a matrix equation with only diagonal matrices. To show this, consider the equation of motion in the physical coordinates as

$$[M]\{\ddot{X}\} + [C]\{\dot{X}\} + [K]\{X\} = -[M]\{I\} / a(t) \qquad (1)$$

where

[M], [C], [K] = mass, damping, and stiffness matrices

$\{X\}, \{\dot{X}\}, \{\ddot{X}\}$ = displacement, velocity, and acceleration vectors for motions relative to the ground

a(t) = earthquake ground motion acceleration

If the building has *n* degrees-of-freedom, then the second order matrix linear differential equation of motion given by Equation (1) represents a coupled set of *n* differential equations because one or more of the matrices [M], [C], and [K] are non-diagonal.

If a special set of new coordinates, called normal mode coordinates, are defined by the equation

$$\{X\} = [\phi]\{q\} \qquad (2)$$

where

$\{q\} = (q(t)\ q_2(t) \ldots q_m(t))^T$ = normal mode coordinate vector ($m \leq n$)

$q_i(t) = i^{th}$ normal mode coordinate

and

$[\phi]$ = transformation matrix from the $\{X\}$ to the $\{q\}$ coordinates

Then it follows if $[\phi]$ is a very special matrix that Equation (1) becomes

$$\left([\phi]^T[M][\phi]\right)\{\ddot{q}\} + \left([\phi]^T[C][\phi]\right)\{\dot{q}\} + \left([\phi]^T[K][\phi]\right)\{q\} \equiv [\phi]^T[M]\{I\}a(t) \qquad (3)$$

Now if we define

$$[M^*] = [\phi]^T[M][\phi]$$
$$[C^*] = [\phi]^T[C][\phi]$$
$$[K^*] = [\phi]^T[K][\phi]$$
$$\{G\} = [\phi]^T[M]\{I\} / [M^*]$$

then

$$[M^*]\{\ddot{q}\} + [C^*]\{\dot{q}\} + [K^*]\{q\} = -[M^*]\{G\}a \qquad (4)$$

The very special matrix $[\phi]$ is called the Modal Matrix. Each column of this matrix is a vector and is called a building mode shape of vibration. The first column of $[\phi]$ is called the first mode shape of vibration, denoted $\{\phi\}_1$, the second column of $[\phi]$ is called the second mode of vibration, denoted $\{\phi\}_2$, etc. When the model matrix is used to define the coordinate transformation from the $\{X\}$ to the $\{q\}$ coordinates, then it can be shown that $[M^*]$, $[C^*]$, and $[K^*]$ are all diagonal matrices. Therefore, the building response in the normal mode coordinates, $\{q\}$, can be calculated by solving up to *n* uncoupled second order differential equation of motion. Equation (2) can now be written as a summation, or power series expansion, of the response $\{X\}$ in terms of the $\{q\}$ coordinates. Equation (2) becomes

$$\{X\} = [\phi]\{q\} = \{\phi\}_1 q_1(t) + \{\phi\}_2 q_2(t) + \ldots + \{\phi\}_m q_m(t) \qquad (5)$$

Each uncoupled equation of motion is of the form

$$\ddot{q}_i(t) + 2\xi_i\omega_i\dot{q}_i(t) + \omega_i^2 q_i(t) = -G_i a(t) \qquad (6)$$

where

G_i = participation factor for the i^{th} mode and i^{th} element in $\{G\}$

$$= \{\phi\}_i^T[M]\{I\} / [M^*] \qquad (7)$$

and

$\{\phi\}_i$ = i^{th} mode shape of vibration of the building

The response of the building is calculated by first representing the acceleration of the ground, *a(t)*, by a function called a Response Spectra, $S_a(T)$, which incorporates the amplitude and frequency response characteristics of *a(t)*. The function $S_a(T)$ is obtained by calculating the response of a series of single degree-of-freedom systems with varying natural frequency of

vibration and modal damping. With a knowledge of $S_a(T)$ the structural engineer can develop a computer model of the building and then calculate the maximum response of q_i, or any associated building force or displacement, for i = 1,2,..., m where m is less than or equal to n. In this response solution, the maximum value of the response is known, but the time at which this maximum response occurs is not retained and thus not used in the analyses.

When this computer model is used to estimate building performance the natural frequencies of vibration, ω_i, modal damping values, ξ_i, and mode shapes $\{\phi\}_i$ are the critical structural modeling parameters. It is very important when using this method to have very accurate estimates of these modeling parameters. Measured full-scale building response is essential in developing models that can be used with confidence when the structural engineer performs a Response Spectra Analysis.

A **LINEAR DYNAMIC TIME HISTORY COMPUTER MODEL** calculates the loads on the structural members from the earthquake, dead and live loads, and compares these loads for each structural member with the yield capacity of the structural member. Equation (1) can be solved directly using direct integration methods such as Newmark-β or Wilson-θ. Alternately, the normal mode method can be used and Equations (5) and (6) are used to calculate the building response. In both methods, the response is calculated as a function of time. Unlike the Response Spectra Method where the time variation of response is lost, here the values of all response quantities are calculated at each instant in time. In both of the above noted linear computer model analysis procedures, the ratio of the Load Demand to the Yield Capacity is termed a Demand-Capacity Ratio (DCR). The value of this ratio is taken as a measure of the inelastic (or ductility) demand on the structural element. A linear elastic time history analysis can provide reasonable estimates of the DCR's for ratios less than 1.5 or 2.0. The accuracy and the range of applications of these linear elastic methods are not well defined primarily because of the inability of a linear elastic model to modify the earthquake load path within the structural system as yielding occurs within the building's structural elements. This load path modification is especially important for brittle, non-ductile elements. Some creative ways have been proposed to soften the stiffness at the structural members as a function of response amplitude. The relationship between the axial load on the vertical structural elements (e.g., columns and walls) and the stiffness and capacity of these elements is not captured by a linear dynamic time history analysis. Measured full-scale response is essential to define the limits of this computer model and especially the DCR limits.

NONLINEAR ANALYSIS MODELS

A **NONLINEAR STATIC COMPUTER MODEL** represents the variation of stiffness with deformation and thus seeks to improve upon the performance prediction accuracy of the linear analysis models. A major shortcoming of this model is that it does not directly model the time variation of building response. This type of model has the advantage that it can modify the load path of the earthquake loads within the structure as the structural elements yield. Also, by its nature it is a displacement-based procedure and the earthquake elements are in displacement-based response variables (e.g., curvature, strains, plastic rotations, etc.) and not forces. It is essential where real accuracy is desired to quantify building response from the deformation

perspective because only by doing so can the structural engineer understand building performance. The inelastic deformation demands can be compared with the inelastic deformation capacities to determine the level of safety associated with any identified limit state.

A basic shortcoming of a Nonlinear Static Computer Model approach can be seen by examining the basic equation of motion in Equation (1) in its rearranged form

$$[K]\{X\} = -[M]\{\ddot{Y}\} - [C]\{\dot{X}\} \qquad (8)$$

where

$$\{\ddot{Y}\} = \{\ddot{X}\} + \{I\}a(t) = \text{absolute acceleration}$$

In a time history analysis, the forcing function acting on the building at any instant in time is the summation of the inertia force, $\{F_I\} = -[M]\{\ddot{Y}\}$, and the damping force, $\{F_D\} = -[C]\{\dot{X}\}$. A static nonlinear analysis uses a static force, denoted here as $\{F\}$, that is intended to provide an acceptable approximation to $\{F_I\}$ and $\{F_D\}$ for the purposes intended by the structural engineer. The difficulty with developing a "good" $\{F\}$ can be seen in Equation (8). In this equation, both $\{F_I\}$ and $\{F_D\}$ are functions of time. Therefore, to develop a "good" $\{F\}$ the force vector must capture with one constant force vector, $\{F\}$, the influence that two time varying force vectors $\{F_I\}$ and $\{F_D\}$ have on the structure. This is very difficult to do even for modest response equivalency goals. Also the building responding in the nonlinear response domain results in the stiffness matrix [K] having a variation as a function of the building displacements and therefore time. However, despite these shortcomings, a static nonlinear analysis is preferred as a preliminary, relatively low cost and effective way to start to understand a building's performance. Full-scale building response measurements are needed to define the limits and the accuracy of this computer model approach.

A NONLINEAR DYNAMIC TIME HISTORY COMPUTER MODEL solves Equation (8) for one or more site specific earthquake ground motions and for one or more sets of possible parameter values. A Nonlinear Dynamic Time History Computer Model will always be more accurate than a Nonlinear Static Computer Model. The criticisms of a Nonlinear Dynamic Time History Computer Model are usually centered around budget limitations placed on the computer analysis phase of a project or the educational limitations of most structural engineers. Both of these limitations are probably true, sad, and inexcusable!

Nonlinear computer models are the most accurate and most valuable computer models. However, the verification of a computer model using measured full-scale building response is also the most difficult. There are several reasons for this. First, it is the authors experience that many structural engineers have a very difficult time learning the topic of linear structural dynamics. This topic is not easy to learn and requires a good understanding of applied mathematics. Second, the step from linear to nonlinear structural dynamics is also very difficult, and thus many structural engineers just do not start the learning process or give up. Third, as pointed out over twenty years ago by Professor Penzien and his Ph.D. student, Dr. Ruiz, the response of a building

modeled using a nonlinear computer model is very sensitive to the values of the parameters in the model and the time variation of the earthquake ground motion. Stated another way, the closer we get to reality the more sensitive the solution is to the parameters of the model and the ground motion. A simple non-engineering example might help understand this point. Assume that you have never had a pair of shoes on your feet and you purchase your first pair. The shoes will feel great especially when walking across a southern California beach on a day where the temperature is 105°. Now time passes and you purchase shoes occasionally and each time you learn more about how to select shoes to make your feet more comfortable. For example, the size, width, vibration soles, arches, etc. Now the process of selecting the correct shoe for you has become more "scientific", more difficult and more time consuming. However, if you are patient and expend the effort your new shoes will fit better than your old shoes. The nonlinear computer analysis is like a new shoe and the linear analysis is like an old shoe.

It is essential to obtain measured full-scale response data to verify our nonlinear computer models. The more locations where the response is measured (both in the building and in the adjacent soil), the better our ability to understand and model the buildings nonlinear response.

The benefit cost ratio for structural engineers of recorded response measurements is very high. However, until recently the structural engineering codes of practice deterred the structural engineering from using improved computer building models and thus indirectly discouraged learning from records of building response.

LEARNING FROM EARTHQUAKES

On occasion the author has told the story of when he was a young, green Assistant Professor at UCLA in the late 1960s and he was attending an earthquake engineering conference. On Day 1 of the conference, the author had given one of his "passionate" talks about earthquake analysis of buildings and the need to incorporate the uncertainty in the computer model and also the uncertainty in the earthquake ground motion. On Day 2 of the conference, the author entered the conference restaurant for breakfast and he was asked by Professor Newmark to join him. Of course the author accepted and of course he shook in his chair all during the breakfast and the estimated peak acceleration was 2g. Little is remembered of that breakfast besides the honor of the invitation and one very wise piece of advice from this great structural engineering professor. What Professor Newmark said was "Things do not change fast in the area of building earthquake engineering so have patience."

The author now, at the age of 50+ and very near the age that Professor Newmark was that day, understands the keen insight in this advice. The author now understand after serving for over 15 years as a member or observer on the SEAOC Seismology Committee and learning from real earthquake experiences many of the justifiable reasons for the slow changes in the accepted use of structural engineering computer modeling methods. The only real time we have to observe, record, and learn from nature is during an earthquake. The single most important item that a structural engineer can have to maximize the learning from the earthquake is to have a measured response of a building. Therefore, the slow change is primarily the result of a lack of good quality

measured building response records combined with the severe consequences that having a wrong model can have on the lives of hundreds or even thousands of people in a building.

VISION 2000 AND COMPUTER MODELING

Consider the quotation from the Vision 2000 part of the SEAOC Blue Book: "A major challenge to performance-based engineering is to develop simple yet effective methods for designing, analyzing, and verifying the design of structures so that they reliably meet the selected performance objectives." This quotation identifies perhaps the single largest reason for the development and use of realistic computer models of buildings. The reason is a lack of respect for the complexity of the problem being solved by the public and structural engineers. Even more, this comment shows a lack of professional respect for the desires and capabilities of Structural Engineers.

Structural Engineering Design is in many ways very similar to the design process that a trained artist uses when designing a painting. Both involve a blend of past life experiences, available technology, and subjective personal feelings. I perform calculations when I design a building until I have a comfort level that tells me that the design is done and the performance goals that have been defined have been satisfied. My own personal line is "That is enough analysis, the design feels right." Design is a process where analysis creativity and effort are at the direction of the structural engineer and the analysis has only one goal and that is to provide the structural engineer with this level of comfort in the design.

To many who have not stamped the plans for the design of a tall building the comments in the preceding paragraph may seem like a bunch of hot air. Also, to many who do not want to do any computer modeling of buildings this many seem like a quick way out. And to many who do not model real buildings on the computer this may seem like an excuse to not perform a "more exact" computer model. However, it is none of the above. It is a realization that we must always push forward our abilities to accurately model real buildings on the computer but we must also recognize the realities of structural engineering.

A major challenge that Performance Based Design faces is the real but well disguised resistance by many, many structural engineers to developing a good analytical model for the building. There are several reasons for this very strong resistance such as: (1) Current staff members are not able to do such analyses and as such must be trained or new staff employed; (2) The current structural engineering value system is often not compatible with rewarding engineers that are good analysts but are not as good at holding a clients' hands; (3) The scope of the required analysis for a project often changes as more is learned about the building and its performance. This often necessitates more effort and the request for more fees; (4) By its very nature computer analysis very often has hidden traps (e.g., bugs, wrong input, etc.) and thus the time line of work is more difficult to predict and control; and (5) Many senior engineers who are really small business operators and who do not really desire to understand how their building performs, see analysis as a very negative cash flow item. Performance Based Design addresses damage and serviceability limit states.

The Vision 2000 document identifies for seismic risk hazards, see Table 1.

The types of computer models of buildings has to be influenced by the different anticipated performance levels. Vision 2000 identifies four performance levels and they are:

- **Fully Operational.** The building continues in operation with negligible damage.
- **Operational.** The building continues in operation with minor damage and minor disruption in nonessential services.
- **Life Safety.** Life safety of the building occupants is substantially protected, but the damage is moderate to extensive.
- **Near Collapse.** The structural collapse of the building is prevented. However, life safety is at risk and the damage is severe.

Tables 2 to 5 expand on the above descriptions. These different performance levels place a special emphasis on obtaining full-scale building response records over a spectrum of amplitudes of motion.

Typical building response parameters are stress ratios, drift and deformation ratios, structural accelerations, ductility demand ratios, and energy dissipation demand vs. capacity.

The Vision 2000 document states: "Typical limiting values for these response parameters must be established for each performance level through research that includes laboratory testing of specific components, as well as calibrating the limiting values by analyzing buildings that have experienced measurable damage in past earthquakes." (The underline is the authors).

Performance-based engineering yields structures with predictable performance within defined levels of risk and reliability. There are multiple sources of uncertainty in the seismic design process. There is uncertainty regarding the seismic ground motions, the design and analysis techniques and modeling assumptions, the variability in the materials, workmanship and construction quality, and the changes to the structure over its life due to material deterioration, wear, and structural or nonstructural modifications.

It is an important task of performance-based engineering to recognize, identify, and quantify those uncertainties using computer models of the structure so that the levels of reliability and risk can be established and acknowledged by the design professional, the client, the legal profession, and the public.

THE 1997 UBC AND COMPUTER MODELING

Some progress to reward more detailed computer models of buildings has been made in the last decade. For example, the 1997 UBC recognizes the improved accuracy of a response spectra analysis versus a static equivalent lateral force analysis. The 1997 UBC allows the elastic response parameters (i.e., design values) that are considered in a response spectrum analysis to be

reduced for regular structures to not less than 80 percent of the basic base shear value from a static lateral load analysis.

The 1997 UBC states that: (1) Nonlinear time history analysis shall use site-specific ground motion time histories, (2) Capacities and characteristics of nonlinear elements shall be modeled consistent with test data or substantiated analysis, (3) The maximum inelastic response displacement shall comply with standard code limits (i.e., 1.5%), (4) A design review of the lateral force resisting system shall be performed by an independent engineering team.

It is also very important to note that the Engineer of Record is required to submit with the plans and calculations a statement by engineering review team stating that the review included the items in the code.

The Base Isolation Design Criteria in the 1997 UBC has provisions that provide a reward to the owner when more detailed analytical computer models are developed and used in the design of the building. These rewards are incentives for the development of more accurate models and are important for inclusion into the building code.

LIMIT STATE DESIGN AND COMPUTER MODELING OF BUILDINGS

Without the reward to the owner of a positive benefit to cost ratio, most owners will never pay the structural engineer for the time required to develop a good analytical computer model of a building. Therefore, because of this belief the author has pushed for over a decade for first the inclusion into design of limit state design concepts, and then the inclusion of capacity reduction factors that are based on structural reliability concepts that quantify the uncertainty in the performance of the designed building. To illustrate the benefits of such an approach and how measured full-scale building response data provides a very strong financial reward to the citizens of California, consider the following discussion.

Consider a building located in Los Angeles and assume that the NEHRP regulations and maps are used to calculate: (1) the earthquake ground motion, (2) the static lateral force at a floor level, and (3) the equivalent elastic rotational demand on the member using an ETAB computer model. Also assume that the failure of the connection is at a plastic rotation of 0.005 radians. Will a specific connection fail? Your answer must be yes or no. You then must quantify how confident you are in your statement. For example, you might reply that you are "70% sure that this connection will fail in this building in the next 10 years." Your confidence will depend on such factors as how much time you spent on constructing your computer model (two days vs. 10 days); how thoroughly you checked out your computer model for input errors (5 minutes vs. 2 days); the type of welding done for the connections; whether the question was asked one day, one year, or one decade after the Northridge earthquake (i.e., the state of knowledge); etc.

Now if you answered the same question after a site-specific hazard analysis by a geotechnical engineer; the development of a nonlinear computer model of the building that included load redistribution because of structural yielding; the performance of a reality check of

your computer model of the building using a previously recorded measurement of the building response; non-destructive testing of 30% of the connections in the building; etc. It is clear that even if the answer is the same, i.e."70% sure that this connection will fail in this building in the next 10 years," the more scientific analysis is, more credible and it should have a much greater weight. That is: Would I accept an answer from the latter method? Yes. Would I accept and answer from the former method? No. What if the former method shows not a 70% but a 99% probability -- would I accept it? Maybe.

A specific limit state that is being addressed as part of the design and rehabilitation of steel frame buildings will now illustrate the benefits of accurate computer modeling of buildings and measured full-scale building response. Imagine that a moment resisting steel frame is being designed. Also imagine that the limit state under consideration is the plastic rotation in the beam just adjacent to the beam-column connection. The limit state equation is

$$F = \text{Limit State Variable}$$

$$= \theta_c - \theta_d \qquad (9)$$

where

θ_c = capacity of the beam-column connection under earthquake loading

θ_d = earthquake induced demand on the beam-column connection

If the demand exceeds the capacity, the connection is defined to have failed. That is

$F > 0$ Safe Behavior

< 0 Failure

The mean value of the demand and capacity are denoted $\overline{\theta_c}$ and $\overline{\theta_d}$,respectively. Then the mean value of F is

$$\overline{F} = \overline{\theta_c} - \overline{\theta_d} \qquad (10)$$

and the Central Safety Factor is

$$FS\ (central) = \overline{\theta_c} / \overline{\theta_d} \qquad (11)$$

If θ_c and θ_d are considered to be independent random variables then the standard deviation of F is

$$V_F = \sqrt{V_c^2 + V_d^2} \tag{12}$$

where

V_c = standard deviation of θ_c

V_d = standard deviation of θ_d

The Safety Index denoted β for this limit state is

$$\beta = \frac{\bar{F}}{V_F} = \frac{\bar{\theta}_c - \bar{\theta}_d}{\sqrt{V_c^2 + V_d^2}} \tag{13}$$

In a rational world a value of the safety index would be set for a specific limit state depending on the consequences of not meeting the limit state (i.e., failure). For example, the more undesirable the failure the larger the value of the safety index. Equation (13) can be rearranged such that

$$\bar{\theta}_c = \bar{\theta}_d + \beta\sqrt{V_c^2 + V_d^2} \tag{14}$$

Assume for purposes of discussion that a simple non-scientific approach produced the same best estimate (mean) demand on the connection as the more sophisticated approach (i.e., the $\bar{\theta}_d$ is the same for both analysis methods). Therefore, the required average capacity is directly related to the square root of the sum of the standard deviation squared (i.e., variance) of the estimated capacity and demand. Assume for purposes of illustration that you had one half the uncertainty in the solution for the more scientific approach. Let $\sqrt{V_c^2 + V_d^2} = V_{ns}$ be the standard deviation of the non-scientific approach. Then the scientific approach would result in $\sqrt{V_c^2 + V_d^2} = 0.5V_{ns}$.

The required mean capacity for a non-scientific solution is

$$\bar{\theta}_{c,n} = \bar{\theta}_d + \beta V_{ns} = \left[1 + \beta\left(\frac{V_{ns}}{\bar{\theta}_d}\right)\right]\bar{\theta}_d \tag{15}$$

and the required mean capacity for the scientific solution is

$$\bar{\theta}_{c,s} = \bar{\theta}_d + 0.5\beta V_{ns} = \left[1 + 0.5\beta\left(\frac{V_{ns}}{\bar{\theta}_d}\right)\right]\bar{\theta}_d \tag{16}$$

If Equation (16) is divided by Equation (15), it follows that

$$\left(\frac{\bar{\theta}_{c,s}}{\bar{\theta}_{c,n}}\right) = \left[\frac{\left[1 + 0.5\beta\left(V_{ns} / \bar{\theta}_d\right)\right]}{1 + \beta\left(V_{ns} / \bar{\theta}_d\right)}\right] \tag{17}$$

For convenience assume that $\left(V_{ns} / \bar{\theta}_d\right)$ is equal to 0.3 and $\beta = 3$, which are both reasonable assumptions. Then

$$\left(\frac{\bar{\theta}_{c,s}}{\bar{\theta}_{c,n}}\right) = \left[\frac{\left[1 + 0.5(3)(0.3)\right]}{1 + (3)(0.3)}\right] = \frac{1.45}{1.90} = 0.8 \tag{18}$$

Therefore, there is a 20% reduction in the acceptable value of the mean capacity associated with this modest increase in confidence. This can be translated into cost savings for construction or perhaps no seismic rehabilitation being required. This value for an increase in confidence could easily result if more measured full-scale building response data was available to help verify our computer model.

In the above example, it was assumed that the same average (or best) estimate was obtained using the non-scientific and scientific computer model. Human nature usually results in more conservative assumptions when there is a lack of sufficient full-scale test data. Therefore, the 1 in the numeration of Equation (17) would probably also reduce with the acquisition of more test data. For example, if the 1.0 were to reduce to 0.7, then Equation (18) will become (1.15 / 1.90) = 0.6 or a 40% reduction in the acceptable value of the mean capacity and an even more significant cost savings.

CONCLUSIONS

The measurement of full-scale building response is a very important part of the development of the performance based design of buildings. Computer models of buildings must be verified using actual building measurements. With the advancement of limit state design methods the reduction in uncertainty associated with a verified computer model has a direct positive impact on new or seismic rehabilitation building costs.

TABLE 1 VISION 2000 SEISMIC HAZARD LEVELS (SEAOC, 1996)

Event	Recurrence Interval (Yrs)	Probability of Exceedence (%)				
		10 yrs	20 yrs	30 yrs	50 yrs	100 yrs
Frequent	43	23	47	50	100	100
Occasional	72	14	28	42	50	100
Rare	475	2	4	6	10	20
Very Rare	970	1	2	3	5	10

TABLE 2 VISION 2000 DAMAGE BY PERFORMANCE LEVEL (SEAOC, 1996)

	Performance Level				
System Description	**Fully Operational**	**Operational**	**Life Safety**	**Near Collapse**	**Collapse**
Overall Building Damage	Negligible	Light	Moderate	Severe	Complete
Permissible Transient Drift	<0.2%±	<0.5%±	<1.5%±	<2.5%±	>2.5%±
Permissible Permanent Drift	Negligible	Negligible	<0.5%±	<2.5%±	>2.5%±
Vertical Load-Carrying Element Damage	Negligible	Negligible	Light to moderate, but substantial capacity remains to carry gravity loads	Moderate to heavy, but elements continue to support gravity loads	Partial to total loss of gravity load support
Lateral Load-Carrying Element Damage	Negligible. Generally elastic response; no significant loss of strength or stiffness	Light. Nearly elastic response; original strength and stiffness substantially retained; minor cracking/ yielding of structural elements; repair implemented at convenience	Moderate. Reduced residual strength and stiffness, but lateral system remains functional	Negligible residual strength and stiffness; no story collapse mechanisms, but large permanent drifts; secondary structural elements may completely fail	Partial or total collapse; primary elements may require demolition

TABLE 3 VISION 2000 FRAME DAMAGE BY PERFORMANCE LEVEL (SEAOC, 1996)

	Performance Level			
Elements	**Fully Operational**	**Operational**	**Life Safety**	**Near Collapse**
Concrete Frames	Negligible	Minor hairline cracking (0.02"); limited yielding possible at a few locations; no crushing (strains below 0.003)	Extensive damage to beams; spalling of cover and shear cracking (<1/8") for ductile columns; minor spalling in nonductile columns; joints cracked <1/8" width	Extensive cracking and hinge formation in ductile elements; limited cracking and/or splice failure in some nonductile columns; severe damage in short columns
Steel Moment Frames	Negligible	Minor local yielding at a few places; no observable fractures; minor buckling or observable permanent distortion of members	Hinges form; local buckling of some beam elements; severe joint distortion; isolated connection failures; a few elements may experience fracture	Extensive distortion of beams and column panels; many fractures at connections

TABLE 4 VISION 2000 SHEAR WALL AND FOUNDATION DAMAGE BY PERFORMANCE LEVEL (SEAOC VISION 2000)

	Performance Level			
Elements	**Fully Operational**	**Operational**	**Life Safety**	**Near Collapse**
Concrete Shear Walls	Negligible	Minor hairline cracking (0.02") of walls; coupling beams experience cracking <1/8" width	Some boundary elements distress including limited bar buckling; some sliding at joints; damage around openings; some crushing and flexural cracking; coupling beams-extensive shear and flexural cracks; some crushing, but concrete generally remains in place	Major flexural and shear cracks and voids; sliding at joints; extensive crushing and buckling of rebar; failure around openings; severe boundary element damage; coupling beams shattered, virtually disintegrated
Reinforced Masonry Walls	Negligible	Minor cracking (<1/8"); no out-of-plane offsets	Extensive cracking (<1/4") distributed throughout wall; some isolated crushing	Crushing; extensive cracking; damage around openings and at corners; some fallen units
Foundations	Negligible	Minor settlement and negligible tilting	Total settlements <6" and differential settlements <1/2" in 30 feet	Major settlements and tilting

TABLE 5 VISION 2000 BUILDING CONTENT DAMAGE BY PERFORMANCE LEVEL (SEAOC, 1996)

	Performance Level			
Element	**Fully Functional**	**Operational**	**Life Safety**	**Near Collapse**
Furniture	Negligible effects	Minor damage; some sliding and overturning	Extensive damage from sliding; overturning, leaks, falling debris, etc.	Extensive damage from sliding; overturning, leaks, falling debris, etc.
Office Equipment	Negligible effects	Minor damage; some sliding and overturning	Extensive damage from sliding; overturning, leaks, falling debris, etc.	Extensive damage from sliding; overturning, leaks, falling debris, etc.
Bookshelves	Negligible damage	Minor damage; some overturning and spilling	Extensive damage from leaks, falling debris, overturning, etc.	Extensive damage from leaks, falling debris, overturning, etc.

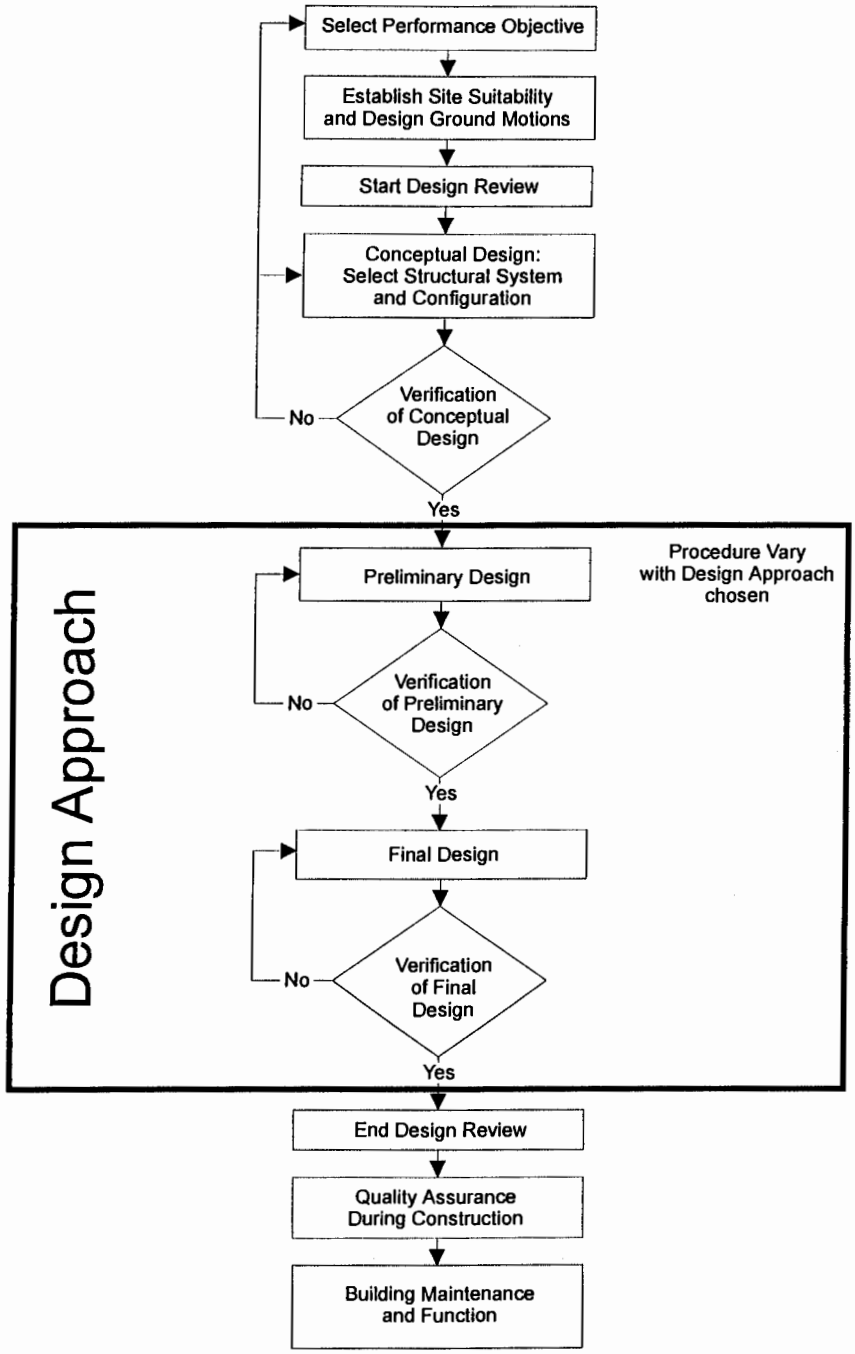

Figure 1: Vision 2000 methodology for performance-based engineering (SEAOC, 1996)

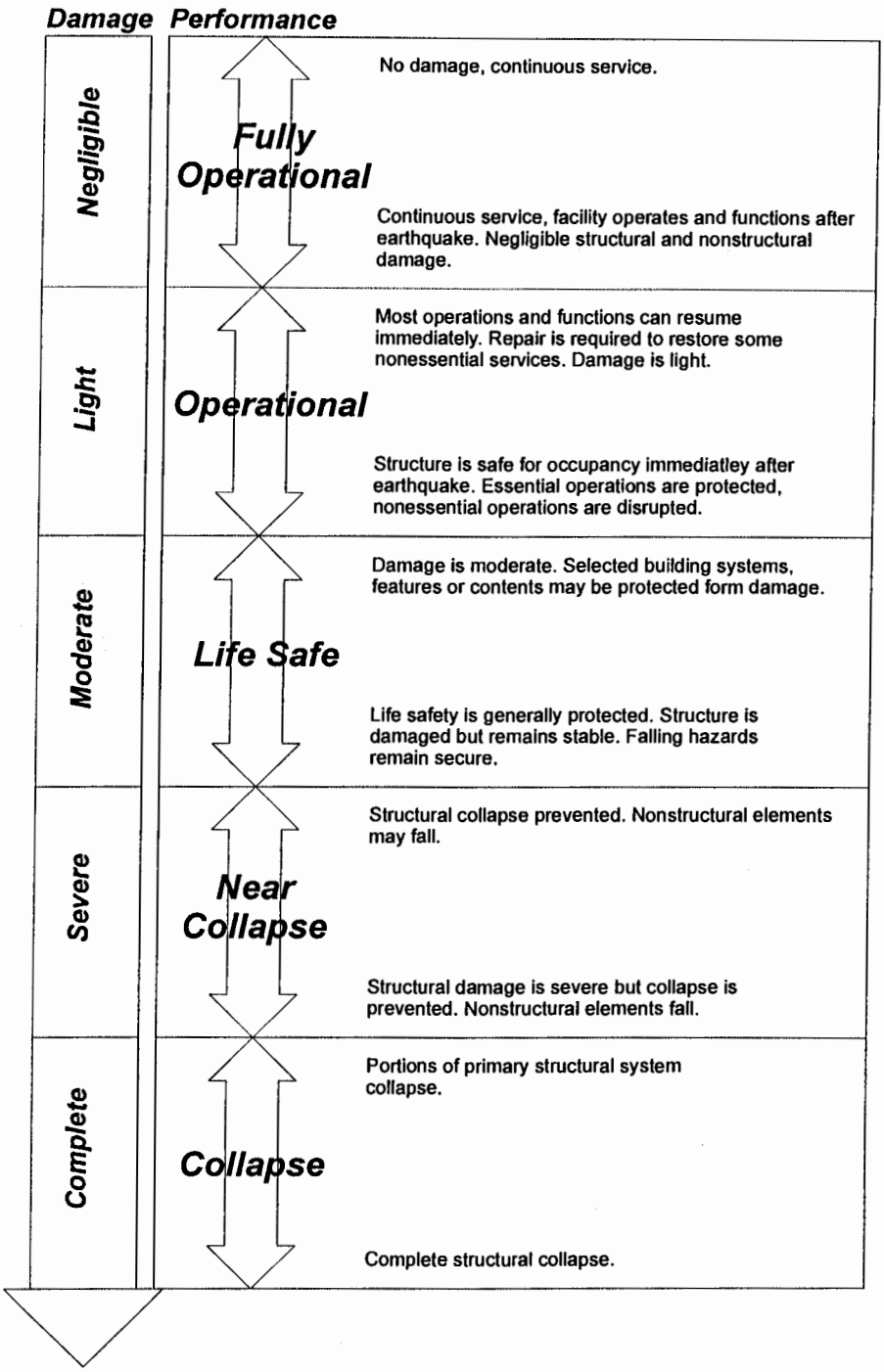

Figure 2: Vision 2000 spectrum of seismic damage states (SEAOC, 1996)

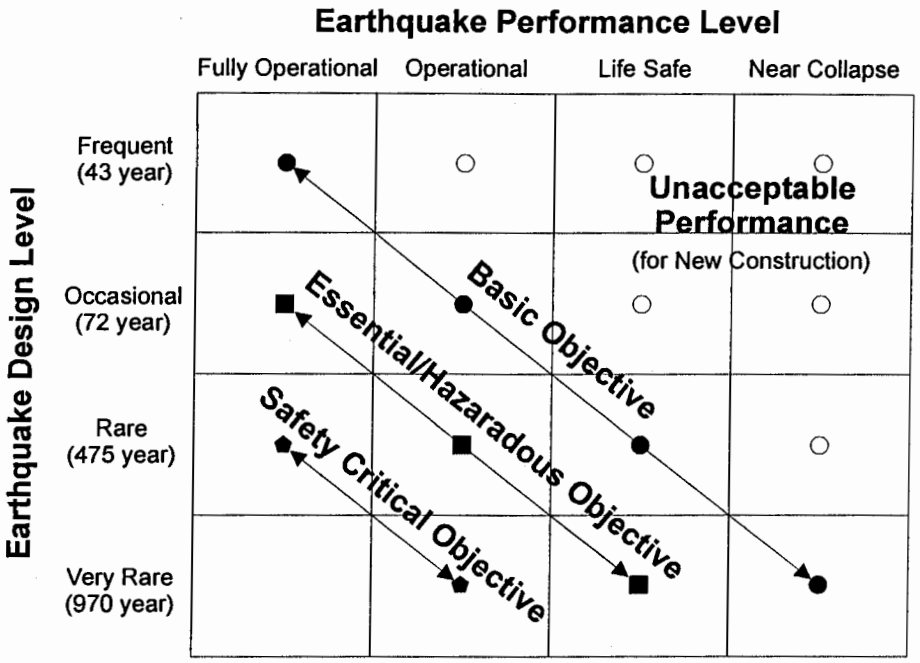

Figure 3: Vision 2000 recommended seismic performance objectives for buildings (SEAOC, 1996)

UTILIZATION OF STRONG–MOTION DATA FROM BRIDGES AND DAMS

Gregory L. Fenves

Earthquake Engineering Research Center
University of California, Berkeley

ABSTRACT

Highway bridges and concrete dams are critical components of California's infrastructure. Because of the difficulty devising experiments to test the complete system response of bridges and dams in earthquakes, the design and safety evaluation of these large structures are primarily based on mathematical models and numerical simulations. Strong–motion data from bridges and dams provide the real–life laboratory for verifying the models. This paper summarizes the results from recent studies of the recorded strong–motion response data from bridges and a dam. Although the strong–motion data are limited, they have provided confirmation that models are capturing the essential features of earthquake response. Limitations of the models, however, are identified and future trends for instrumentation and data utilization for bridges and dams are discussed.

INTRODUCTION

Although very different structural systems, bridges and dams have several common characteristics. Both types of structures are critical components of the infrastructure for transportation and water resources, respectively, for which a high level of performance during an earthquake is expected by society. Considering the dynamic characteristics, interactions of the structures with the surrounding media, such as soil and water, play an important role in the earthquake response. They are large structures for which length scales of thousands of feet are common. The large size and multiple or continuous connections with the ground, over a varying topography and soil conditions, mean that the assumption of uniform free-field ground motion is seldom valid. Because of the large size of the bridges and dams, experimental testing of system performance in earthquakes presents profound difficulties with similitude, boundary conditions, and limited capacity of earthquake simulators. Consequently, mathematical modeling and numerical simulation of bridge and dams systems are the primary method for assessing earthquake performance and safety.

How accurate are the mathematical models of bridge and dam systems? One way that we can answer this question is by examining and interpreting their performance as recorded by strong–motion instrumentation during an earthquake. The recorded responses of structures in earthquakes provide the laboratory in which engineers can study characteristics, assess the validity of mathematical models, and improve understanding of earthquake performance. The instruments for the modern full-scale earthquake laboratories in the field are digital strong–motion accelerometers strategically located to capture input motion, global response characteristics, and important local response. The methodologies include direct interpretation of strong–motion records, system identification for vibration properties or system and component properties, and direct comparison numerical simulation results from models.

The goal of this paper is to examine retrospectively the use of strong–motion records for bridges and dams. The California Strong Motion Instrumentation Program (CSMIP) has instrumented bridges, and to a lesser extent dams, in addition to its basic mission and funding base for instrumenting buildings. This review will concentrate on results from bridges and one case of a concrete dam. Although numerous data utilization studies are referenced, previous studies in which the author has been involved are emphasized. The paper concludes with comments about needs for the instrumentation of bridges and dams and future trends.

INSTRUMENTATION OF BRIDGES

At the time of the 1989 Loma Prieta earthquake, CSMIP had instrumented six bridges, a segment of the BART elevated structure, and one tunnel. Three of the bridges were short with two to six spans (156/101 Separation in Hollister, Painter Street Overcrossing in Rio Dell, and Meloland Road Overcrossing in El Centro) and one was a ten span bridge retrofitted with seismic isolators (Seirra Point Overhead in South San Francisco). The other two pre–1989 instrumented bridges were the 6000 ft long Vincent Thomas suspension bridges and the 8600 ft long Dumbarton bridge with prestressed concrete and steel box girder construction. These two long bridges each had 26 accelerometers and limited free–field ground motion instruments. The Loma Prieta earthquake demonstrated the fragility of several bridge types. The only strong–motion records from bridges in Loma Prieta, as will be discussed later, were from the Sierra Point Overhead and the Dumbarton bridge. Because of the limited instrumentation a valuable opportunity to improve understanding about earthquake response of bridges was lost.

After the Loma Prieta earthquake the California Department of Transportation recognized the importance of installing strong–motion instrumentation in a variety of bridge types, and it began funding an expanded instrumentation program. Between 1989 and 1993, Caltrans and CSMIP installed strong–motion instrumentation in 14 additional bridges, including a limited number of channels (nine or less) on three toll bridges. From this era significant strong–motion records were obtained from curved connector bridges in the Landers, Big Bear, and Northridge earthquakes. Another important record was obtained at the Painter Street Overcrossing in the 1992 Petrolia earthquake, with a peak horizontal acceleration of 1.09 g.

The Caltrans–CSMIP instrumentation program accelerated after the 1994 Northridge earthquake. Through mid–1996, 24 additional bridges have been instrumented. The majority of the bridges are reinforced or prestressed concrete box girder bridges, the predominant construction type in California. Most instrumented bridges have six to twelve accelerometers, but two curved connectors have 30 to 36 channels. Two of the sites have downhole arrays with six accelerometers. The downhole arrays will provide invaluable information about the propagation of free–field motion through the site up to the bridge footings and ground surface, and provide opportunities for verifying soil models, which is an urgent need.

At this time, Caltrans plans to instrument seventeen additional freeway bridges and five downhole arrays. Also under planning are instrumentation networks for the toll bridges in conjunction with the toll bridge retrofit program. The Golden Gate Bridge District also plans to install a network as part of the seismic retrofit for that vital transportation link.

DATA UTILIZATION STUDIES FOR BRIDGES

Wilson (1984) examined the response of the first instrumented bridge in California (Route 156/101 Separation in Hollister) to the 1979 Coyote Lake earthquake. Later the two–span Meloland Road Overcrossing in the 1979 Imperial Valley earthquake was the subject of several studies (Werner, et al., 1987; Werner, et al., 1993). The Meloland studies have shown large damping ratios, in excess of 20%, for the embankment abutments. The study also showed the importance of using cracked section properties in the model for a valid comparison with the recorded response.

In the 1989 Loma Prieta earthquake, strong–motion data was recovered from the Dumbarton bridge. A study by Fenves, et al. (1992) obtained spectral estimates of vibrations properties and compared the recorded response with models using various assumptions. The results showed the sensitivity of the response to assumptions about the articulations at the hinges and also to the soil properties. Another examination of the Dumbarton bridge by McCallen (1992) using a refined

finite element model made similar observations and noted the difficulty with fully reproducing the recorded response by numerical simulation.

A set of Loma Prieta records was obtained from the Sierra Point bridge. The heavily skewed, steel girder bridge was retrofit in 1985 with lead–rubber isolation bearings replacing older steel bearings. However, no seismic gap was provided for at the abutments, apparently because the primary objective of the isolators was to limit forces into the tops of the non–ductile columns, and the expectation that the abutment backwalls would fail during a large earthquake. A study of the records by Kelly, et al. (1991) showed the strains in the bearings did not exceed 4%, barely yielding the lead core, and the effective isolation vibration period was a short 0.75 sec. Although the stiff bearings provide little isolation at small shear strain, there was some reduction in short period energy transmitted from the superstructure and abutments to the columns below the isolators.

Another Loma Prieta study involved a section of the elevated BART structure in Hayward. Tseng, et al. (1992) examined the significant effects of soil–structure interaction on the response of the single column bents supporting the tracks.

The 1992 Petrolia earthquake produced peak free–field ground acceleration of 0.52 g at the Painter Street Overcrossing, and 1.09 g at one abutment of the structure. Records from eight other earthquakes and aftershocks have been recorded at the bridge, making it one of the most studied (Maroney, et al., 1990). McCallen and Romstad (1994) developed a very refined solid nonlinear, finite element model of the bridge, embankments, and abutments. The advanced simulation showed the importance of hysteretic energy dissipation in the embankment soils. Sweet and Morrill (1993) examined a simpler nonlinear model of the soil to explain the bridge response. Using a different approach, Goel and Chopra (1997) directly estimated the time–varying abutment stiffness and torsional response from the records caused by the skew and differences in transverse stiffness of the two abutments. They concluded that the Caltrans guidelines for computing abutment stiffness based on the capacity of the abutment divided by the assumed failure displacement of 2.4 in. were reasonable. The results also show significant hysteretic energy dissipation in the abutments, which is typically not recognized in bridge design.

A CASE STUDY: CURVED CONNECTOR BRIDGE

The Northwest Connector bridge at the Interstate 10/215 interchange in Colton, Calif., was the first bridge with single column bents to undergo an extensive column and footing retrofit. As part of the 1992 retrofit, Caltrans and CSMIP installed 34 channels of accelerometers, as shown in Fig. 1. This section summarizes a study by the author (Fenves and Desroches, 1994; Desroches and Fenves, 1997) and to a lesser extent a later study by Liu, et al. (1996).

Table 1 lists the strong–motion records obtained at the Northwest Connector. The response spectra for the free–field site for 1992 Landers and Big Bear earthquakes are shown in Fig. 2. The response spectra can be compared with the smooth design spectrum used by Caltrans for a deep alluvial site and PGA of 0.70 g. Also, shown in Fig. 2 is the smoothed elastic response spectrum reduced by a factor of four, a typical value to account for inelastic behavior of single column bents. For periods less than one second, the spectra for the recorded motion exceed the reduced spectrum. For longer periods the design spectrum mostly envelopes the spectra for the two earthquakes. The spectral ordinates for the Northridge earthquake are much less than for Landers and Big Bear at periods greater than 1.5 seconds. From system identification results described later, the important vibration modes of the bridge have periods between 1.0 and 1.7 sec. In this period range there is not a large difference between the reduced design spectrum and actual spectra, so it can be expected that the forces developed in the columns approached the nominal design strengths.

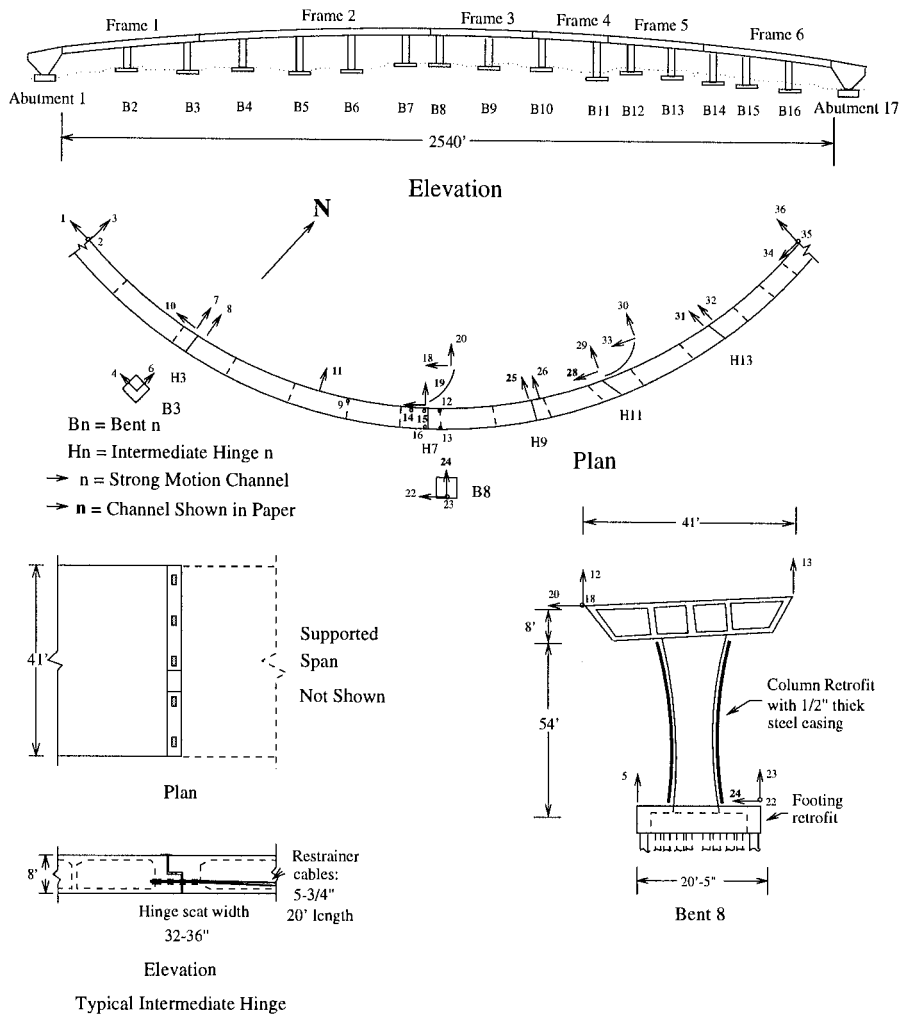

Fig. 1 General plan and instrumentation for the Northwest Connector at the Interstate 10/25 Interchange.

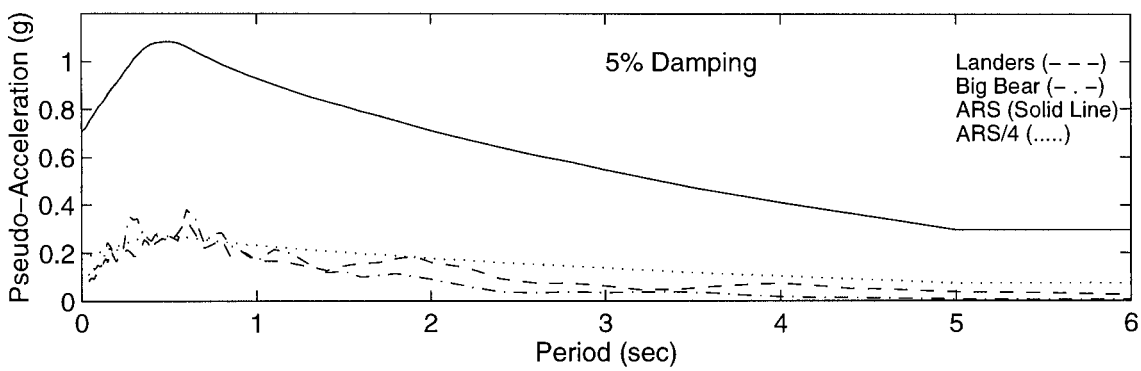

Fig. 2 Response spectra for Landers and Big Bear free–field ground motions (major axis) compared with Caltrans design spectrum.

Table 1. Earthquakes and Free–Field Ground Motion Recorded at the Northwest Connector

Event	Magnitude M_s	Epicentral Distance (miles)	Peak Acceleration (g)	
			Horizontal[a]	Vertical
1992 Joshua Tree[b]	6.3	52	—	—
1992 Landers	7.6	50	0.09	0.06
1992 Big Bear	6.6	28	0.11	0.07
1994 Northridge	6.8	72	0.08	0.04

[a]Instantaneous peak horizontal acceleration.
[b]Records not processed.

The instrumentation allows examination of the spatial variation of the input motion over the length of the bridge. Figure 3 shows the displacement time histories at the free–field site and at four supports for the bridge (two abutments, bents 3 and 8) in the Landers earthquake, and the maximum displacements are plotted in Fig. 4. The coherency functions for the pairs of input acceleration histories show a general loss of coherency for frequencies greater than 2 Hz, as typically expected.

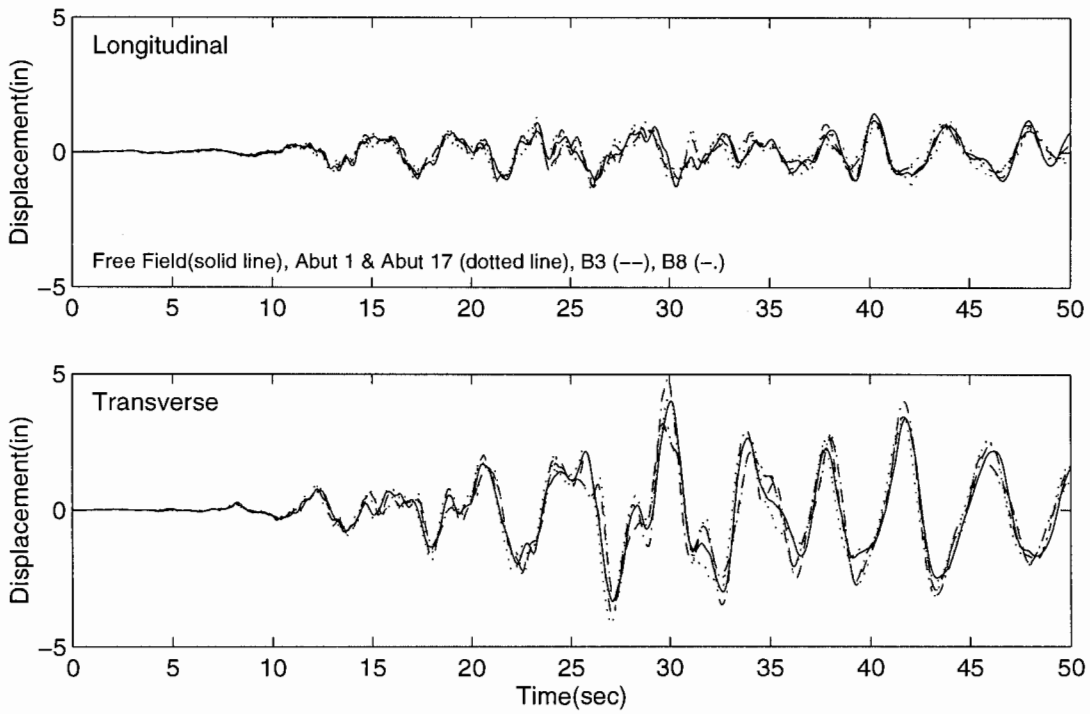

Fig. 3. Horizontal displacement at four support and free–field in global longitudinal and transverse directions for the Landers earthquake.

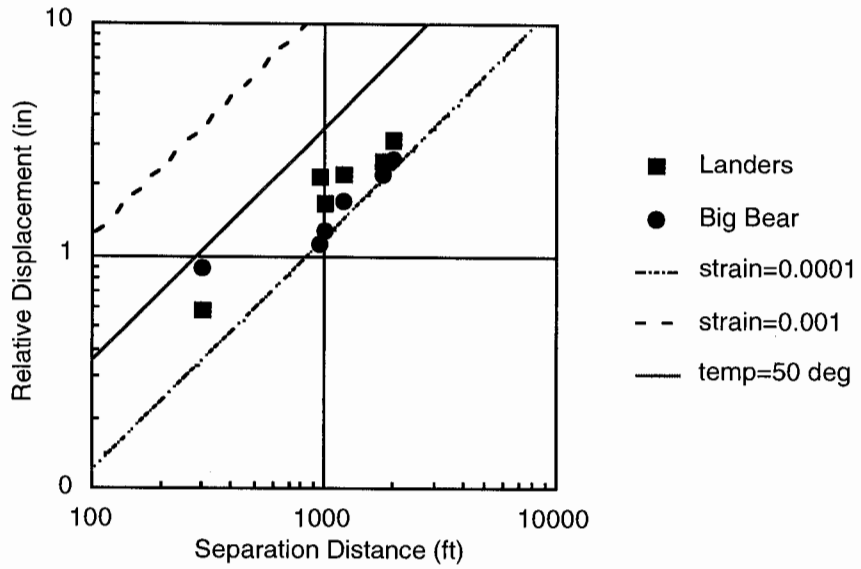

Fig. 4 Maximum relative displacement between supports as a function of distance between supports.

Evaluation of Earthquake Response

The instrumentation at bent 8 allows direct evaluation of the column deformation accounting for footing and superstructure rotation. The maximum column deformation for bent 8 near the center of bridge is 4.8 in. for Landers (0.86% drift) and 3.0 in. for Big Bear (0.54% drift). The Liu (1996) study reports bent 8 column deformations of 5.6 in. and 3.5 in. for the two earthquakes, respectively, although it is not clear if the superstructure rotation was accounted for in these calculations. Foundation flexibility through pile cap rotation are significant, contributing about 15% to the displacement of the superstructure. Based on analysis of a calibrated model and estimates of capacities, bent 8 reached 80% and 87% of the yield moment in the longitudinal and transverse direction, respectively, in the Landers earthquake. This is consistent with the post–earthquake inspection which did not reveal any evidence of cracking or other signs of deformation.

The thorough instrumentation in the bridge allowed evaluation of the opening and closing of intermediate hinges in the bridge, which are used to take temperature induced strains and simplify construction and post–tensioning. The hinge near bent 8 opens a maximum of 1.41 in. and 1.70 in. in Landers and Big Bear, respectively, which is less than the yield displacement of the cable hinge restrainers (and much less than the 32 in. hinge seat width). As a result, the cable restrainers had a small effect on the response of the bridge because of the small hinge opening. Malhotra, et al. (1994) also examined the hinge response, particularly looking at the acceleration spikes caused by pounding.

Two system identification techniques were used to identify the vibration properties of the Connector. The first method involved transmissibility functions were computed using cross–power spectral density estimators. The second method used parametric time domain identification (Safak, 1990). Table 2 summarizes the results of the identification. The periods from the two identification procedures are similar, except for the second mode for the Landers earthquake, although it is possible there are two closely spaced modes which are identified differently by the two methods. Liu (1997) study identified somewhat shorter periods of 1.67 sec, 1.47 sec, and 1.19 sec, although it is not clear for which earthquake these periods pertain.

Table 2. Identified Vibration Periods and Damping Ratios for the Northwest Connector

	Landers Earthquake			Big Bear Earthquake		
	Spectral Analysis	Parametric Identification		Spectral Analysis	Parametric Identification	
Mode	Period (sec)	Period (sec)	Damping Ratio (%)	Period (sec)	Period (sec)	Damping Ratio (%)
1	1.51	1.56	3.1	1.78	1.75	8.2
2	1.19	1.30	11.0	1.24	1.29	2.1
3	1.02	0.98	5.0	1.14	1.09	15.0
4	0.79	0.83	7.0	0.95	0.96	7.0

The most significant finding in Table 2 is the difference in the fundamental mode period of the bridge in the Landers and Big Bear earthquakes. Although there is little change in the second mode, the third and fourth mode period are long in the Big Bear earthquake. The change in the fundamental mode implies a 20% reduction in stiffness of the bridge, and the damping increases from 3.1% to 8.2%. The lengthening of the vibration periods and generally increased damping indicate that the bridge softened during the Landers earthquake. Since the column forces were less than the yield strength, the increased flexibility is due to column cracking and softening of the pile footings and soil. The identified results show the footing rotational stiffness was smaller in the Big Bear earthquake than in Landers, possibly due to compaction and gapping of soil around the piles or a change in the ground water table between the two earthquakes. The Liu (1996) study tracked the decrease in bent 8 lateral stiffness as a function of displacement and only a slight increase in flexibility due to soil–structure interaction in Big Bear.

Verification of Mathematical Models

The major objective of the Fenves and Desroches study (1994) was to examine the efficacy of typical lumped–parameter models used in bridge design. Since the structural components did not experience inelastic deformation, it was appropriate to use a linear elastic model. However, the nonlinear behavior of hinge opening and closing are included in the model with gap elements. Generally, the modeling followed guidelines in the recent ATC–32 report (ATC, 1996). The effective stiffness of the steel jacketed columns was selected to match identified vibration properties. The best fit model give an effective stiffness of $1.20EI_g$ and $0.95EI_g$ for the Landers and Big Bear earthquakes, respectively, for the columns with full–length steel jackets, where EI_g is based on the gross section properties. A factor of 1.20 EI_g is consistent with a cracked stiffness of $0.75EI_g$ and an increase in stiffness from the steel jackets of 60%. The calibration represents the reduction in stiffness apparent in the lengthening of the vibration periods between the earthquakes.

The comparison of total displacements for Landers is shown in Fig. 5 assuming uniform free–field ground motion. Overall, the comparison is reasonable although some of the peak displacements are underestimated by the model, particularly during the strong–motion response. The model does not produce as accurate accelerations because of the greater participation of the high frequency modes, which are not represented well in the coarse lumped parameter model. The model captures the captures the acceleration spikes characteristic of the impact between adjacent frames as the hinges pound closed. Figure 5 shows that the model represents adequately the response of the hinge. In addition the model gives the propagation of acceleration pulses from impact at the hinge.

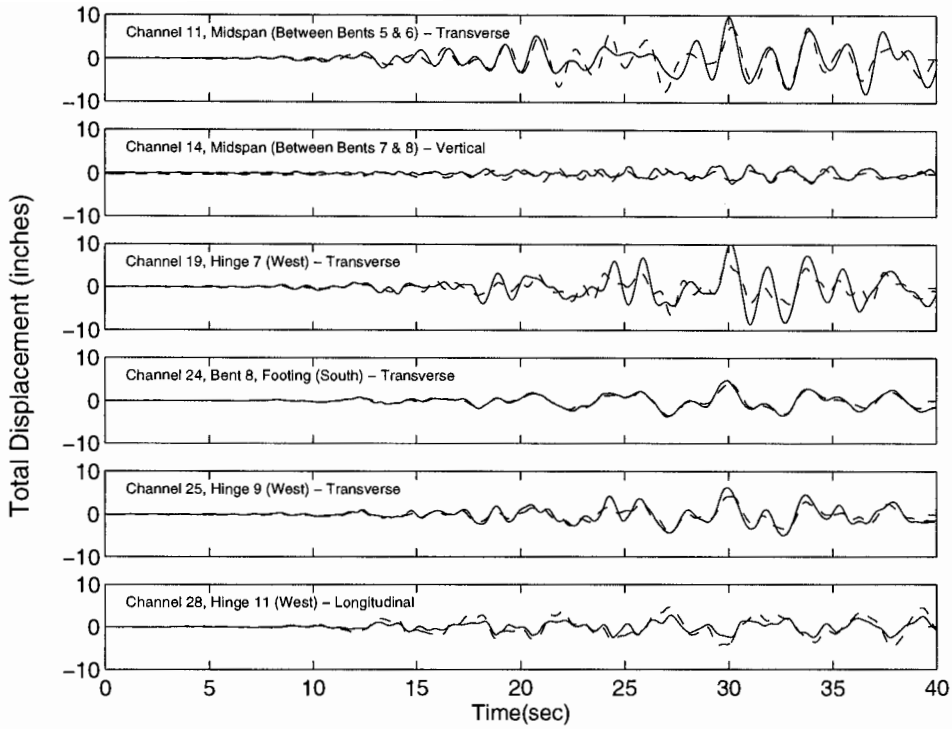

Fig. 5 Comparison of recorded displacement (solid line) with computed displacement (dashed line) using uniform free–field Landers earthquake ground motion.

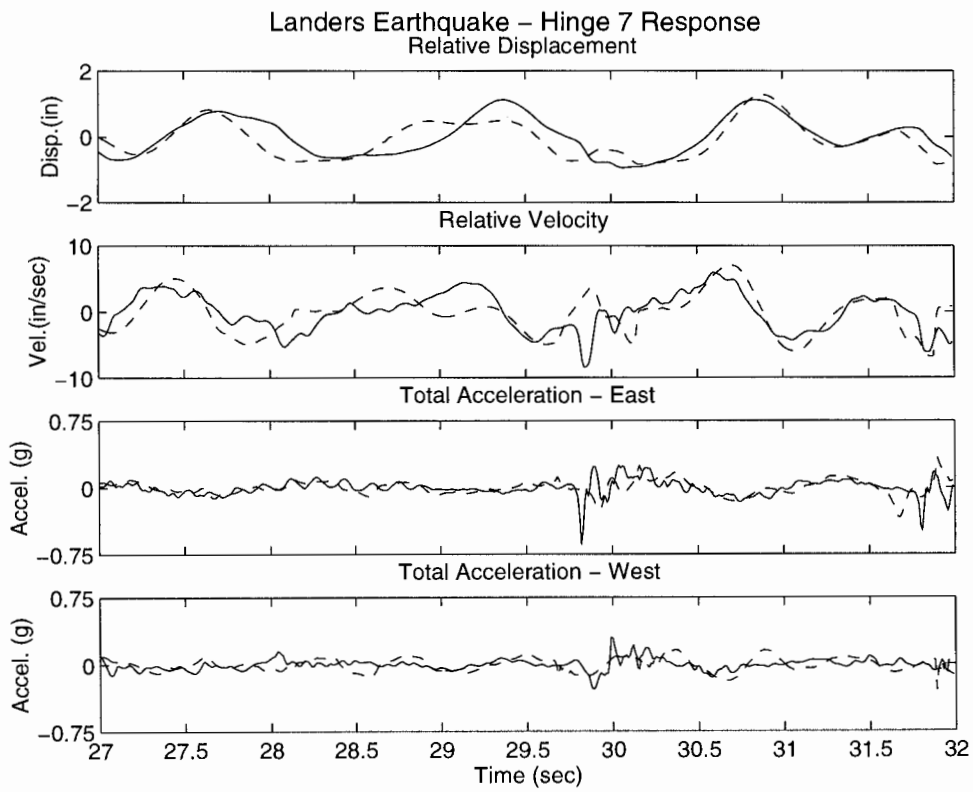

Fig. 6 Comparison of recorded longitudinal hinge motion (solid line) and response from model (dashed) for the Landers earthquake.

To examine the effect of non–uniform ground motion on the response of the bridge, the recorded displacements at the four supports were imposed using a simple interpolation scheme. Figure 7 shows the comparison for the Landers earthquake, which is a considerable improvement over the results in Fig. 5 for uniform free–field input motion. These results indicate that the apparently small differences in input displacement (see Fig. 3) have a fairly important effect on the displacement histories of the bridge. To examine the effect on column moments, Fig. 8 shows the non–uniform input motion has a more important effect on the transverse bending moment than on the longitudinal moment. Most of the difference is caused by dynamic response, because the pseudo–static forces are relatively small.

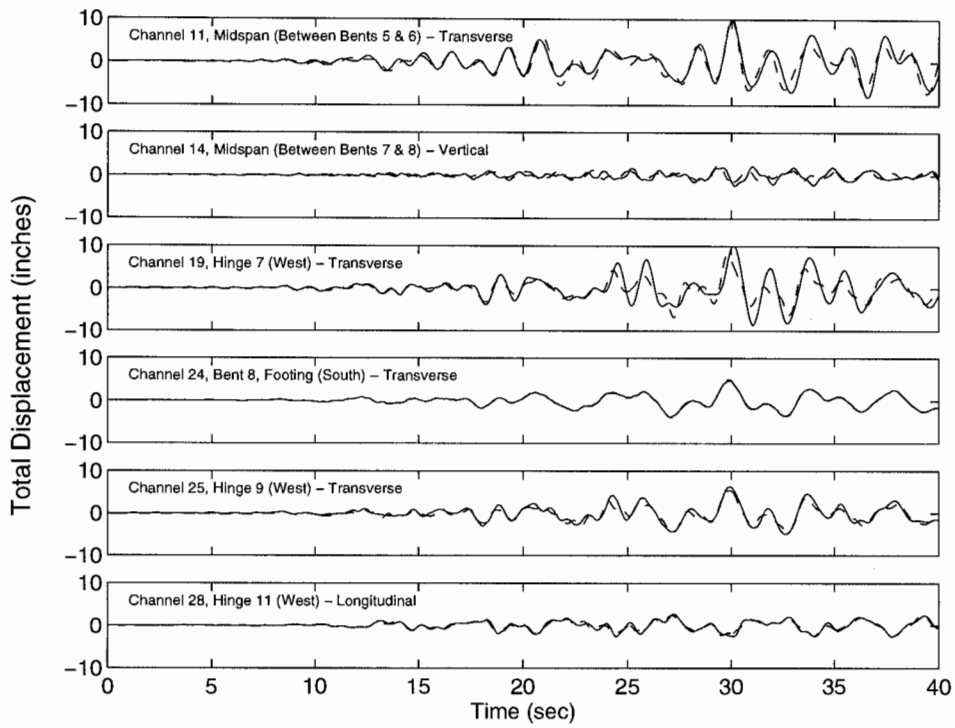

Fig. 7 Comparison of recorded displacement (solid line) with computed displacement (dashed line) using non–uniform input motion from the Landers earthquake.

Evaluation of Design Models

Bridge design is generally based on a linear global model to compute the displacement demands and elastic forces. To account for the effects of the hinge opening and closing, it is common to bound the response by two linear models: a tension model and compression model. The tension model essentially represents the hinges as open and compression model as hinges closed. Using the calibrated model, Fig. 9 plots the column moments for the design model with uniform free–field motion compared with the moments from the nonlinear model with non–uniform input motion. Considering the longitudinal response, the compression model gives larger moments than the tension model for the short columns, particularly at the end frames. The tension model gives larger moments for the taller, flexible columns. Generally the two models bound the nonlinear response within about 10%. However, in the transverse direction the nonlinear model produces up to 50% larger moments for five columns. This is primarily due to larger response for the non–uniform input motion compared with the uniform motion in the design models.

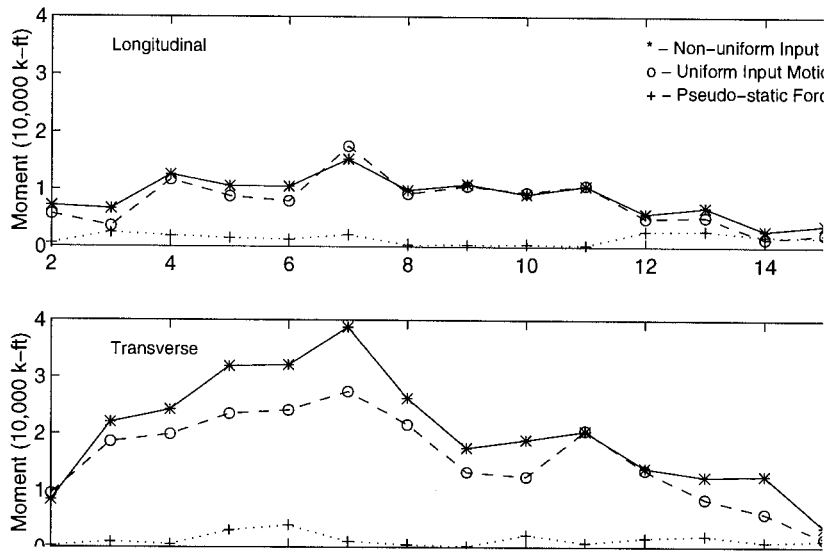

Fig. 8 Maximum column moments for uniform and non–uniform input motion in the Landers earthquake.

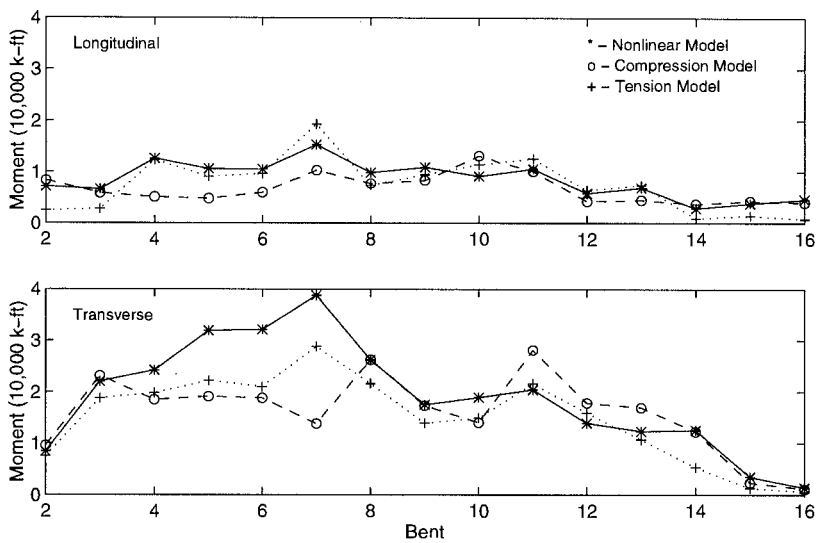

Fig. 9 Comparison of column moments from nonlinear model with moments from design models.

DATA UTILIZATION FOR CONCRETE DAMS

Compared with bridges, few dams have been instrumented with strong–motion accelerometers. Strong–motion records from several earth dams in the Loma Prieta and Northridge earthquakes are available and have been studied by geotechnical engineers. However, there is only one set of strong–motion records for a concrete dam. This section summarizes the results of a recent study of Pacoima dam in the 1994 Northridge earthquake (Mojtahedi and Fenves, 1996).

Pacoima dam is illustrated in Fig. 10. It is a 365 ft tall, 589 ft long flood control arch dam located 4.5 miles northeast of San Fernando, California. Uniformly spaced contraction joints with 12 in. deep beveled keys divide the dam into eleven cantilevers. The left abutment is supported by

a concrete thrust block through a 60 ft tall joint. The dam was subjected to severe shaking in the 1994 Northridge earthquake, with the epicenter 11 miles from the dam. The peak accelerations of 1.6 g and 1.2 g, at the left abutment in the horizontal and vertical directions, respectively, are among the largest ever measured during an earthquake. The reservoir level was 233 ft above the base (about two–thirds full including the silt).

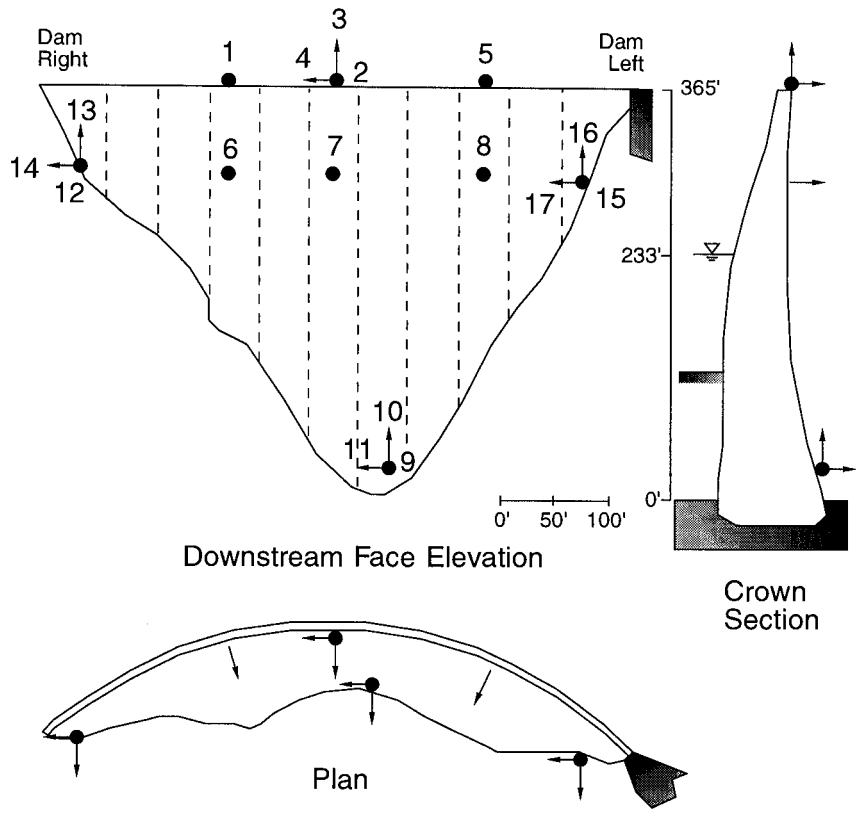

Fig. 10 Pacoima dam and strong–motion instrumentation plan.

Over–stressing of the dam occurred during the earthquake, as indicated by cracks and permanent movements of the concrete blocks. Most of the damage, however, can be attributed to the movement of the thrust block due to a failure in the supporting foundation rock. The contraction joint between the dam and the thrust block opened and remained open after the earthquake: about 2 in. at the crest and 1/4 in. at the bottom. Some permanent differential movement in the vertical direction also occurred at the joint, with the thrust block lower with respect to the dam. A diagonal crack occurred in the thrust block near the bottom of the thrust block joint. The dam body suffered less damage, with minor cracking permanent offsets of some blocks. There was evidence that the vertical contraction joints opened because of their subsequent clean appearance. This was the first evidence of contraction joint opening in a concrete dam during an earthquake.

The strong–motion records provided a unique opportunity to examine the contraction joint behavior in an arch dam subjected to a large earthquake. The locations of the accelerometers on the dam are shown in Fig. 10. Several of the records could not be digitized completely because large acceleration peaks, which exceeded the range of instruments, were intertwined on the film. Processed records are available for two locations in the canyon, one at the downstream and the other 50 ft above the left abutment, and channels 8 to 11 on the dam. The peak accelerations

recorded in the canyon were 0.43 g and 1.58 g for the downstream and the upper left abutment (ULA) instruments, respectively, indicating the amplification of ground motion by the canyon topography. The stream component of these motions are shown in Fig. 11. Channel 8 recorded the radial acceleration, with a peak of 1.31 g, at the left quarter point at 80% height of the dam. Figure 12 shows the radial accelerations of the dam at three different elevations, the base, 80% height and the crest. The partially digitized but unprocessed acceleration records from the crest of crown section are plotted in Fig. 13,

Development of the Model

The finite element computer program ADAP–88 (Fenves, Mojtahedi, et al., 1989; Fenves, Mojtahedi, et al., 1992) was used for the earthquake analysis of the dam. Nonlinear joint elements simulate opening–closing of the contraction joints, lift joints, and the dam–foundation interface. Spatially non–uniform seismic input, can be specified through displacement histories at the dam–foundation interface (Mojtahedi and Tseng, 1994).

Two types of earthquake analysis were performed. The first type used a uniform free–field motion, whereas non–uniform free–field motion was considered in the second type. The free–field motions for both cases were derived from the motions recorded in the canyon during the Northridge earthquake. For determining the non–uniform free–field motion, it was not possible to separate dam–foundation interaction effects from the spatial variation of the canyon motion. Hence, those dam–foundation effects were neglected and the recorded motion at the interface was assumed to be the free–field motion. Due to the profound difficulties in determining the motion of canyon and also lack of sufficient acceleration records from the earthquake, a simple approach was adopted for specification of the non–uniform free–field motion. The same motion was specified for the right and the left abutments. The ULA and the dam base records were specified for the crest and the base of the dam, respectively. The motion at intermediate elevations was computed by linear interpolation from these records, as illustrated in Fig. 14.

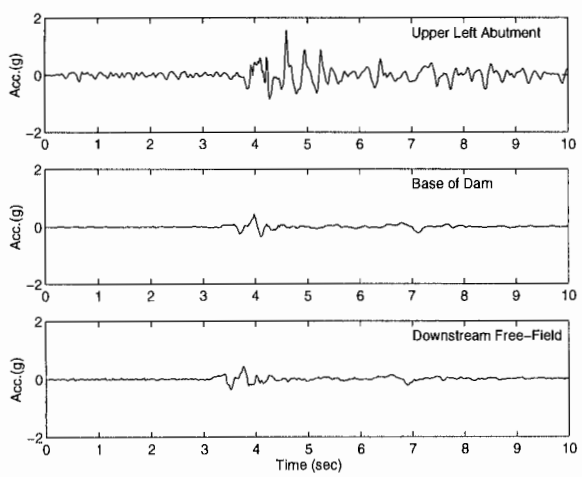

Fig. 11 Recorded acceleration histories for the canyon of Pacoima dam.

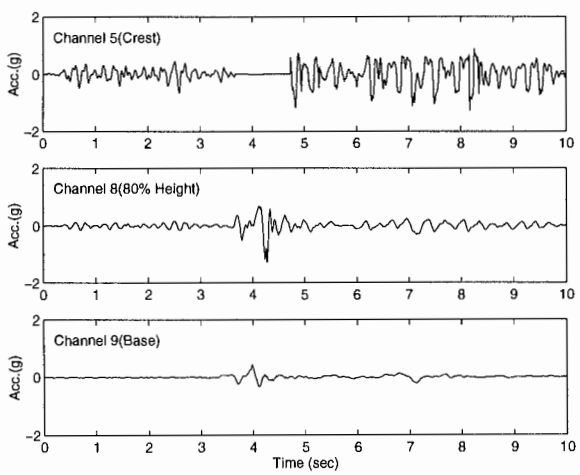

Fig. 12 Recorded radial acceleration history of dam. Zero acceleration shown for gaps in digitization of Channel 5.

For the finite element analysis, a total of 588 eight–node 3–D elements model the dam body. The number of contraction joints and lift joints in the dam model was selected from trial analyses.

Of the twelve vertical joints in the dam, only five were included in the model. In addition, five horizontal joints, at 50, 97, 135, 202, and 282 ft above the base, were included to represent lift joints. A foundation rock region with a depth approximately equal to the height of the dam was included in the model to account for dam–foundation interaction effects. Although the foundation rock geometry and material properties are complicated, a prismatic shape was assumed for the canyon using a coarse mesh of the foundation rock region with 220 3–D solid elements. To suppress the propagation of seismic waves, the foundation rock was assumed to be massless. Rayleigh damping was assumed for the dam–foundation system with parameters selected to produce 10% damping at 5 Hz and 20 Hz. The assumed damping is relatively high, but is justified considering that radiation damping in the massless foundation is not explicitly included in the model. For analysis with uniform free–field motion, the acceleration was specified at the rigid base of the foundation model. For analyses with non–uniform free–field motion, the displacement was specified at the nodes on the dam–foundation interface.

The first natural frequency computed for the dam using these properties, with the 233 ft reservoir level, was 4.3 Hz with an anti–symmetric mode shape. To confirm the selected properties, the transmissibility function was computed for the radial motions recorded at the base and channel 8. The fundamental frequency of the dam from the transmissibility function was 4.0 Hz which, considering the limited data, is in reasonable agreement with the model frequency.

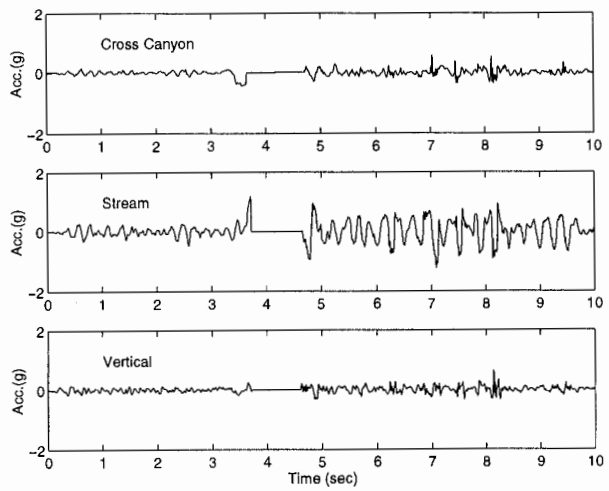

Fig. 13 Unprocessed acceleration histories at crest (channels 2–4). Zero acceleration shown for gaps in digitizing.

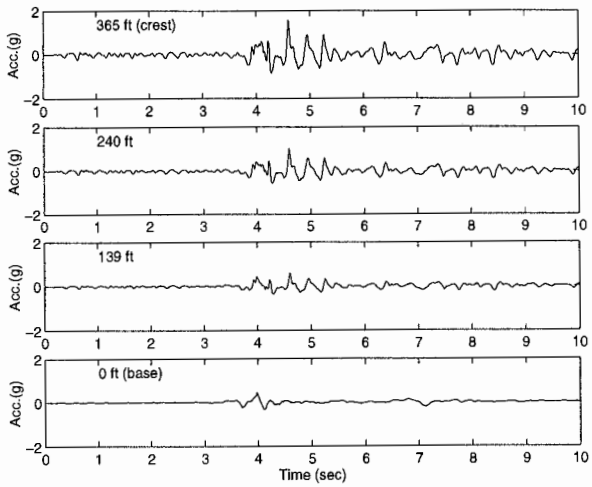

Fig. 14 Assumed non–uniform acceleration histories at the dam–canyon interface in stream direction.

Evaluation of the Model

The amplification of seismic waves in the canyon was indicated by variation in the acceleration amplitudes recorded at the downstream, base, and upper left abutment (Fig. 11). To assess the effects of the ground motion input on the response of the dam, two cases were analyzed with all joints closed. Following previous studies of the dam (Dowling and Hall, 1989), two–thirds of the ULA motion was considered as the average motion of the canyon and was specified as uniform input motion for the first case. The previously described non–uniform free–field motion was used for the second case.

The recorded and computed accelerations for channel 8 are shown in Fig. 15. The accelerations computed for the two closed joint cases differ in amplitude and phase. The case with non–uniform input agrees better with the recorded acceleration than does the uniform input case. However, the responses computed for both cases contain a large amplitude cycle which is not present in the recorded motion. The overestimation of the vibration is most likely caused by the lack of radiation damping in the foundation model. The sliding of the foundation rock mass near the left abutment, not accounted for in the model, may also be responsible for the discrepancy.

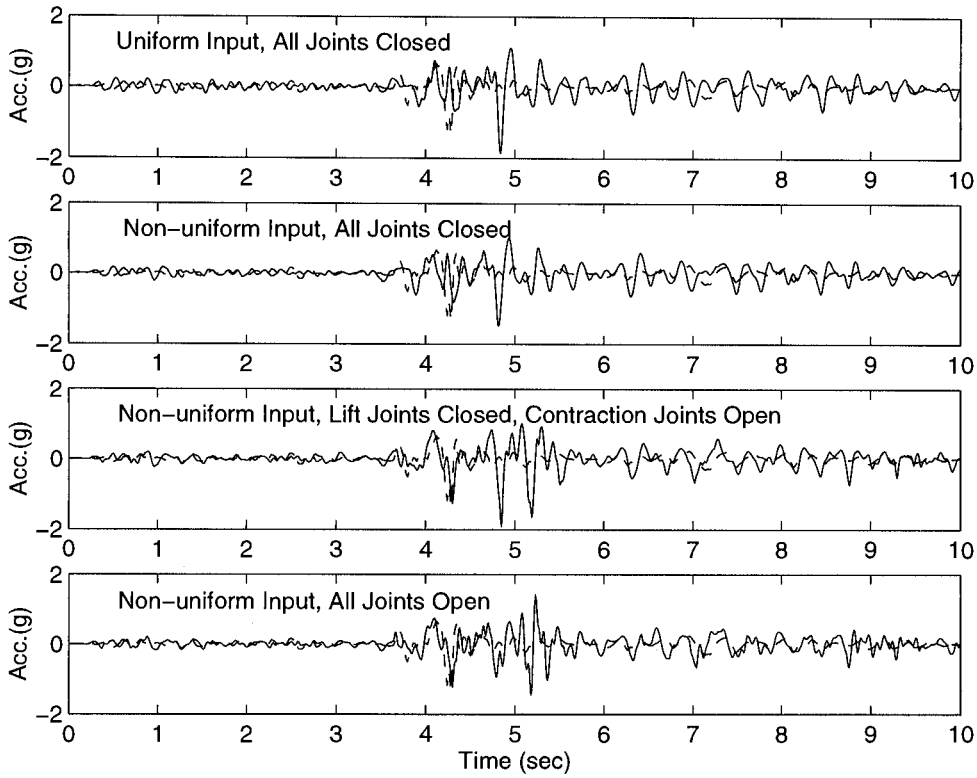

Fig. 15 Comparison of recorded acceleration for channel 8 (dashed line) with computed acceleration (solid line) at the same location.

To examine the effects of contraction joints, as well as opening at the dam–foundation interface due to tensile stresses, the analysis with non–uniform input motion was repeated with these joints allowed to open. From the channel 8 acceleration comparison in Fig. 15, the agreement between computed and recorded acceleration improves significantly when the joints are allowed to open. However, the computed response again contains spikes not present in the recorded motion for the reasons mentioned previously. The cantilever stresses computed for the case with contraction joint opening exceed the tensile strength of concrete and the lift joints. To account for the opening of lift joints, the dam was analyzed with all vertical, horizontal and abutment joints allowed to open, and considering the non–uniform input motion. In view of the permanent opening of the thrust block joint, the tangential stiffness of the joint was omitted. The last history in Fig. 15 for non–uniform input and all joints open shows the best comparison between the computed and recorded acceleration at channel 8.

Mojtahedi and Fenves (1996) present contours of peak tensile stresses from the various models. The maximum cantilever stress of downstream face reduces to 1000 psi from 1800 psi for lift joints assumed closed. Significant opening occurs at the top lift joint with a maximum value of

2.6 in. at the base of thrust block on the downstream face. The opening for all other locations is less than 0.5 in. The simulations show complete separation through the thickness over a short length occurs at a several locations.

While this study has shown that the non–uniform canyon motion affected the response of Pacoima dam, and the opening of contraction joints was confirmed by the model and simulation, the lack of processed strong–motion data limited the quality of information from the Northridge earthquake. Although further attempts at digitizing and processing the film records may be futile, there is an important need for a thorough study of the records and deconvolution analysis to identify the free–field motion in the canyon.

FUTURE NEEDS

Strong–motion instrumentation of structures always involves a tradeoff between the number of instruments (i.e. the cost) and the richness of the data for one structure or over an expected epicentral region. As with most endeavors, cost is the controlling factor. However, the costs of not recording data in a major earthquake are rarely quantified. Increasing the instrumentation program for bridges and dams will require well–reasoned arguments that the current costs are justified by the future costs avoided.

There has been tremendous progress for bridges in the past four years. The next northern or southern California urban earthquake should produce information about the response of bridges including the effects of structural yielding and near field effects. The performance of a retrofitted bridge or a post–1990 designed bridge in a near field event has not yet been recorded. The collection of such data will provide essential information to improve understanding of system response in the nonlinear range. The plans for instrumenting the toll bridges is a welcome development. However, the relatively light instrumentation on large flexible bridges will not provide a complete picture of system response. Careful studies on how to deploy instruments optimally should be undertaken before finalizing the instrumentation plans for the toll bridges.

The studies of strong–motion records from bridges have shown the importance of capturing the non–uniform free–field and input motions at multiple supports. The recent deployment of downhole arrays will help in understanding the propagation and reflection of earthquake waves to the surface and the distribution of input motion over footings and kinematic soil–structure interaction effects. Although inertial soil–structure interaction has always been considered in the design and analysis of bridges, the recent studies are increasing are appreciation of the importance of interaction and recognizing nonlinearities of the footings and abutments. The hysteretic behavior of footings and abutments may be providing significant energy dissipation that is not recognized when assessing the inelastic demands on columns. Although there have been limited studies for abutments, there has not been a similar study for footings because it requires a dense array. Critical bridges on soft soils should be provided instrumentation at the footings to capture nonlinear soil–structure interaction effects. This should be done at sites with downhole arrays.

The instrumentation of concrete dams is inadequate considering the importance of dams for water supply and the strict review of dams required by the State. Unlike bridges, for which the owner (Caltrans) funds the instrumentation, there is no requirement or incentive for dam owners to instrument their dams. Instrumentation for Pacoima dam should be upgraded with a modern digital system. It is strongly recommended that the canyon downstream of the dam be instrumented to capture the free–field motion of the canyon without the effects of the dam.

Collecting strong–motion data is only the first step. System identification for linear, time invariant systems is fairly mature. System identification for nonlinear systems has primarily considered simple systems with simple nonlinearities. However, improvements are needed for

identifying the behavior of large structures such as bridges as they enter the nonlinear range. Identification procedures that provide changes in mode shapes, vibration periods, and damping over time are useful for understanding global changes in behavior. However, the time–varying procedures do not provide information about the underlying nonlinear component behavior that is leading to the change in vibration properties. There is a critical need to validate the nonlinear models that are beginning to be used in bridge design.

A final comment is that particularly for bridges, we are often more interested in deformation, that is displacements between two points, rather than forces (i.e. acceleration). Deformations can be determined from double integrating differences of accelerations but these requires enough accelerometers and entails error because of random noise and other factors. Direct dynamic measurement of deformation and even strain would be very useful for validating models. Rugged and reliable displacement instruments with a wide dynamic range, possibly using fiber optics or lasers, should be developed.

ACKNOWLEDGMENTS

The work on the Northwest Connector and Pacoima dam were supported by two grants from CSMIP as part of its data utilization program. The author is grateful to Dr. Anthony Shakal and Dr. Moh Huang for their support. The California Department of Transportation has funded related studies as part of its seismic retrofit program. James Roberts, James Gates, Brian Maroney, and Pat Hipley have been particularly helpful. For the study of Pacoima dam, the author wishes to acknowledge the assistance of Dr. Rashid Amad of the California Division of Safety of Dams and Robert Kroll of the Los Angeles Department of Public Works.

REFERENCES

ATC (1996). "Improved Seismic Design Criteria for California Bridges," *ATC–32*, Applied Technology Council, Redwood City.

Desroches, R., and Fenves, G.L. (1997). "Evaluation of Recorded Earthquake Response of a Curved Highway Bridge," accepted for publication, *Earthquake Spectra.*

Fenves, G.L., Filippou, F.C., and Sze, D.T., "Response of the Dumbarton Bridge in the Loma Prieta Earthquake," *Report No. UCB/EERC–92/02*, Earthquake Engineering Research Center, University of California, Berkeley.

Fenves, G.L., and Desroches, R. (1994). "Response of the Northwest Connector in the Landers and Big Bear Earthquakes," *Report No. UCB/EERC–94/12*, Earthquake Engineering Research Center, University of California, Berkeley.

Fenves, G. L., Mojtahedi, S., and Reimer, R.B. (1989). "ADAP–88: A Computer Program for Nonlinear Earthquake Analysis of Concrete Arch Dams," *Report No. UCB/EERC–89/12*, Earthquake Engineering Research Center, University of California, Berkeley.

Fenves, G. L., Mojtahedi, S., and Reimer R.B. (1992). "Effect of Contraction Joints on Earthquake Response of an Arch Dam," *Journal of Structural Engineering*, ASCE, Vol. 118, No. 4, pp. 1039–1055.

Kelly, J.M., Aiken, I.D., and Clark, P.W., "Response of Base–Isolated Structures in Recent California Earthquakes," *Proceedings*, SMIP91 Seminar, California Strong Motion Instrumentation Program, Division of Mines and Geology, Sacramento.

Liu, W.D, Kartoum, A., Dhillon, S, Chen, X., and Imbsen, R.A. (1996). "Implications of the Strong–Motion Records from a Retrofitted Curved Bridge on Seismic Design and Performance," *Proceedings*, SMIP96 Seminar, California Strong Motion Instrumentation Program, Division of Mines and Geology, Sacramento.

McCallen, D.B. (1992). "Response Studies of the Dumbarton Bridge," Lawrence Livermore Laboratory.

McCallen, D.B., and Romstad, K.M. (1994). "Dynamic Analysis of a Skewed Short–Span Box–Girder Overpass," *Earthquake Spectra*, Vol. 10, No. 4, pp. 729–755.

Malhotra, P.M., Huang, M., and Shakal, A.F. (1994). "Interaction at Separation Joints of a Concrete Bridge During 1992 Earthquakes in California," *Proceedings*, Fifth U.S. National Conference on Earthquake Engineering, Chicago, Vol. I, pp. 347–356.

Maroney, B., Romstad, K.M., and Chajes, M. (1990). "Interpretation of Rio Dell Freeway Response During Six Recorded Earthquakes," *Proceedings*, Fifth U.S. National Conference on Earthquake Engineering, Chicago, Vol. I, pp. 1007–1016.

Mojtahedi, S., and Fenves, G.L. (1996). "Response of a Concrete Arch Dam in the 1994 Northridge, California Earthquake," *Proceedings,* Twelfth Word Congress on Earthquake Engineering, Acapulco.

Mojtahedi, S., and Tseng, W.S. (1994). "ADAP–NF, A Computer Program for Nonlinear Analysis of Arch Dams Considering Nonuniform Seismic Input," International Civil Engineering Consultants, Inc., Berkeley.

Nowak, P. S., and Hall, J.F. (1990). "Arch Dam Response to Nonuniform Seismic Input," *Journal of Engineering Mechanics*, ASCE, Vol. 116, No. 1, pp. 125–139.

Safak, E. (1990). "Identification of Linear Structures Using Discrete–Time Filters," *Journal of Structural Engineering*, ASCE, Vol. 116, No. 7, pp. 2008–2021.

Sweet, J., and Morrill, K.B. (1993). "Nonlinear Soil–Structure Interaction Simulation of the Painter Street Overcrossing," *Proceedings*, Second Annual Caltrans Seismic Research Workshop, Sacramento.

Tseng, W.S., Yang, M.S., and Penzien, J. (1992). "Seismic Performance Investigation of the Hayward BART Elevated Section," *Data Utilization Report CSMIP/92–02*, California Strong Motion Instrumentation Program, Sacramento.

Werner, S.D., Beck, J.L., and Levine, M.B. (1987). "Seismic Response Evaluation of Meloland Road Overcrossing using the 1979 Imperial Valley Earthquake Records," *Journal of Structural Dynamics and Earthquake Engineering*, Vol. 15, No. 2, pp. 249–274.

Werner, S.D., Crouse, C.B., Katafygiotis, L.S., and Beck, J.L. (1993). *Model Identification and Seismic Analysis of Meloland Road Overcrossing*, Technical Report to Caltrans, Dames & Moore, Oakland.

Wilson, J.C. (1984). "Analysis of the Observed Earthquake Response of a Multiple Span Bridge," *Report No. EERL 84–01*, Earthquake Engineering Research Laboratory, California Institute of Technology.